HYDROTHERMALLY PREPARED VANADIUM OXIDE-CHITOSAN NANOCOMPOSITE FOR ELECTROCATALYTIC APPLICATION

A Major Project Submitted In the Partial Fulfillment of the Requirement

For the Award of the degree of

MASTER OF TECHNOLOGY

IN

POLYMER TECHNOLOGY

Under the Supervision of

Prof. D.KUMAR

(Project Guide & Head)

Department of Applied Chemistry

& Polymer Technology

Delhi Technological University

Delhi - 110042

BY

MANISH KUMAR

(2K12/PTE/06)

DEPARTMENT OF APPLIED CHEMISTRY & POLYMER TECHNOLOGY

DELHI TECHNOLOGICAL UNIVERSITY, DELHI- 110042

DELHI TECHNOLOGICAL UNIVERSITY

(Govt. of National Capital Territory of Delhi)

Shahbad Daulatpur, Main Bawana Road,

Delhi - 110042

CERTIFICATE

*This is to certify that Mr. Manish Kumar has Satisfactorily Completed this Major project entitled "**Hydrothermally Prepared Vanadium Oxide-Chitosan Nanocomposite for Electrocatalytic Application**" in the Partial Fulfillment for the Award of the Degree of Master of Technology in Polymer Technology of Delhi Technological University, Delhi during the Academic Session 2013-2014.*

To the Best of my knowledge and Belief, this Work has not been submitted to any other University or Institutions for the Award of any Degree or Diploma.

Prof. D. Kumar

Project Guide & Head

Department of Applied Chemistry &

Polymer Technology,

DTU, Delhi-110042

ACKNOWLEDGEMENT

Taking the opportunity of this column, I would like to express my sincere gratitude to all those who directly or indirectly helped me in successful completion of my project.

First of all I heartedly express my humble gratitude to **Prof. D.KUMAR**, Department of Applied Chemistry & Polymer Technology, Delhi Technological University (Formerly Delhi College of Engineering), for providing me the facilities, guidance, suggestions and constant encouragement throughout the tenure of my project work. I am deeply indebted to him for giving me an opportunity to work with him and helping me in every possible way in bringing out this work to reality.

I also would like to express any sincere gratitude to **Dr. Jay Singh**, Department of Applied Chemistry & Polymer Technology, Delhi Technological University (Formerly Delhi College of Engineering), complete my entire project under their valuable guidance, constant support and encouragements.

I am also thankful to Dr. Sameer Sapra, Professor Department of Chemistry, Indian Institute of Technology, Delhi, for his kind assistance for providing XRD spectra.

I am very much thankful to Dr. Pamela, Department of Biotechnology, Murthal, for carrying out antibacterial study.

I also express my deep sense of gratitude to Ms. Reetu Prabhakar, Ms. Sarita S. Nair and Ms. Nidhi, Research Scholar Department of Applied Chemistry and Polymer Technology for their kind discussion and valuable suggestion.

I would like to extend our thanks to all the non-teaching staff of the Polymer Technology Department, especially Mr. Aman and Mr. Sandeep of Polymer Department.

I am thankful to all my colleagues (friends) Priya Malik and Alkesh Kumari whose inspiring suggestion and ceaseless enthusiasm for the topic explored in this thesis has meant a great deal to me.

Last, but not the least, my parents and my well-wishers have been with me at every step of this exciting journey. I thank them for all their prayers, encouragements and best wishes.

Date:

MANISH KUMAR
2K12/PTE/06
M.TECH (Polymer Technology)
Dept. of Applied Chemistry & Polymer Technology
DTU, Delhi-110042

UNDERTAKING

I declare that the work presented in this thesis titled "**Hydrothermally prepared Vanadium Oxide/Chitosan nanocomposite for electrocatalytic application**", submitted to the Department of Applied Chemistry & Polymer Technology, is an authentic record of my own work carried out under the supervision of **Prof. D Kumar**, Head of the Department, Department of Applied Chemistry and Polymer Technology, Delhi Technological University, Delhi.

I have not submitted the matter embodied in this major project as whole or in part, for the award of any other degree.

Date:
Place: DTU, Delhi

Signature of the candidate

ABSTRACT

In this project work, the nanostructured vanadium penta oxide (V_2O_5) has been prepared using the hydrothermal method. These nanostructured vanadium penta oxide (V_2O_5) used for fabrication of efficient non-enzymatic sensor for electro-oxidation of hydrazine. A colloidal solution of prepared nanostructures has been electrophoretically deposited (EPD) onto an indium-tin-oxide (ITO) glass substrate and and utilized for electro-oxidation of hydrazine. The crystalline structure and morphology of prepared sample have been determined by X-ray diffraction (XRD) (particle size ~25nm), scanning electron microscopy (SEM), transmission electron microscopy (TEM), atomic force microscopy (AFM) and Fourier transform infrared (FTIR) spectroscopic techniques. The optical properties of prepared sample have been examined by ultra-violet (UV–Vis), photoluminescence (PL). Chitosan(CHIT) (a biopolymer) was used as a matrix to prepare the nanocomposite. The V_2O_5 nanoparticles were then ultrasonically dispersed in chitosan (CHIT) solution, and then used to form V_2O_5-CHIT/ITO nanocomposite electrode by drop casting method on the ITO plate. The V_2O_5-CHIT/ITO nanocomposite electrode was found to provide improved sensing characteristics to the electrode interface in terms of electroactive surface area, diffusion coefficient, charge transfer rate constant and electron transfer kinetics. This interfacial platform has been used for fabrication of a non-enzymatic sensor for electro-oxidation of hydrazine. The results of response studies of the fabricated V_2O_5-CHIT/ITO electrode catalytic oxidation peak current shows a linear dependence on the hydrazine concentration and a linear calibration curve is obtained in the concentration range of 2-22 mM, lower detection limit of 1.6239 mM, standard deviation of 0.00249μA and high sensitivity of 0.00460 μA/(mM cm^2) with a response time of 20 s. The utilization of this V_2O_5 modified electrode for electo-oxidation of hydrazine offers an efficient strategy and a novel interface for application of vanadium penta oxide (V_2O_5) in the field of electrochemical sensors. The obtained results indicate that the nanostructured V_2O_5 based electrode offers an efficient strategy and a new promising platform for application of the metal oxide material in electrochemistry and bioelectronics.

TABLE OF CONTENTS

CHAPTER 1. INTRODUCTION

CHAPTER 2: EXPERIMENTAL TECHNIQUES

LIST OF FIGURES

LIST OF TABLE

1. Introduction

1.1 Nanotechnology

The term "nanotechnology" was introduced by Norio Taniguchi for the first time in 1974 during the session of International Conference on Precision Engineering (ICPE). He defined the term nanotechnology as production technology to achieve accurate and ultra-fine dimensions at the level of 1 nm in length. The fast and effective progress in nanotechnology could take place only after the invention of sensitive tools for the characterization of nanomaterials. Scanning tunnelling microscopy (STM) was invented by Gerd Binnig and Heinrich Rohrer and they were awarded with the Nobel Prize in 1986 for the invention of this sensitive tool for the characterization of nanomaterials. At the present time the resolution of modern electron microscopes is enough to get the image of individual atoms and they are generally fitted with detectors which are able to determine the chemical composition or the oxidation state of surface related atoms.

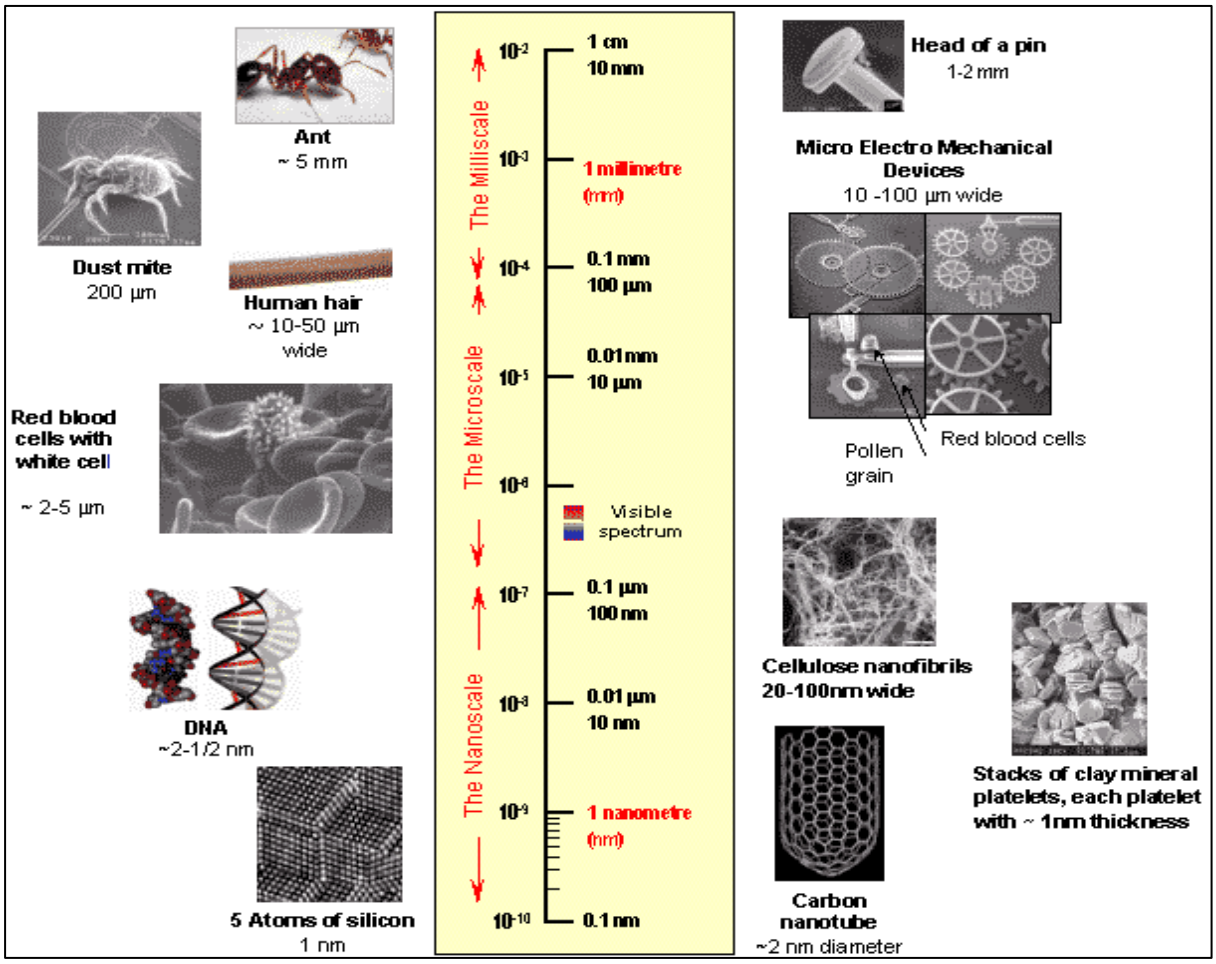

Figure 1.1: Schematic diagram showing the nanoscale to the milliscale dimensions.

Nanotechnology is an interdisciplinary field of science that encompasses the production and application of physical, chemical and biological systems at scales ranging from individual atoms or molecules to submicron dimensions, as well the integration of the resulting nanostructures into larger systems. It is the study of manipulating matter on an atomic and molecular scale. Generally, nanotechnology deals with developing materials, devices, or other structures possessing at least one dimension sized from 1 to 100 nm which literally means nanotechnology is any technology performed on a nanoscale that has applications in the real world. When a matter is brought from the bulk to nano (10^{-9}) range some unique properties like electrical, optical, mechanical, magnetic etc. have been observed which are totally different from its bulk state. Nanotechnology refers to the preparation, characterization, exploration and utilization of nanostructured materials that can be characterized by at least one dimension in the nm range [1]. Nanostructured objects constitute a bridge between single molecule and bulk system. Individual nanostructure involves clusters; quantum dots (QDs), nanoparticles (NPs), nanowires and nanotubes, while collections of nanostructures include arrays, assemblies and super lattices [2]. The chemical and physical properties of nanomaterials can be significantly different from those of atomic, molecular and bulk materials of same composition. The uniqueness of chemistry, structure, response and dynamics of the nanostructures is indispensable motivation for the study of this class of materials. Suitable control of the properties of nanomaterials can lead to new science as well as new products, devices and technologies. The concept of making materials of nanometer size is fundamentally interesting because as the size approaches atomic dimensions, energy level bands are slowly transformed into quantized discrete levels resulting in the change of the properties of materials that are not exhibited by the bulk matter of the same composition [3]. These unique properties provide great potential for the nanoparticles to be used in various applications.

Therefore it draws much attention for the researchers to manipulated thing at that low dimensions to discover the noble and unique world in the low dimension. Nanotechnology has turned out to be the hot buzz word of the new millennium finding its application in almost all applications. Nanotechnology is playing an increasingly important role in the development of sensors, especially exciting opportunity for high-impact applications benefiting from “nano” attributes. A wide variety of nanomaterials, especially nanoparticles with different properties have found broad application in many kinds of analytical methods.

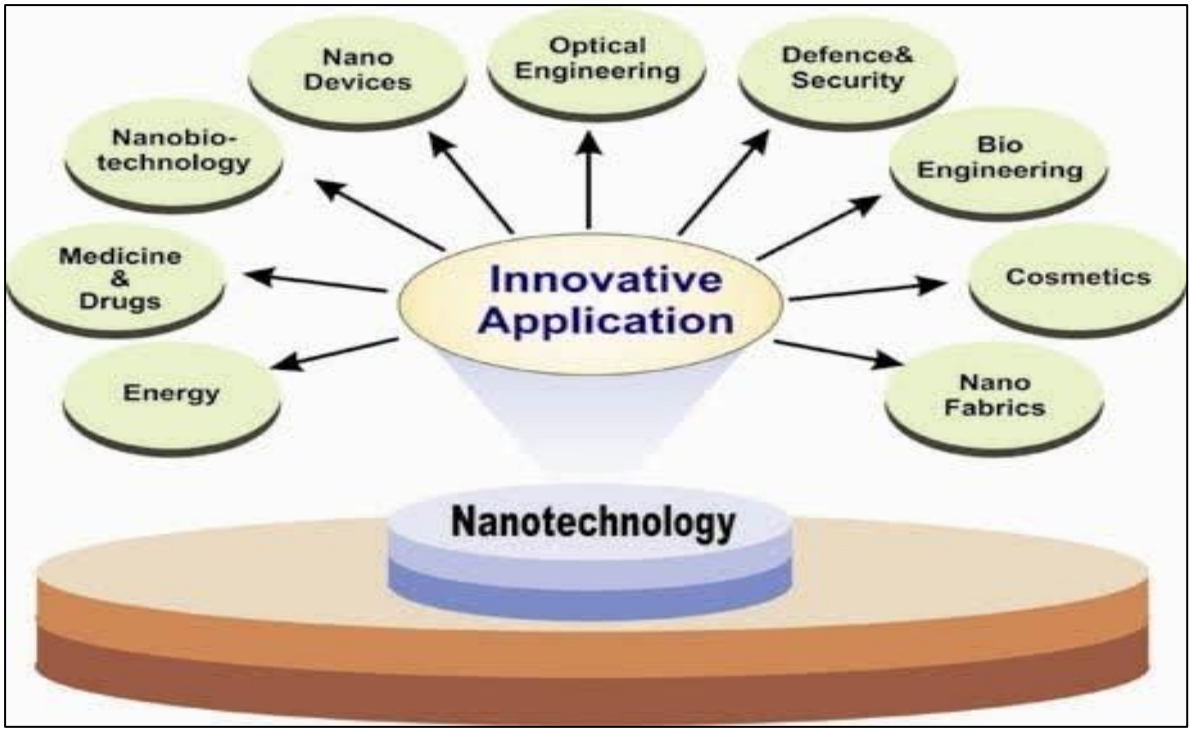

Figure 1.2: Applications of Nanotechnology in various fields

1.2 Metal oxide nanoparticles for electrocatalytic application

In recent years, applications of nanomaterials in biosensors provide novel opportunities for developing a new generation of sensor technologies. Nanomaterials can improve mechanical, electrochemical, optical and magnetic properties of sensor. There are various types of nanomaterials like metal nanoparticles, metal oxide nanoparticles, carbon nanotubes, nanowires, nanorodes that have been used for sensor development but among them metal oxide nanoparticles have recently drawn much interest [4]. Oxide nanoparticles are often used due to their biocompatibility, while semiconductor nanoparticles are often used as label or tracers for electrochemical analysis.

Metal oxide nanomaterials such as vanadium, nickel, zinc, iron, cerium, tin, zirconium, titanium, metal and magnesium have been found to exhibit interesting nano morphological, functional biocompatible, non-toxic and catalytic properties. These materials also exhibit enhanced electron-transfer kinetics and strong adsorption capability and resulting in enhanced electron transfer and improved electrocatalytic characteristics.

Applications of nanomaterials to electrocatalytic applications have recently aroused much interest. This is because these interesting materials exhibit the following properties:

1. Large surface-to-volume ratio
2. High surface reaction activity
3. High catalytic efficiency,
4. Low toxicity
5. Chemical stability

Addition to this these nanostructures show fast electron communication properties which is very important for electrocatalytic applications.

1.2.1. Vanadium penta oxide (V_2O_5)

Vanadium (V) oxide is a yellow to red crystalline powder with the chemical formula V_2O_5 and also known as vanadic acid [5]. The V_2O_5 is thermochromic material a transition temperature of about 375 °C, melting temperature of 690 °C. It is a poisonous orange solid, because of its high oxidation state, is both an amphoteric oxide and an oxidizing agent. This thermochromic material has orthorhombic crystal structure [6]. It is used as a catalyst in various organic reactions and as a starting material (precursor) for other vanadium salts. It has been shown that upon heating V_2O_5 reversibly loses oxygen [7].

Vanadium exists in a number of oxide forms, the di-, sesqui- and penta oxides (VO_2, V_2O_3 and V_2O_5). Vanadium oxygen systems (V_2O_5, VO_2) have been studied extensively by theoretical and experimental techniques. They show metal-semiconductor transition, which implies an abrupt change in optical and electrical properties. That is why this oxide is used in electrocatalytic applications. Especially vanadium oxide (V_2O_5), as a wide band gap and n-type semiconductor material, was widely investigated because of its interesting electrochemical performance, its thermochromic and electrochromic properties [8].

1.2.2. Orthorhombic structure of V_2O_5

This thermochromic material has orthorhombic crystal structure; and belongs to P_{mnm} space group with a lattice parameters a = 11.510Å, b = 3.563Å, c = 4.369Å, where the b and c axes are often interchanged. The vanadium atoms form five bonds with oxygen V-O bond lengths vary from 1.585 Å to 2.021 Å: one with O (1) atoms, one with the O (2) atom and three with the O (3) atoms [9].

.

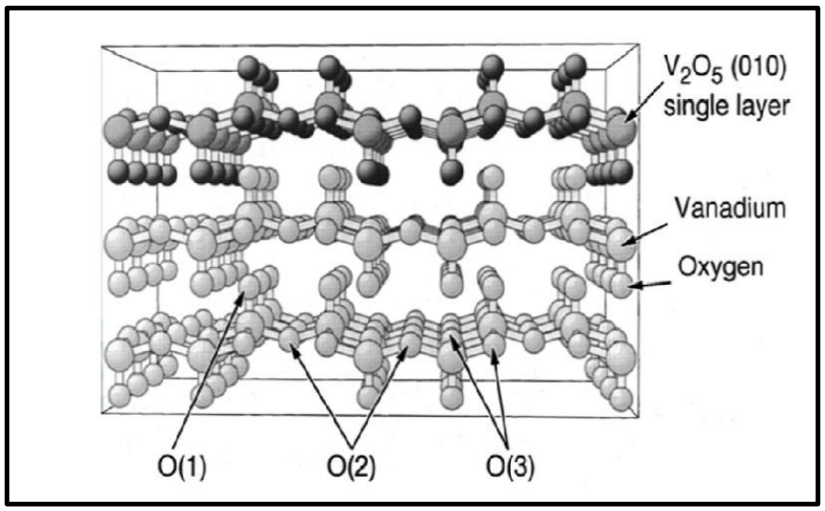

Figure 1.3: Crystal structure of the orthorhombic V_2O_5 with net plane stacking along the (010) direction. Vanadium and inequivalent oxygen centres, singly coordinated O (1), doubly coordinated O (2), and triply coordinated O (3), are marked accordingly.

1.2.3. Physical properties of V_2O_5

Vanadium is a transition metal with an atomic number 23 and atomic mass of 50.9414gmol^{-1}. The melting point of vanadium is 1910 °C and its boiling point is 3407 °C. There are five isotopes of vanadium. The vanadium is a rare, soft, ductile grey-white element found combined in certain minerals and used mainly to produce certain alloys. The protective film of oxide on the surface of vanadium makes it to resist. The common oxidation states of this element include +2, +3, +4 and +5 [10]. After vanadium has been oxidized, it produces all the vanadium oxides with different colours, transition temperature, melting point and boiling point.

1.3 V_2O_5 nanoparticles Synthesis

Anqiang Pan et al have done the facile synthesis of nanorod structured vanadium penta oxide for high-rate lithium batteries. V_2O_5 nanoparticles produced by this method exhibit much better electrochemical performance than commercial micro-sized V_2O_5. The optimized-nanorod electrodes give the best specific discharge capacities of 270 mAh g^{-1} at C/2 (147 mA g^{-1}) coupled with good cycle stability with only 0.32% fading per cycle. Even at a high rate of 4C (1176 mA g^{-1}), the nanorod electrode still delivers 198 mAh g^{-1} [11].

Waldir Avansi Jr. et al worked to fabricate V_2O_5 nanostructures with an effective control of morphology and crystal structure in hydrothermal conditions. They have reported that morphologies, crystal structure, and amount of water molecules between the layered structures were regulated by strictly controlling the hydrothermal treatment variables. X-ray diffraction (XRD) and scanning transmission electron microscopy (STEM) revealed the formation of monoclinic phase and nanowires or nanorods of the $V_2O_5{\cdot}nH_2O$ orthorhombic phase [12].

Li Li et al have synthesized and characterized self-assembled V_2O_5 mesostructures intercalated by polyaniline. This group has reported a new nanocomposite of vanadium penta oxide (V_2O_5) and polyaniline (PANI) synthesized by in situ oxidative polymerization/intercalation on V_2O_5 powder at room temperature. The reaction was facile and topotactic, forming polyaniline as the emeraldine salt. It was indicated that V_2O_5 itself can catalyze the oxidative polymerization of aniline and that layered structure could make aniline intercalate into the V_2O_5 framework. XRD results showed PANI/ V_2O_5 nanocomposite possessed lamellar mesostructure, which was determined by an X-ray diffraction peak at 6.5° and SEM photograph. And FT-IR spectrum suggested that there was interaction between PANI and V_2O_5 [13].

1.4 Importance of V_2O_5 nanoparticles

Among the various nanomaterials, V_2O_5 nanoparticles have recently gained increased interest due to promising applications for applications in catalysis, as sensors, in electrochromic devices, in electrochemistry, photocatalytic activities and in spintronic devices etc. Vanadium exists in a number of oxide forms, the di-, sesqui- and penta oxides (VO_2, V_2O_3 and V_2O_5).They show metal-semiconductor transition, which implies an abrupt change in optical and electrical properties. That is why this oxide is used in electrocatalytic applications. Especially vanadium oxide (V_2O_5), as a wide band gap and n-type semiconductor material, was widely investigated because of its interesting electrochemical performance, its thermochromic and electrochromic properties. That's why V_2O_5 nanoparticles have been considered as interesting nanomaterial for electrocatalytic applications.

1.5 Chitosan (CHIT)

1.5.1. Structure of chitosan

CHIT is a fibre-like substance derived from chitin, a homopolymer of ß-(1→4)-linked *N*-acetyl-D-glucosamine. Chitin is the second most abundant organic compound in nature after cellulose. With regards to their chemical structure **Figure 1.4**, chitin and CHIT have similar chemical structure. Chitin is made up of a linear chain of acetyl glucosamine groups while CHIT is obtained by removing enough acetyl groups (CH_3-CO) for the molecule to be soluble in most diluted acids. This process is called deacetylation. The actual difference between chitin and CHIT is the acetyl content of the polymer. CHIT having a free amino group is the most useful derivative of chitin.

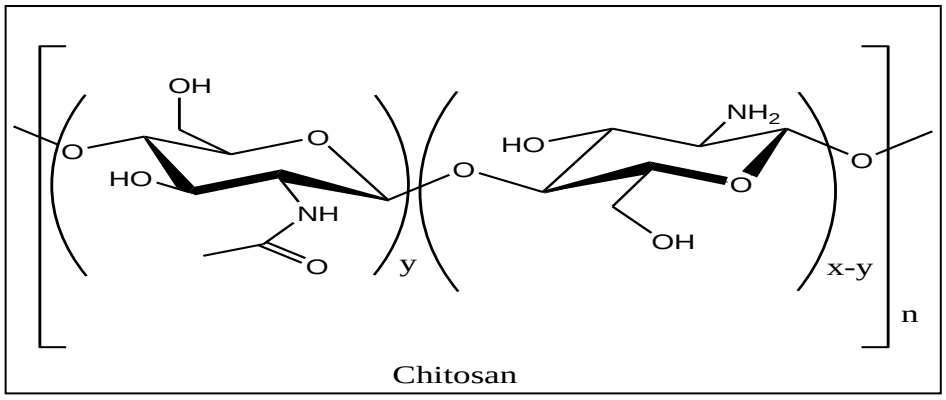

Figure 1.4: Chemical structure of Chitosan

1.5.2. Preparation of chitosan from chitin

CHIT is prepared from the deacetylation of chitin. The process of deacetylation involves the removal of acetyl groups from the molecular chain of chitin, leaving behind a compound (CHIT) with a high degree chemical reactive amino group (-NH_2). This makes the degree of deacetylation an important property in CHIT production as it affects the physicochemical properties, hence determines its appropriate applications. Deacetylation also affects the biodegradability and immunological activity. The degree of deacetylation of CHIT ranges from 56% to 99% with an average of 80%, depending on the crustacean species from which

chitin is obtained and the preparation methods. Chitin with a degree of deacetylation of 75% or above is generally known as CHIT.

deacetylation

CHITIN ⟶ CHITOSAN

1.5.3. Characteristics of chitosan

CHIT is a non-toxic, biopolymer of high molecular weight. CHIT possesses positive ionic charges, which give it the ability to chemically bind with negatively charged fats, lipids, cholesterol, metal ions, proteins, and macromolecules. In this respect, chitin and CHIT have attained increasing commercial interest as suitable resource materials due to their excellent properties including biocompatibility, biodegradability, adsorption, and ability to form films, and to chelate metal ions.

1.5.4. Chitosan (CHIT) for nanocomposite formation

CHIT (electroactive biopolymer) has been attracted much interest for electrocatlytic applications because of the following features: Among the various biopolymers, chitosan (CHIT) along with nanoparticles has been utilized as a stabilizing agent due to its following properties [14].

1. Susceptibility towards chemical modifications
2. Excellent film forming ability
3. Mechanical strength
4. Biocompatibility
5. Non-toxicity
6. High permeability towards water
7. Cost-effectiveness
8. Possible to modulate required electrical and mechanical properties.

Though CHIT is of great importance in electrocatalytic applications but still there is a vast scope of improvement in this material. The improvement is subject to the incorporation of nanoparticles in the biopolymer because they promote electron-transfer reactions and hence increase the charge conduction.

1.6 Nanocomposites

Nano-composite material has broadened significantly to encompass a large variety of systems such as one-dimensional, two-dimensional, three-dimensional and amorphous materials, made of distinctly dissimilar components and mixed at the nanometer scale.

1.6.1. Organic - inorganic hybrid nanocomposites

The combination of inorganic and organic building blocks on the molecular or nanometer scale leads often to materials with novel properties that lie between the properties of the two original compound classes or entirely new properties are generated. Many different reaction parameters have to be controlled to get homogeneous materials with the desired properties. The focus is currently on investigations in the preparation of well-defined nanobuilding blocks, their attachment to the polymer backbone and the influences of the attached systems on the properties of the polymer and vice versa. Among various organic inorganic nanocomposite systems, biopolymer (chitosan) – nanomaterials based nanocomposite systems have recently been attracted interest of researchers for biosensor development. Organic - inorganic hybrid nanocomposites have promising applications in many areas: optics, electronics, ionics, mechanics, energy, environment, biology, medicine for example as membranes and separation devices, functional smart coatings, fuel and solar cells, catalysts, sensors, etc.

1.7 Nanocomposite of CHIT-Nanomaterials

Different type of nanomaterials such as Fe_3O_4, ZnO, TiO_2, CNT, Au etc. have been incorporated in CHIT matrix to fabricate nanocomposite for various application. The electrocatalytic applications of these nanocomposites are discussed below as-

1.7.1. CHIT-ZnO Nanocomposite

ZnO NPs uniformly dispersed in CHIT has been used to fabricate a hybrid nanocomposite film onto indium-tin-oxide (ITO) glass plate. ChOx has been immobilized onto this Nano ZnO–CH composite film using physisorption technique. The ChOx/NanoZnO-CH/ITO bioelectrode exhibits linearity from 5 to 300 $mgdl^{-1}$ of cholesterol with detection limit as 5 mg dl^{-1}, sensitivity as 1.41×10^{-4} $Amgdl^{-1}$ and the value of K_m as 8.63 $mgdl^{-1}$. This cholesterol biosensor can be used to estimate cholesterol in serum samples [15].

1.7.2. CHIT-Au nanocomposite

There is a systematic exploration of a natural polymer, CHIT, as a structural material for designing functional layers on electrode surfaces in this work. Au colloid films are organized on CHIT layer by adsorption. These assemblies of colloid Au multilayer are highly stable, and can be kept for a long time in distilled water, only being removed by scratching or extreme electrochemical conditions [16].

A new strategy for immobilization of horseradish peroxidase (HRP) has been presented by self-assembling AuNPs on CHIT hydrogel modified Au electrode. The resulting biosensor (HRP-modified electrode) showed wide linear range of 8.0 mM to 0.50 mM, with a detection limit of 2.4 μ. Moreover, the biosensor remained about 85% of its original sensitivity after four weeks storage [17].

The nanocomposite composed of carboxymethyl CHIT and AuNPs was successfully prepared by a novel and in situ process. Good stability and sensitivity were assessed for the biosensor [18].

A novel method for preparation of hydrogen peroxide biosensor was presented based on immobilization of haemoglobin (Hb) on CIN. The designed biosensor exhibited acceptable stability, long-term life and good reproducibility [19].

1.7.3. CHIT-Fe_3O_4 nanocomposite

Fe_3O_4 nanoparticles prepared using co-precipitation method has been dispersed in CHIT solution to fabricate nanocomposite film on indium-tin-oxide (ITO) glass plate. GOx has

been immobilized onto this CH-Fe_3O_4 nanocomposite film via physical adsorption. This GOx/CH-Fe_3O_4/ITO nanocomposite bioelectrode has response time of 5 s, linearity as 10-400 mg dL^{-1} of glucose, sensitivity as 9.3 µA/ (mg dL^{-1} cm^{-2}) and shelf life of about 8 weeks under refrigerated conditions. The value of K_m constant obtained as 0.141 mM indicates high affinity of immobilized GOx towards the substrate (glucose) [20].

A novel amperometric glucose biosensor was developed by entrapping GOx in CHIT composite doped with ferrocene monocarboxylic acid-modified magnetic core-shell Fe_3O_4-SiO_2 NPs (FMC-AFSNPs). This immobilization approach effectively improved the stability of the electron transfer mediator and is promising for construction of biosensor and bioelectronic devices [21].

1.7.4. CHIT-CNT/Fe_3O_4 nanocomposite

Nanosized flower-like ZnO was synthesized by a simple hydrothermal method which is a convenient, environment friendly, inexpensive and efficient process. The biosensor exhibited satisfactory reproducibility and stability and retained about 78% of its original response after 40 days storage in a phosphate buffer at 4 °C [22].

1.7.5. CHIT-SiO_2 nanocomposite

This study primarily aims to explore the strength and thermal properties of various hybrid materials that are made of tetraethoxysilane/ vinyltriethoxysilane (TEOS/VTES) and CHIT in different weight ratios. It is confirmed, from micro FT-IR and nuclear magnetic resonance (NMR) analysis that hydrogen bonds emerge between CHIT and SiO_2 in hybrid materials. With the addition of more VTES and TEOS, the surface of the hybrid material features thick granules. In addition, the mechanical performance and thermostability of both types of hybrid are better than pure CHIT. The former is enhanced with an increasing amount of TEOS until it exceeds 2.4 g and the latter is also improved with an increasing amount of TEOS [23].

1.7.6. CHIT-TiO_2 nanocomposite

FT-IR and UV-visible spectroscopy were used to optimize TiO_2 concentration in CHIT to develop a sensitive CHIT/TiO_2 bioactive electrode. EIS used to measure electro-activity of

these bioactive electrodes associated with enhance oligosaccharide containing –C=O groups from degradation of CHIT molecules. This matrix has free $–NH_2$ and –OH functional groups due to higher probability of hydrogen and covalent bonding between –OH group in CHIT molecules with Ti–O–Ti which supported immobilization of rabbit antibodies (I_gGs) and proteins. Ochratoxin A (OTA) was detected and showed a linear response up to 10 ng/mL with CHIT/TiO_2 bio-electrode. The OTA detection sensitivity of 7.5 mM TiO_2 added CHIT bioactive electrode was four times higher than only CHIT [24].

1.7.7. CHIT-CeO_2 Nanocomposite

CeO_2/CHIT nanocomposite matrix was firstly developed for the single-stranded DNA (ssDNA) probe immobilization and the fabrication of DNA biosensor related to the colorectal cancer gene. Such matrix combined the advantages of CeO_2 and CHIT, with good biocompatibility, nontoxicity and excellent electronic conductivity, showing the enhanced loading of ssDNA probe on the surface of electrode. The preparation method is quite simple and inexpensive. The hybridization detection was accomplished by using methylene blue (MB), an electro active lable, as the indicator. The established biosensor has high detection sensitivity, a relatively wide linear range from 1.59×10^{-11} to 1.16×10^{-7} mol L^{-1} and the ability to discriminate completely complementary target sequence and four-base-mismatched sequence [25].

1.8. V_2O_5-CHIT nanocomposite

It has been seen that the problem of aggregation and rapid biodegradation of V_2O_5 onto a desired matrix containing can perhaps be overcome by modifying these interesting nanoparticles using inorganic semiconductors, conducting polymers and biopolymers (polysaccharides) etc. Among the various biopolymers, CHIT along with nanoparticles has been utilized as a stabilizing agent due to its excellent properties such as Excellent film forming ability, Biocompatibility, Nontoxicity, High mechanical strength, Cheapness, Susceptibility to chemical modifications. Moreover, amino groups of CHIT provide a hydrophilic environment compatible with most of the biomolecules.

In this study V_2O_5 nanoparticles were synthesized and V_2O_5-CHIT/ITO electrode was fabricated through appropriate addition of V_2O_5 nanoparticle and CHIT solution by drop casting method. The prepared electrode has been characterized by XRD, SEM, FTIR, UV-Vis, PL and electrochemical techniques for enhancing the electrocatalytic properties of hydrazine. This work provides an easy going and effective route for synthesis of V_2O_5-CHIT nanocomposite.

1.9. Hydrazine

Hydrazine and its derivatives have found a wide range of applications, including as antioxidants, pharmaceutical intermediates, pesticides, plant-growth regulators, blowing agents, corrosion inhibitors, dyes and in photography. Furthermore, hydrazine is a high energy fuel molecule and reducing agent as well and can be used as the fuel in explosives and rocket propulsion systems. Direct hydrazine (N_2H_4)-air fuel cells are highly attractive because of their superior theoretical standard equilibrium potential and high power density.

1.9.1. Importance of electro-oxidation of Hydrazine

Hydrazine is toxic and probably even mutagenic. In order to better utilize hydrazine as a fuel and resolve these environmental issues, the development of a catalyst that can oxidize at a high rate is required. However, a major barrier to the wide application of direct hydrazine (N_2H_4)-air fuel cells is the expensiveness of the noble metal catalysts that are generally required [26-27]. To overcome this problem, research has been focused on developing various types of catalysts for the electro oxidation of hydrazine. Recently, gold nanoparticles supported on a TiO_2 nanotube matrix [28], titanium-supported Ag/Ti electrodes [29], metal electrodes [30], carbon nanotubes/Ni-Fe alloys [31], carbon-supported metalloporphyrins [32], iridium [33], palladium/ polyaniline nanocomposites [34] and nickel-palladium nanoparticles [35] have been studied for use as a catalyst for the electrooxidation of hydrazine hydrate. Chinchilla et al reported the use of Ni−Co alloy as an electrocatalyst for the oxidation of (N_2H_4) [36]. Zhong et al synthesized Ni–Fe/MoS_2 hybrids by the in situ growth of Ni–Fe alloy on graphene-like MoS_2 using different molar ratios of Ni: Fe [37]. In this work, we synthesized **V_2O_5/CHIT nanocomposites** by a simple hydrothermal treatment. Moreover, by combining the advantages of Chitosan and V_2O_5 nanoparticles together with their good conductivity and electrocatalytic activity, the V_2O_5/CHIT nanocomposites were

studied for their application to the electrochemical oxidation of hydrazine. It was observed that the V_2O_5/CHIT modified electrode exhibited excellent catalytic activity for the oxidation of hydrazine as compared to bare V_2O_5.

1.10. Objective of present work

For the fabrication of V_2O_5-CHIT nanocomposite electrode for Electro-oxidation study of hydrazine following experiments have been conducted:

(i) Synthesis of the vanadium penta oxide (V_2O_5) nanoparticles.
(ii) Structural and morphological characterization of prepared V_2O_5 nanoparticles.
(iii) Investigation of Optical properties of prepared V_2O_5 and V_2O_5-CHIT nanocomposite.
(iv) Bonding characteristics of these fabricated electrodes through FTIR studies.
(v) To fabricate V_2O_5 /ITO and V_2O_5 -CHIT/ITO electrode.
(vi) Electro-oxidation of hydrazine by using fabricated V_2O_5 -CHIT/ITO electrode.
(vii) Electrochemical response studies of V_2O_5 -CHIT/ITO electrode are measured in terms of linearity, sensitivity, low detection limit, linear regression, and standard deviation.
(viii) Antibacterial activity test was performed with different micro-organism.
(ix) Optimization of various parameters (effect of potential, pH, response time) during electro-oxidation of hydrazine.

1.11. Methodology adopted to achieve the above objective

To achieve the above objective, we plan to follow the methodology described below**:**

(i) Synthesis of the V_2O_5 nanoparticles using hydrothermal homogeneous method.
(ii) Structural and crystalline size of V_2O_5 nanoparticles through XRD, TEM and AFM.
(iii) V_2O_5 /ITO electrode was prepared by EPD and V_2O_5-CHIT/ITO nanocomposite electrodes fabricated by drop casting.

(iv) Preparation of polymer (chitosan) solution and chitosan based V_2O_5 nanocomposite film on ITO.

(v) Surface morphological studies and element analysis of the electrodes by using SEM, EDX and AFM.

(vi) Optical properties were measured by UV-Vis and PL spectrophotometer.

(vii) Bonding characteristics of those fabricated electrodes through FTIR.

(viii) Electro-oxidation of hydrazine was done by amperometric measurement (CV, and DPV).

(ix) Electrochemical response studies of the V_2O_5-CHIT/ITO nanocomposite electrodes using sensing parameter like linearity, sensitivity, low detection limit, linear regression, and standard deviation.

(x) Investigation of the effect of potential, pH, response time, stability on the fabricated V_2O_5-CHIT/ITO nanocomposite electrode.

(xi) Antibacterial activity test was performed in CHIT, prepared V_2O_5 nanoparticles and V_2O_5-CHIT/ITO nanocomposite with Gram positive and Gram negative was done by well diffusion method.

(xii) Application of prepared nanocomposite electrode for Hydrazine sensing.

2. Materials and methods

This chapter gives details about the various materials, methods and characterization techniques used for the preparation of V_2O_5/CHIT nanocomposite for electro-oxidation of Hydrazine.

2.1 Materials

Vanadium penta oxide (V_2O_5), Sodium Hydroxide Pellets (NaOH), Hydrogen Peroxide (30%) (H_2O_2), Sodium Phosphate, Monobasic (NaH_2PO_4), Sodium Phosphate, Dibasic (Na_2HPO_4) were obtained from were obtained from CDH (Delhi). Potassium ferrocyanide (5mM) ({$K_4[Fe(CN)_6]$}), Potassium ferricyanide (5mM) ({$K_3[Fe(CN)_6]$}), Sodium Chlorideb (NaCl) were purchased from MARC (New Delhi).Ammonia Solution (70%) (NH_3), Glacial Acetic Acid($C_2H_4O_2$), Acetone, Hydrazine ($NH_2NH_2.H_2O$) were purchased from Thomas Baker, Chitosan Powder (CHIT) was purchased from was purchased from Sigma–Aldrich (USA) and Nutrient Agar (NA) was a product of Hi Media. The bacterial cultures of *B. cereus* and *P. aeruginosa* were procured from Department of Biotechnology, DCRUST, Murthal. The pre-cleaned functionalized indium-tin-oxide (ITO) coated glass sheets of resistance 15 W/cm was used as the substrate for the deposition of composite electrode and treated as working electrodes. All other chemicals were of analytical grade and were used without further purification. The stock solutions of hydrazine (2-22 mM) were freshly prepared in phosphate buffer (5 mM, pH 6.4). De-ionized water (resistivity not less than 18 MΩ cm) was taken from Milli-Q water purification system (Milli-Q, USA) and used for the preparation of buffer and other solutions.

2.2 Apparatus

X-ray diffraction (XRD) studies have been carried out to characterize the structure and particle size of V_2O_5 nanoparticles and V_2O_5-CHIT nanocomposite using Bruker D8 Advance Diffractometer with Ni-filtered Cu Kα radiation (IIT, New Delhi) with Voltage- 30 kV, 35 mA. The surface morphological studies of V_2O_5, CHIT and V_2O_5-CHIT nanocomposite film have been investigated using scanning electron microscope (HITACHI, Model No.S-3700N with EDS-X with X-ray). The atomic force microscopic studies have been done using Park Systems, XE-100. Transmission electron microscopy was done for the V_2O_5 nanoparticles

using FEI Tecnai S Twin (AIIMS, New Delhi). Fourier transform infrared (FTIR) spectrophotometer (Thermoscientific, Nicolet-380) has been used to characterize V_2O_5, CHIT and V_2O_5-CHIT nanocomposite. The UV-visible spectroscopic studies have been conducted on UV/VIS/NIR spectrometer (PerkinElmer, Lambda 950). The PL emission studies have been done using Fluorolog 3, made by Horiba. The electrochemical studies and amperometric measurements have been recorded on an Autolab Potentiostat/Galvanostat (Metrohm). The electrochemical measurements have been conducted on a three-electrode system with V_2O_5-CHIT nanocomposite electrode as the working electrode, a platinum (Pt) wire as the counter electrode, and saturated Ag/AgCl electrode as a reference electrode in phosphate buffer saline (5 mM, pH 6.4, 0.9% NaCl) containing 5 mM $[Fe(CN)_6]^{3-/4-}$ mediator.

2.3. Methods

2.3.1. Synthesis of Vanadium pent oxide (V_2O_5) nanoparticles

The V_2O_5 nanoparticles were synthesized by hydrothermal and melt quenching method as reported earlier with some modification [38]. Firstly, 5 g V_2O_5 powder was weighed and placed in the crucible. Now, crucible was placed in muffle furnace and heated up to 850 $^{\circ}$C till it get melted and, then melt quenching was done with 100 ml deionized water at room temperature. After stirring for 7-8 h obtained V_2O_5 sol was poured in sealed air tight bottle at room temperature and kept overnight for ageing. In second step, V_2O_5 sol was added to Teflon-lined stainless steel hydrothermal vessel. Now, hydrothermal vessel was placed in hot air oven at 180 $^{\circ}$C for 15 h, afterwards, the Teflon cup was taken out from oven and allowed to cool at room temperature by natural convection. Precipitates were obtained which are washed with deionized water and dried at 70 $^{\circ}$C. **Figure: 2.1** shows schematic representation of V_2O_5 nanoparticles preparation by hydrothermal method.

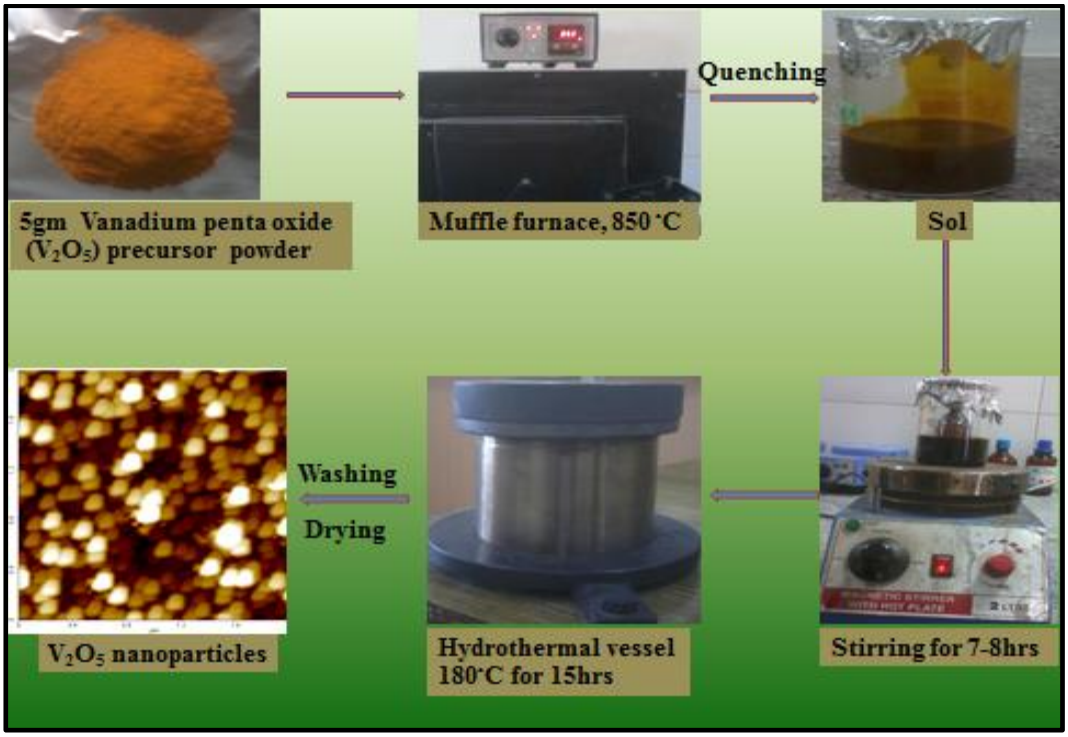

Figure: 2.1: Schematic representation of V_2O_5 nanoparticles preparation by hydrothermal method.

2.3.2. Functionalization of ITO (Indium Tin Oxide) glass plates

Indium Tin Oxide (ITO) coated glass plates were cut into small pieces of 0.5×2 cm^2 area and then immersed in the solution of H_2O_2 : NH_3 :H_2O in the ratio 1:1:5 (v/v) respectively and then kept in oven for 2 h at 90 °C. This leads to formation of uniformly distributed OH groups on the surface of Indium Tin Oxide (ITO) coated glass plates. Afterwards, functinalized ITO plates were rinsed with de-ionized water and dried at room temperature. Further that ITO plates were cleaned with acetone and stored in dust free environment for future use. There functionality was checked by using ammeter. **Figure: 2.2** shows schematic representation of functionalization of ITO plates.

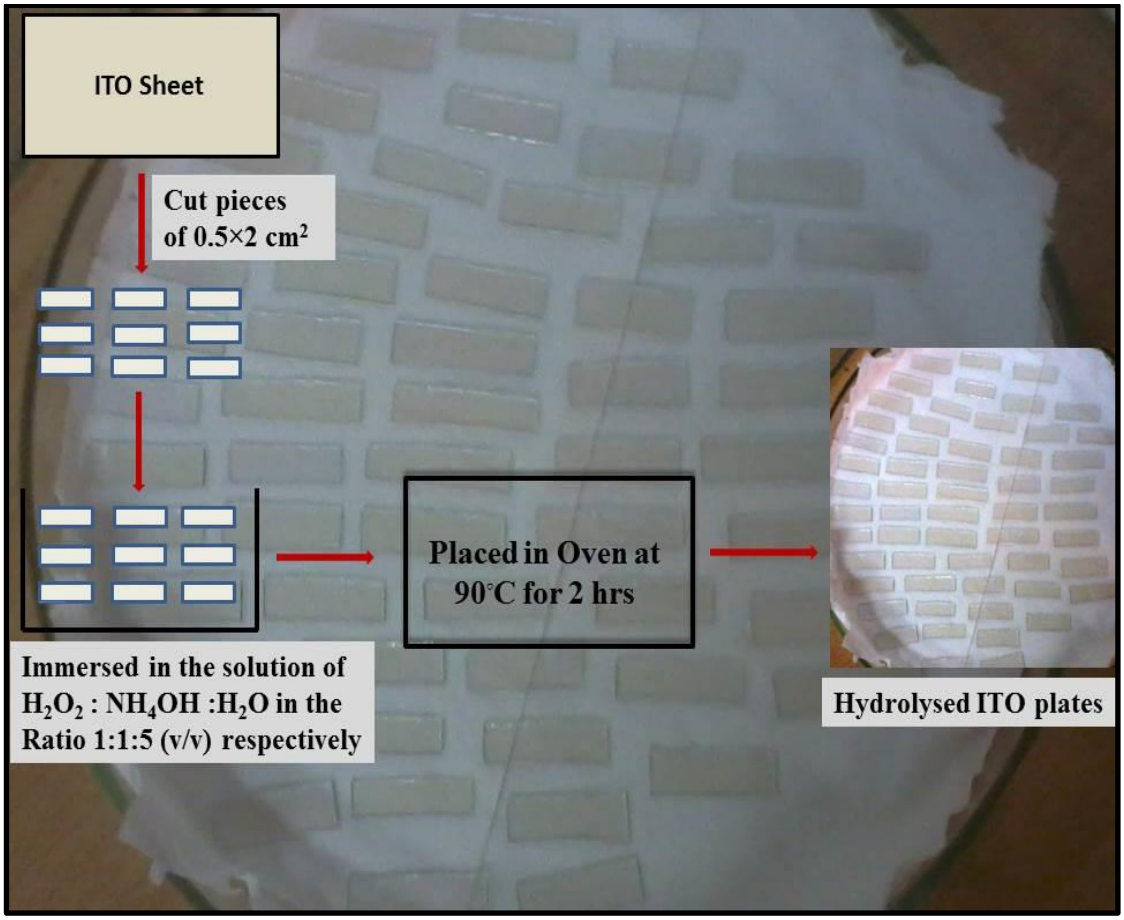

Figure: 2.2: Schematic representation of functionalization of ITO plates.

2.3.3. Preparation of Phosphate Buffer solution

Phosphate Buffer solution was prepared by mixing of freshly prepared two different solutions:- Solution **A** and Solution **B**.

Solution **A:**-Prepared by dissolving 6 g of monobasic sodium phosphate (NaH_2PO_4) in 250 ml of de-ionized water.

Solution **B:**-Prepared by dissolving 7.1 g of dibasic sodium phosphate (Na_2HPO_4) in 250 ml of de-ionized water.

Now Phosphate Buffer solution of different pH can be obtained by mixing different proportions of solution-**A** and solution-**B** (X ml of Solution-**A** + Y ml of solution-**B**, diluted to a total of 200 ml).

For pH 6.0 : (87.7 ml of solution-**A** + 12.3 ml of solution-**B**) + 100 ml of distilled H_2O

For pH 6.4 : (73.5ml of solution-A + 26.5 ml of solution-B) + 100ml of distilled H_2O

For pH 7.0 : (39.0 ml of solution-**A** + 61.0 ml of solution-**B**) + 100 ml of distilled H_2O

For pH 7.5 : (16.0 ml of solution-**A** + 84.0 ml of solution-**B**) + 100 ml of distilled H_2O

For pH 8.0 : (5.30 ml of solution-**A** + 94.7 ml of solution-**B**) + 100 ml of distilled H_2O

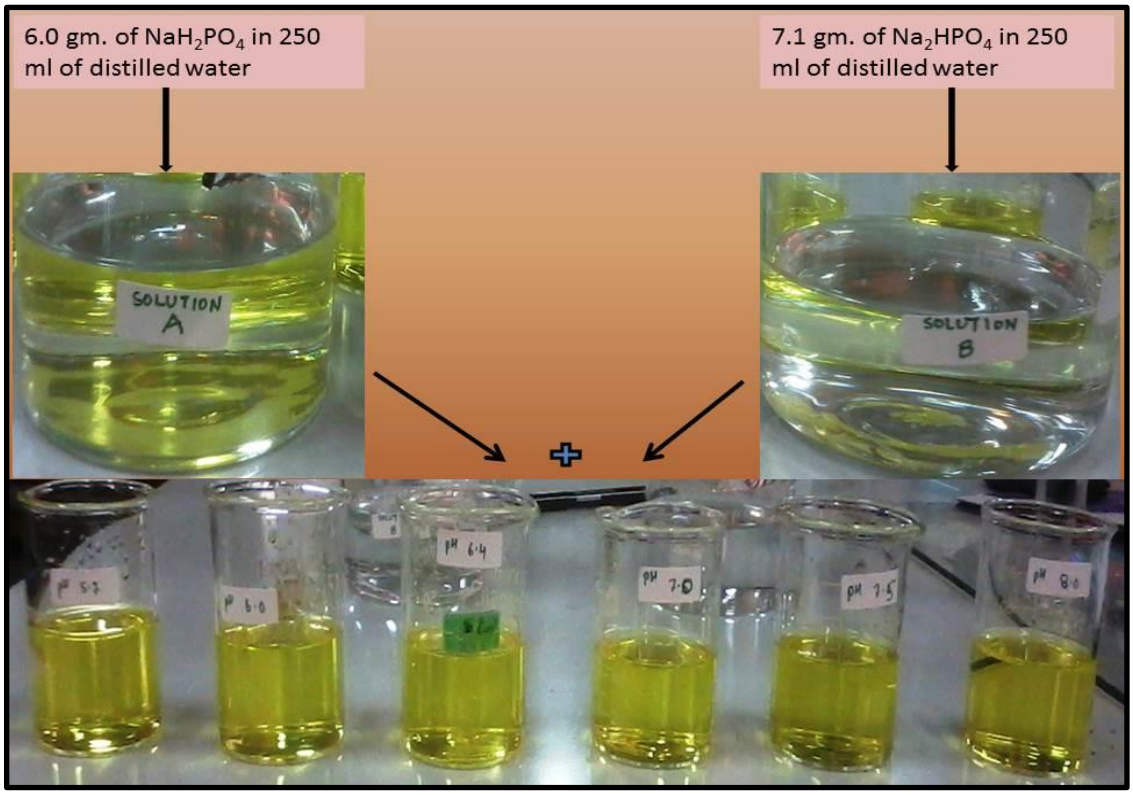

Figure 2.3: Schematic representation of preparation of PBS buffer solution of different pH (5.7 to 8).

2.3.4. Preparation of Phosphate Buffer Saline Solution

0.9% of NaCl (1.8 g) salt per 200 ml was added to phosphate buffer solution for making Phosphate buffer saline (PBS). Further, 422 mg of Potassium Ferrocyanide $\{K_4Fe(CN)_6\}$ and 329 mg of potassium ferricyanide $\{K_3Fe(CN)_6\}$ were added to the Phosphate Buffer Saline (PBS) where potassium ferro-Ferri cyanide are mediator solution and after that shaken well until it became yellowish clear solution. This resultant 5 mM phosphate buffer saline solution

was then stored in refrigerator for further use. **Figure: 2.4** shows schematic representation of preparation of phosphate buffer saline solution.

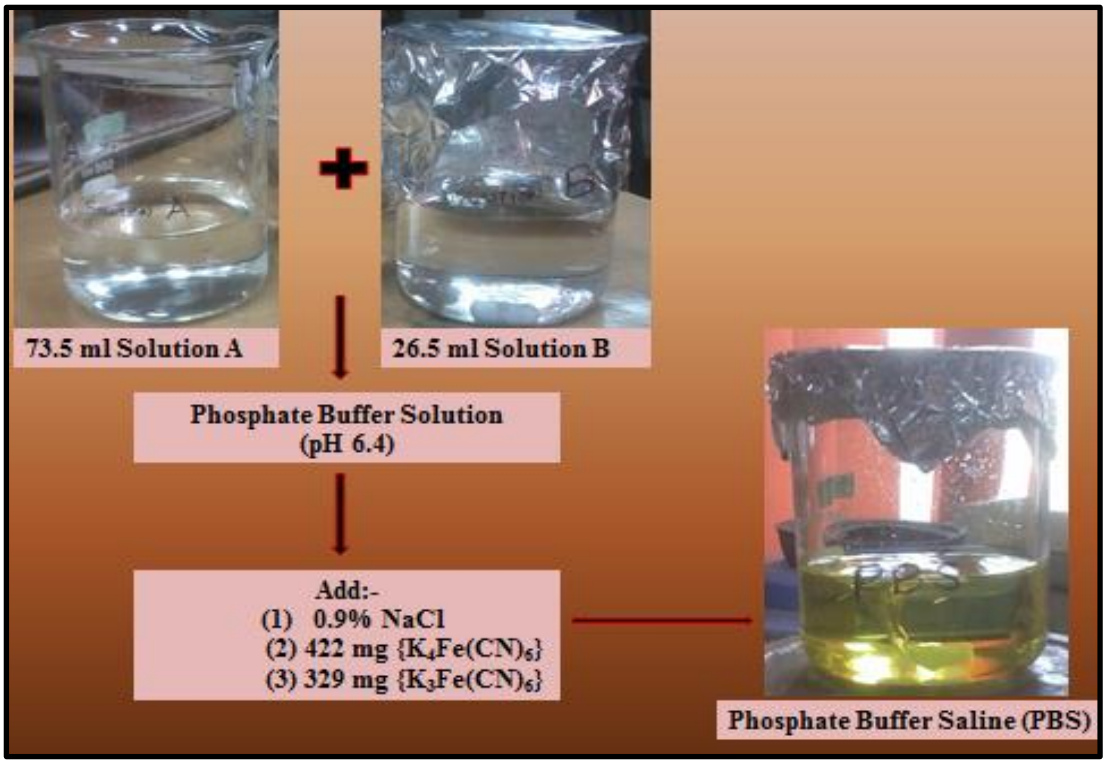

Figure: 2.4: Schematic representation of preparation of phosphate buffer saline solution.

2.3.5. Preparation of Chitosan Solution

For preparing 1%(v/v) chitosan solution initially 49 ml deionised water was mixed with 1 ml glacial acetic acid, then 0.5 g high molecular weight chitosan powder was added to it slowly with constant stirring over magnetic stirrer for 12 h at room temperature. This leads to formation of a highly viscous homogenous and clear solution. This solution was again filtered through synthetic cloth to remove any dissolved particles and then kept overnight to remove trapped air bubbles. The solution was further stored in air tight vial for future use.

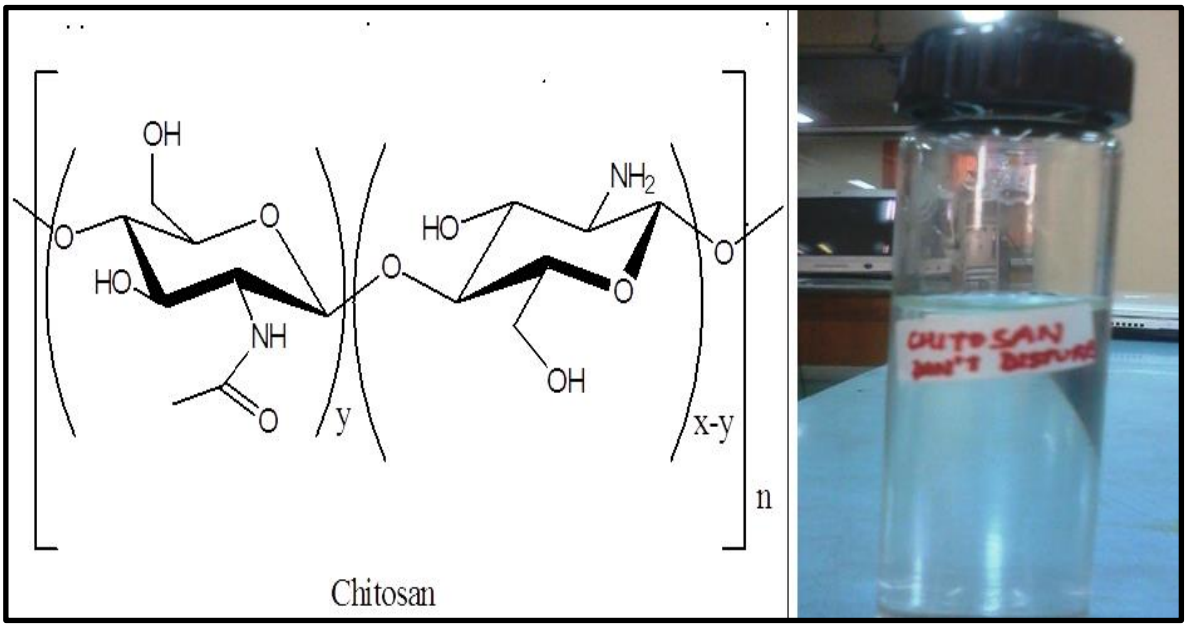

Figure: 2.5: Structure of Chitosan and Prepared chitosan solution in vial.

2.3.6. Preparation of V_2O_5-CHIT/ITO Nano-composite

30 mg of V_2O_5 nanoparticles were dispersed into 5 ml of CHIT solution with stirring at room by sonication for about 2 h to get a highly viscous CHIT solution with uniformly dispersed V_2O_5 nanoparticles. The Nano composite thin films were fabricated by uniformly spreading 10 µl solution of V_2O_5-CHIT Nano composite onto an ITO-coated glass surface (0.25 cm^2) and dried for 12 h at room temperature in a controlled environment and then washed with de-ionized water to remove any unbound particles. **Figure: 2.6** shows schematic representation of preparation of V_2O_5-CHIT nanocomposite.

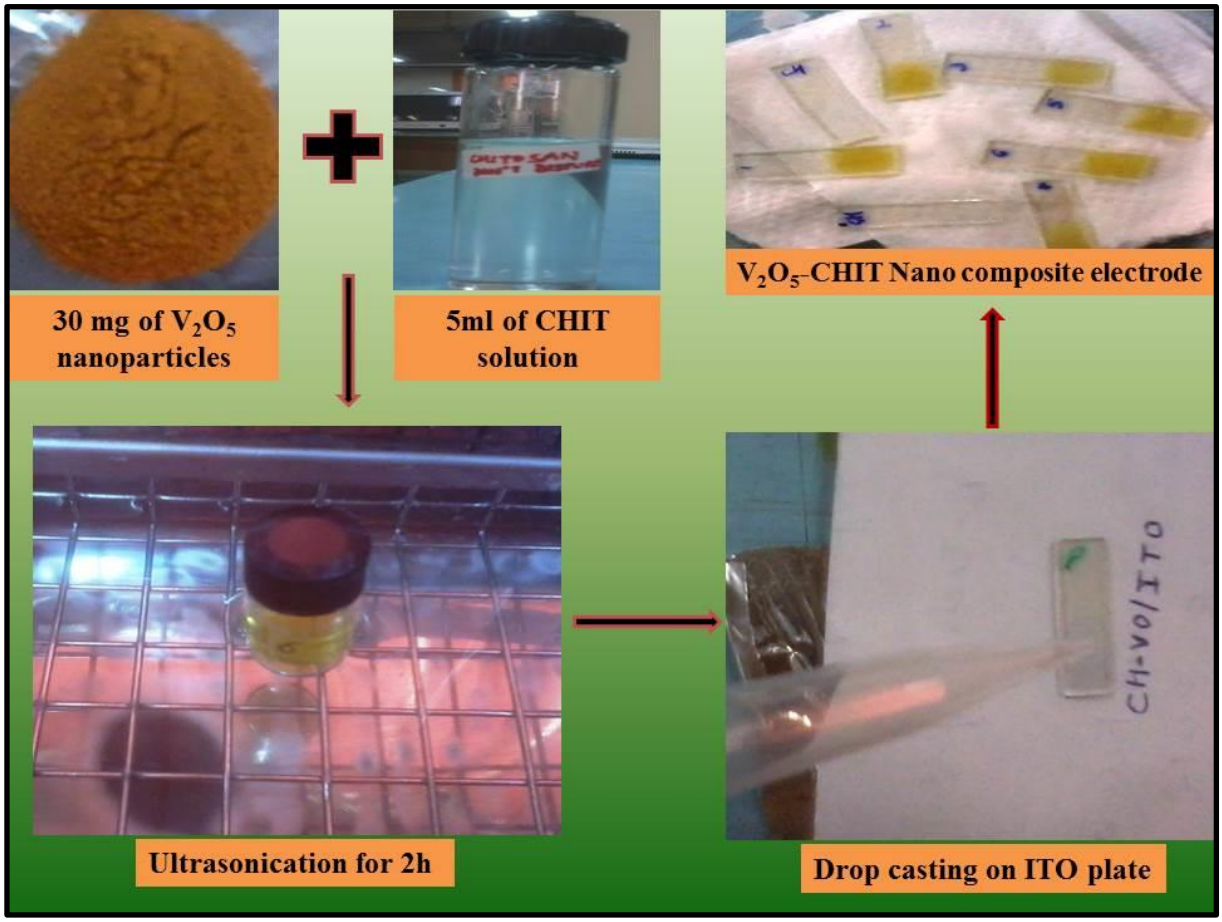

Figure: 2.6: Schematic representation of preparation of V_2O_5-CHIT Nano-composite

2.3.7. Preparation of stock solutions Of Hydrazine

Hydrazine solution (M_w = 50.06) of 20.58 M was taken. Then the solution of hydrazine of different concentration from 2 to 22 mM (2, 5, 8, 12, 15, 20 and 22 mM) was prepared by serial dilution with de-ionised water. **Figure: 2.7** show hydrazine stock solution preparation of various concentrations (2 to 22 mM).

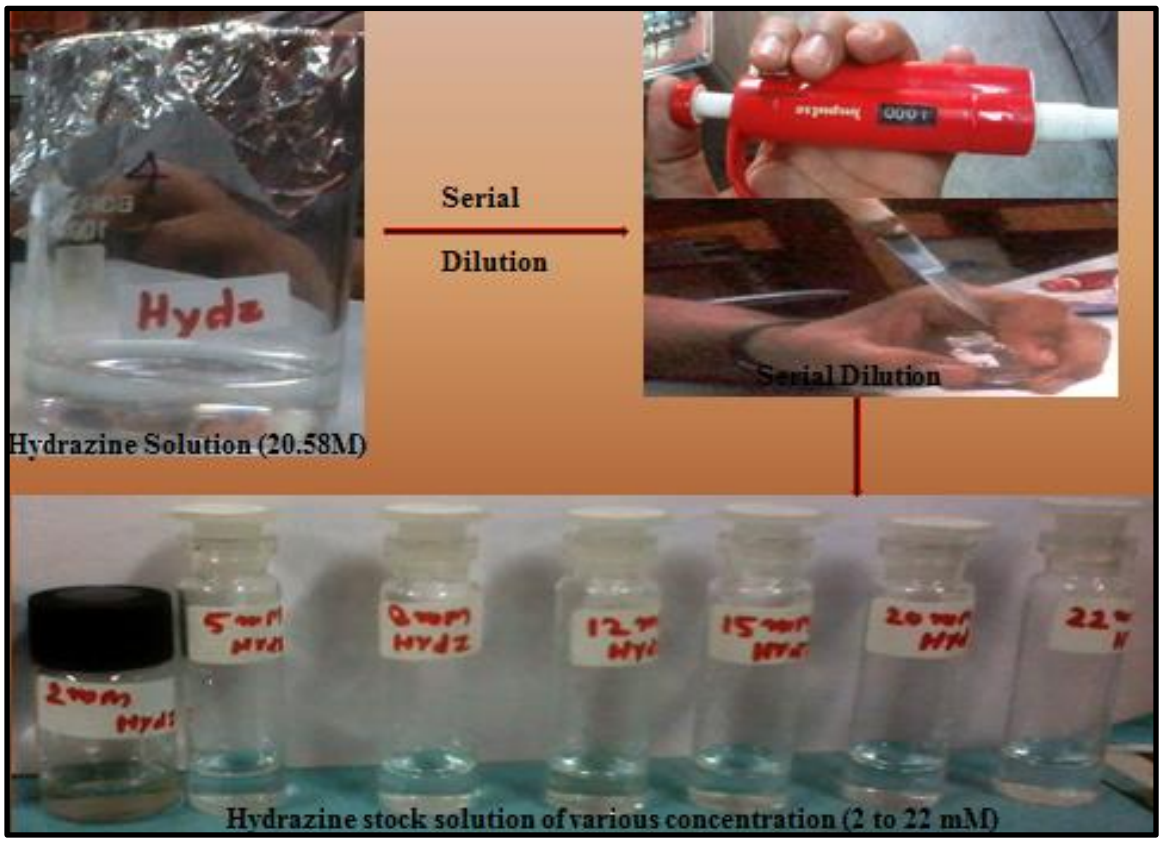

Figure: 2.7: Hydrazine stock solution preparation of various concentrations (2 to 22 mM)

2.3.8. Preparation of Electrode

2.3.8.1. Preparation of V_2O_5 films by Electrophoretic Deposition (EPD) Technique

Nanostructured V_2O_5 was deposited onto hydrolysed ITO (0.25 cm^2) coated plates by electrophoretic deposited technique. The calculated amount (10 mg) of V_2O_5 nanoparticles was uniformly dispersed in 10 ml of distilled water by ultra-sonication. This prepared suspension solution consists of positively charged V_2O_5 nanoparticles. Since ITO (0.25 cm^2) plates were hydrolysed, -OH group would be present on its surface. Thus ITO plate was made cathode and platinum was made anode and cathodic electrophoretic deposition was carried out. It has been found that optimized condition for electrophoretic deposition of V_2O_5 nanoparticles onto ITO plates is 25 V for 15 s. During the process positively charged nanoparticles V_2O_5 nanoparticles were attracted with -OH group

present on ITO surface. Thus nV_2O_5 is deposited onto ITO plate. This nV_2O_5 film is washed with deionized water followed by ethanol to remove any unbound particles.

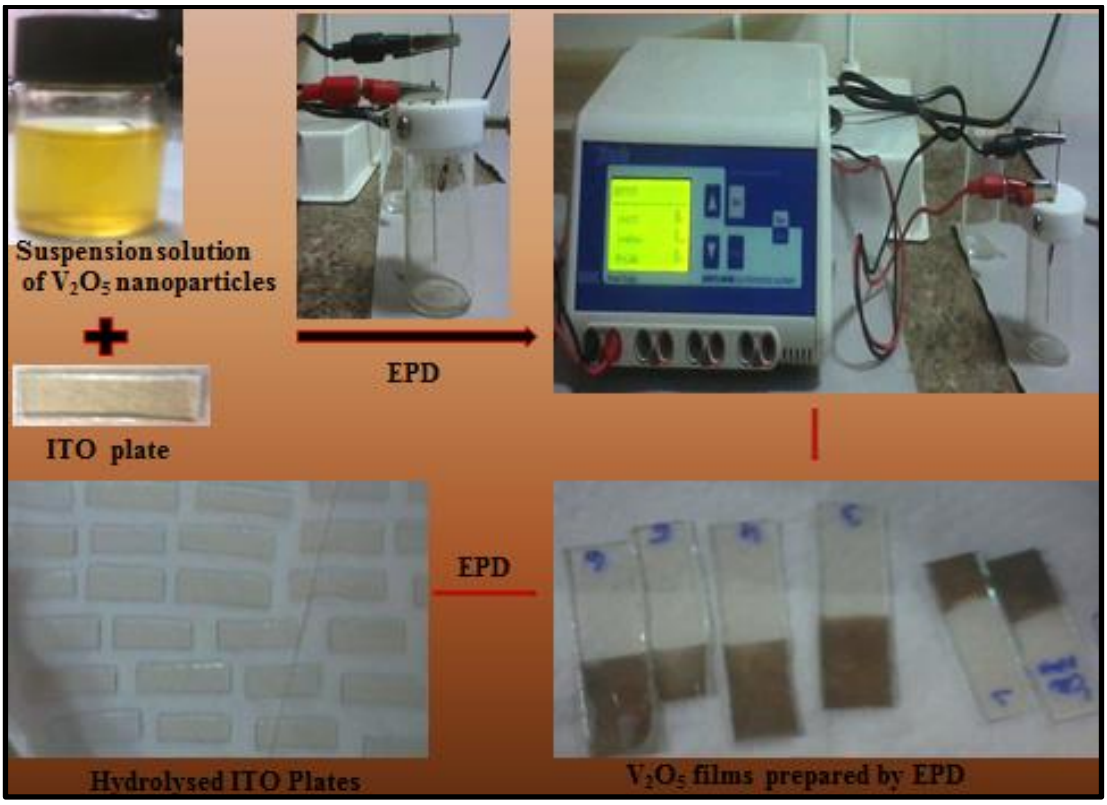

Figure: 2.8: EPD of V_2O_5 nanoaparticles on ITO plate.

2.3.8.2. Preparation of V_2O_5-CHIT/ITO electrode

The Nano composite thin films were fabricated by uniformly spreading 10 µl solution of V_2O_5-CHIT Nano composite onto an ITO-coated glass surface (0.25 cm^2) by drop casting method and dried for 12 h at room temperature in a controlled environment and then washed with de-ionized water to remove any unbound particles. **Figure: 2.9:** Shows schematic representation of fabrication of V_2O_5-CHIT/ITO electrode.

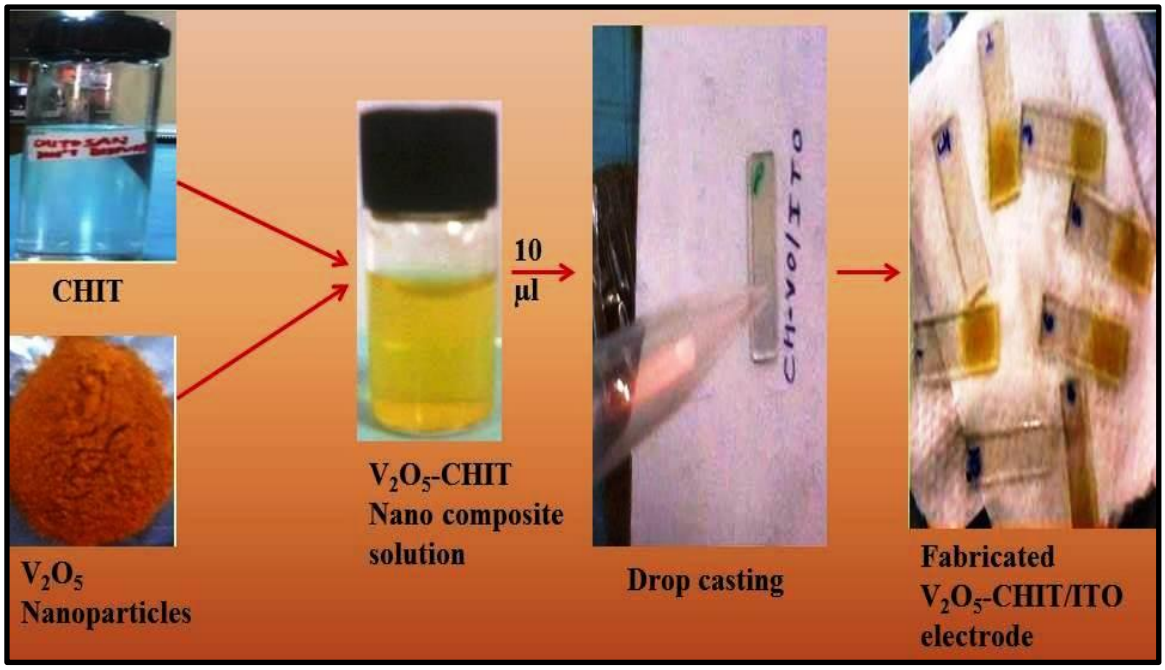

Figure: 2.9: Schematic representation of fabrication of V_2O_5-CHIT/ITO electrode.

2.3.9. Antibacterial activity assay

2.3.9.1. Preparation of Nutrient Agar Media

Ingredients	**g/ l**
Peptone	5.000
Beef Extract	3.000
Agar	15.000

Preparation

28gm nutrient agar powder was suspended in 1000ml of distilled water. This was heated to boiling to dissolve the medium completely. Put this now in autoclave vessel to sterilize it at 15 psi pressure (121 C) for 15 minutes. After sterilization open the valves of autoclave and take out the media and pour in petri plates under laminar air flow.

The antibacterial activity of the synthesized V_2O_5 nanoparticles, CHIT, and the V_2O_5-CHIT nanocomposite was evaluated by swabbing method against *B. cereus* and *P. aeruginosa*. First of all, nutrient agar media was prepared in the autoclave at 121°C at 15 psi. After release of pressure from the autoclave, the media was poured aseptically into the petri plates in laminar

air flow. The plates were allowed to cool down inside the laminar air flow so as to solidify the agar. After that bacterial colonies were picked from the sub cultured bacterial plates with the help of autoclaved cotton swabs. The cotton swab was dipped into autoclaved normal saline solution (0.9% NaCl solution) and then used to pick the bacterial colony. The swab was rubbed into the respective agar plate thoroughly at an angle of 360°. The agar plates were kept still for 10 min so that the bacterial culture gets little absorbed into the media. Then the wells were created in the swabbed agar plate for 4 samples using autoclaved wire loop. 30-40 µl samples were added into the respective wells in desired concentrations. Four different samples i.e. V_2O_5 nanoparticles, CHIT, V_2O_5-CHIT nanocomposite and water as control, were loaded in respective wells of two different bacterial plates, i.e., Gram positive and Gram negative. Now, both the bacterial plates with loaded wells were incubated at 37 °C +/- 2 °C for 24 h in BOD incubator. Next day the respective value of the inhibition zones were collected.

2.4. Characterization

The various characterization techniques and instruments used in this study are:-

2.4.1. Instruments used

Nanoparticles are the intermediate state of atoms and bulk. So they carry some unique structure and properties which are different from the bulk. Therefore it is seen that from a few decades nanomaterials are of great interest for the researchers toward its application in electrocatalytic applications. In order to establish the interrelationship between the structure and properties, it is very much required to know the physical as well as chemical structure as well as properties of the material. For this purpose, a lot of sophisticated instruments are available which can give all detailed information about the nanocrystalline material and its composites. These include Transmission Electron Microscope (TEM), Scanning Electron Microscope (SEM), Atomic Force Microscope (AFM), X-Ray diffraction (XRD) techniques, Fourier Transform Infra-Red spectrometry (FTIR), UV-visible (UV-Vis) Spectrometer, Cyclic Voltammetry (CV), Differential Pulse Voltammetry (DPV) etc. Some of these instruments are elucidated below:

2.4.1.1 X-ray diffraction (XRD) studies

X-ray diffraction (XRD) is one of the most powerful techniques for qualitative and quantitative analysis of crystalline compounds. The technique provides information which includes types and nature of crystalline phases present, structural make-up of phases, degree of crystallinity, amount of amorphous content, micro-stain and size [39] and orientation of crystallites. When a material (sample) is irradiated with a parallel beam of monochromatic X-rays, the atomic lattice of the sample acts as a three dimensional diffraction grating causing the X-ray beam to be diffracted to specific angles. The diffraction pattern, that includes position (angles) and the intensity of the diffracted beam, provides several information about the samples and are discussed below:

- Angles are used to calculate the interplanar atomic spacings (d-spacings). Because every crystalline will give a characteristic pattern and can act as a unique 'fingerprint', the position (d) and intensity (I) information are used to identify the type of material by comparing them with patterns over 80,000 data entries in the International Powder Diffraction File (PDF) database, complied by the Joint Committee for powder Diffraction Standards (JCPDS). By this method, identification of any crystalline compounds, even in a complex sample can be made.

- The position (d) of the diffracted peaks also provides information about how the atoms are arranged within the crystalline compounds (unit cell size or lattice parameter). The intensity information is used to assess the type and nature of atoms. Determination of lattice parameter helps understand to the extent of solid solution (complete or partial substitution of one element for another, as in some alloys) in a sample.

- Width of the diffracted peak is used to determine crystallite size and micro-stain in the sample.

- The 'd' and 'I' from a phase can also be used quantitatively estimate the amount of that phase in a multi-component mixture.

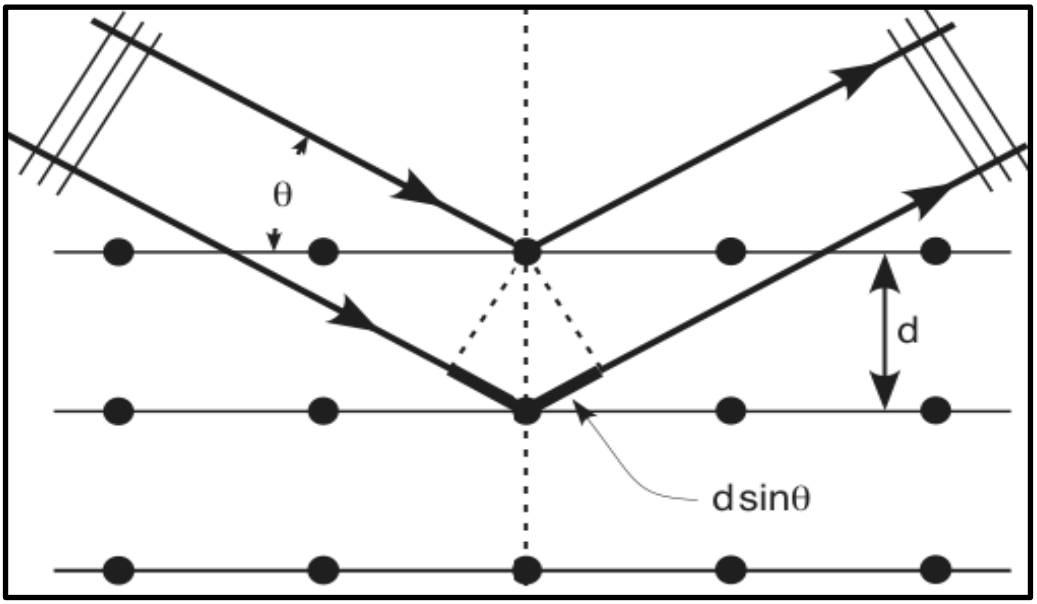

Figure: 2.10: Basic principle of Bragg's law

The X-ray diffraction experiment requires an X-ray source, the sample under investigation and a detector to pick up the diffracted X-rays. The X-ray radiation most commonly used is that emitted by copper, whose characteristic wavelength for the K radiation is 1.5418 Å. When the incident beam strikes a powder sample, diffraction occurs in every possible orientation of 2θ. The diffracted beam may be detected by using a moveable detector such as a Geiger counter, which is connected to a chart recorder. In normal use, the counter is set to scan over a range of 2θ values at a constant angular velocity. Routinely, a 2θ range of 5° to 70° is sufficient to cover the most useful part of the powder pattern [40]. The scanning speed of the counter is usually 2θ of 2° min^{-1} and therefore, about 30 minutes are needed to obtain a trace.

In this project we have used Bruker D8 Advance Diffractometer with Ni-filtered Cu K_α radiation (Voltage- 30 kV, 35 mA), at IIT, New Delhi.

2.4.1.1.1 .Theoretical formulation:

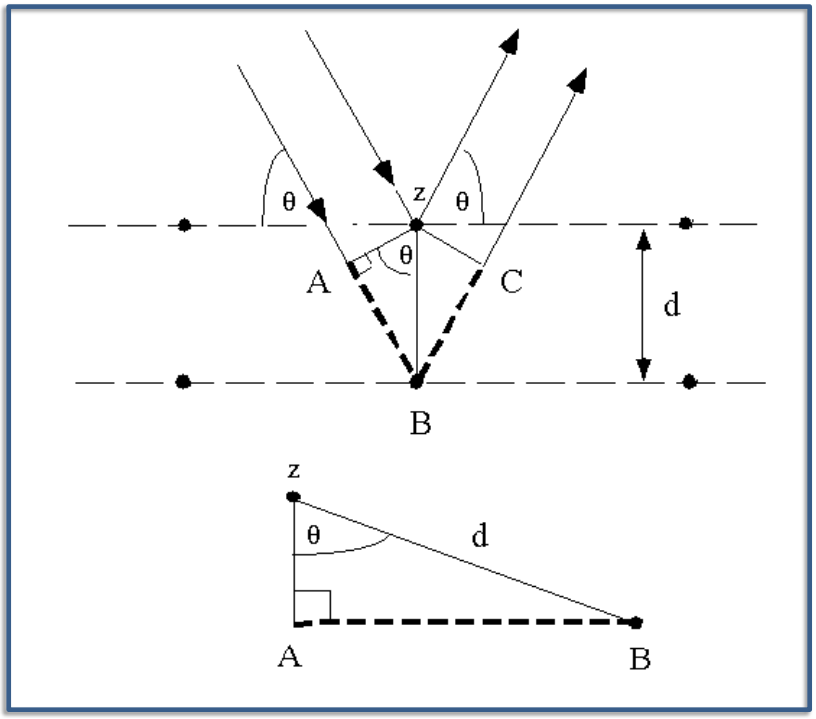

Figure: 2.11: Reflection of X-rays from two planes of atoms in a solid.

The path difference between two waves:

$$2\lambda = 2d\sin\theta \qquad \text{…….. (2.1)}$$

For constructive interference between these waves, the path difference must be an integral number of wavelengths:

$$n\lambda = 2x \qquad \text{……. (2.2)}$$

This leads to the Braggs equation:

$$\mathbf{n\lambda = 2d\sin\theta} \qquad \text{……. . (2.3)}$$

The basic difference between coherent scattering from planes of atoms of spacing ‘d’ in a single crystal and a random powder is that diffracted beams from individual crystallites in the latter generate cones with semi-angle 2θ, where

$$2\theta = \sin^{-1}(\lambda/2d) \qquad \text{……..... (2.4)}$$

Where λ being the wavelength of the radiation used and θ being the Bragg's angle. This is the basis and justification for the Bragg reflection analogy.

If the physical origin of peak broadening is due to the small grain size alone, the relationship between grain size (D) and FWHM (δ=θ) in radians is given by

$$D = 0.94\,\lambda / \delta 2\theta \cos\theta \quad \ldots\ldots\ldots\ldots\ldots\ldots \quad (2.5)$$

Where, λ is wavelength and θ is diffraction angle. In this case, the obtained grain size is volume averaged in the direction perpendicular to the plane of diffraction.

2.4.1.2 Fourier Transform Infrared Spectroscopy (FTIR)

Fourier transform infrared spectroscopy (FTIR) is a technique which is used to obtain an infrared spectrum of absorption, emission, photoconductivity or Raman scattering of a solid, liquid or gas [41]. An FTIR spectrometer simultaneously collects spectral data in a wide spectral range. The term Fourier transform infrared spectroscopy originates from the fact that a Fourier transform (a mathematical algorithm) is required to convert the raw data into the actual spectrum. In infrared spectroscopy, IR radiation is passed through a sample. Some of the infrared radiation is absorbed by the sample and some of it is passed through (transmitted). The resulting spectrum represents the molecular absorption and transmission, creating a molecular fingerprint of the sample. Like a fingerprint no two unique molecular structures produce the same infrared spectrum. This makes infrared spectroscopy useful for several types of analysis. FT-IR can identify unknown materials; determine the quality or consistency of a sample and the amount of components in a mixture.

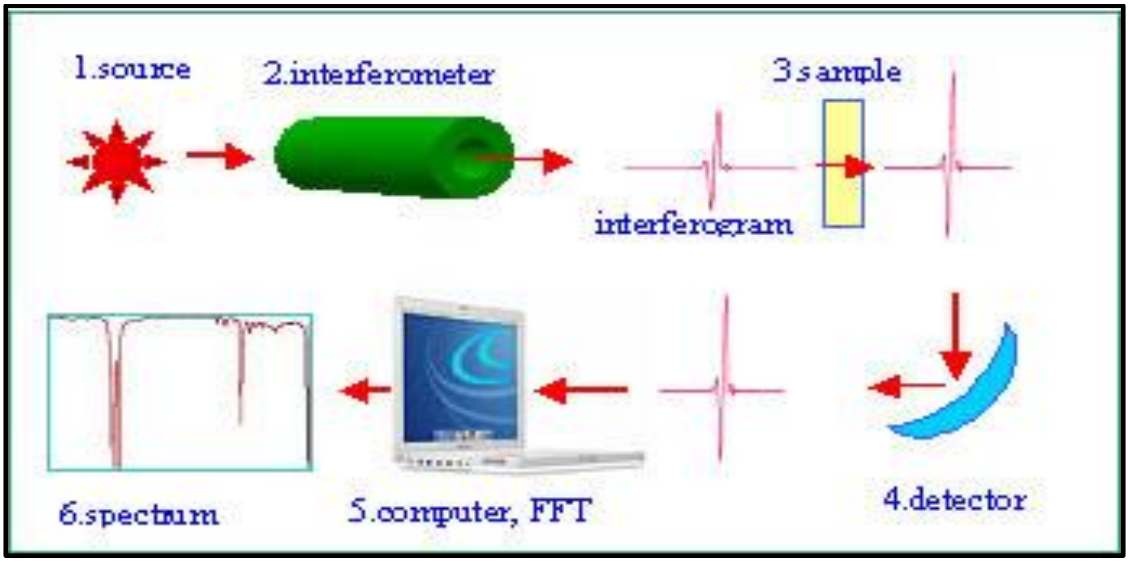

Figure: 2.12: Various components of Fourier Transform Infrared System.

2.4.1.2.1 Basic principle of FTIR

There are two kinds of fundamental vibrations for molecules: stretching, in which the distance between two atoms increases or decreases, but the atoms remain in the same bond axis, and bending (or deformation), in which the position of the atom changes relative to the original bond axis. The various stretching and bending vibrations of a bond occur at certain quantized frequencies. When infrared light of that same frequency is incident on the molecule, energy is absorbed and the amplitude of that vibration is increased. When the molecule reverts from the excited state to the original ground state, the absorbed energy is released as heat [42].

The most powerful function of infrared spectroscopy is establishing conclusively the identity of two samples that have identical spectra when determined in the same medium. The region 1430-910 cm^{-1} contains many absorptions caused by bending vibrations as well as absorptions caused by C-C, C-O and C-N stretching vibrations. As there are many more bending vibrations in a molecule than stretching vibrations, this region of the spectrum is particularly rich in absorption bands and shoulders. For this reason, it is frequently called the fingerprint region. Although similar molecules may show very similar spectra in the region 4000-1430 cm^{-1}, there will nearly always be discernible differences in the fingerprint region.

Infrared absorption spectra is obtained by placing the sample, in one beam of a double beam IR spectrophotometer and measuring the relative intensity of transmitted (and therefore absorbed) light energy versus wave number (or wave length). The peaks in the IR spectrum at different wave numbers indicate the presence of different identities with varying bond nature. The wave numbers for corresponding peaks in the plot are compared with the standard characteristic IR peaks of functional group, to reveal the exact bond nature and bond intensity levels.

In this project FT-IR studies were carried out by using Thermoscientific, Nicolet-380 spectrophotometer, at DTU, New Delhi.

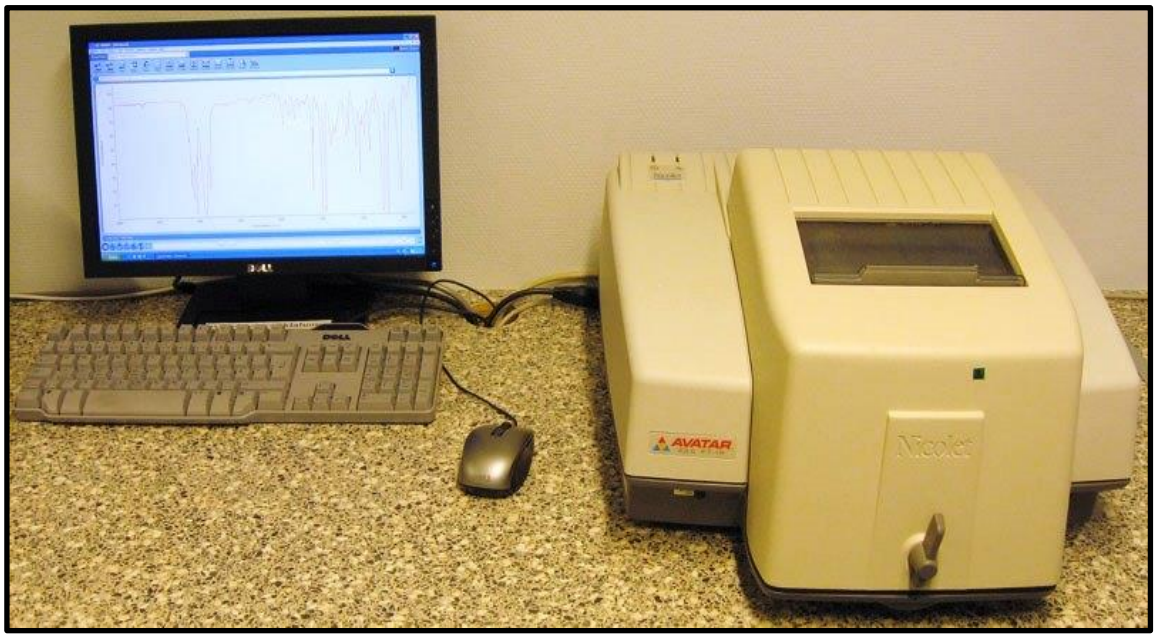

Figure: 2.13: FTIR spectrophotometer Thermoscientific, Nicolet-380 at DTU, Delhi.

2.4.1.3. Ultraviolet-Visible (UV-Vis) Spectroscopy

Ultraviolet–visible spectroscopy (UV-Vis) refers to absorption spectroscopy or reflectance spectroscopy in the ultraviolet-visible spectral region. This means it uses light in the visible and adjacent (near-UV and near-infrared (NIR)) ranges. The absorption or reflectance in the visible range directly affects the perceived colour of the chemicals involved. In this region of

the electromagnetic spectrum, molecules undergo electronic transitions. Ultraviolet (UV) and visible radiation compromise a small part of the electromagnetic spectrum, which include such other forms of radiation as radio, infrared (IR), cosmic, and X rays. The principle of UV Vis is that the molecules containing π-electrons or non-bonding electrons (n-electrons) can absorb the energy in the form of ultraviolet or visible light to excite these electrons to higher anti-bonding molecular orbitals. The more easily excited the electrons (i.e. lower energy gap between the HOMO and the LUMO), the longer the wavelength of light it can absorb.

In the practical sense, spectroscopy measures the absorption, emission or scattering of electromagnetic radiation by atoms or molecules. By such measurements, the type of atoms or molecules present in a sample, as well as a measure of their concentration or abundance, can be made to an astonishing degree of accuracy. When radiation interacts with matter, a number of processes can occur, including reflection, scattering, absorbance, fluorescence/phosphorescence (absorption and re-emission), and photochemical reaction (absorbance and bond breaking). In general, when measuring UV-visible spectra, we want only absorbance to occur. Because light is a form of energy, absorption of light by matter causes the energy content of the molecules (or atoms) to increase. The amount of energy a molecule possesses in each form is not a continuum but a series of discrete levels or states.

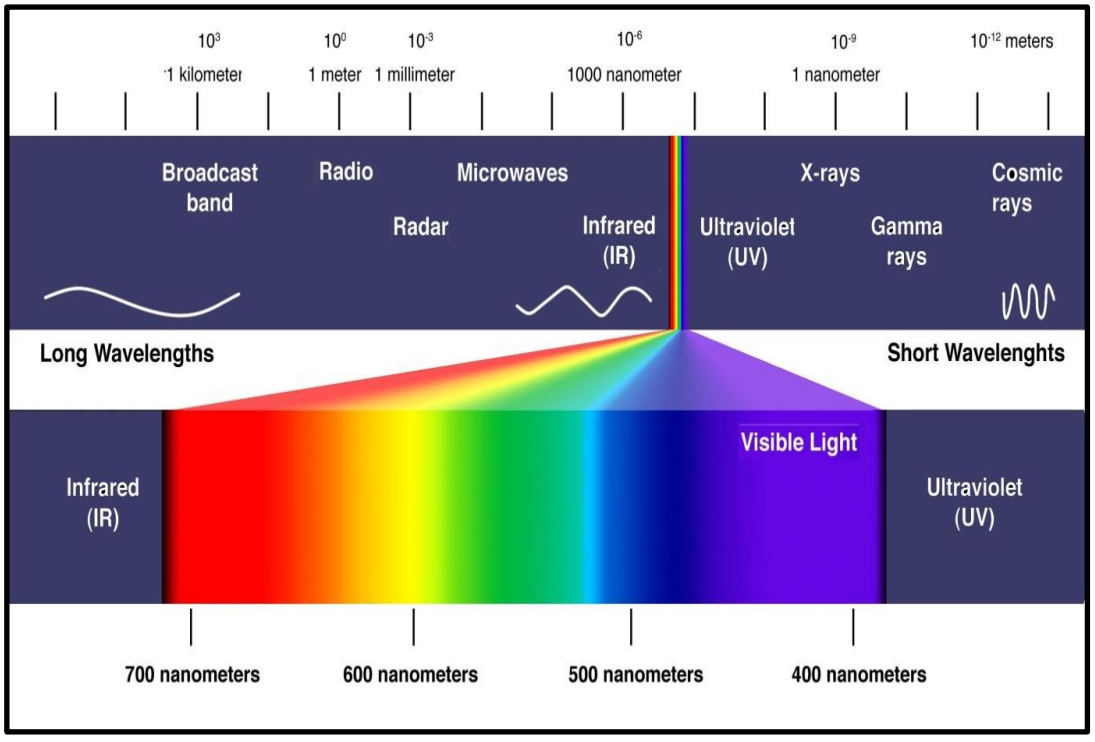

Figure: 2.14: Range of electromagnetic spectrum

In some molecules and atoms, photons of UV and visible light have enough energy to cause transitions between the different electronic energy levels. The wavelength of light absorbed is that having the energy required to move an electron from lower energy level to a higher energy level. When ultraviolet or visible light strike atoms or molecules they can either bounce off or cause electrons to jump between energy levels. Absorption of ultraviolet or visible light electromagnetic radiation causes electron to moves from lower energy levels to a higher energy levels. This type of transition is called electronic transition.

Ultraviolet-visible absorption spectroscopy measures the absorption of ultraviolet or visible light. Because the spectrum of an atom or a molecule depends on its electron energy levels, UV-Vis absorption spectra are useful for identifying unknown substances. In UV spectroscopy, a beam of light is split into a sample and reference beams. As its name implies, the sample beam is allowed to pass through the target sample. Alternatively, the reference beam passes through the control solvent or a portion of the solvent that does not contain the actual target. Once the light passes through the target of interest, it is measured by a special meter termed a spectrometer designed to compare the difference in the transmissions of the sample and reference beams. Double beams UV spectroscopy instruments allow scientists to measure transmissions through the target sample and solvent. The wavelength of ultraviolet or visible light absorbed by a substance results in a unique ultraviolet visible spectroscopic signature for each substance.

The amount or percentage of a substance present is often of great importance. Chemists doing UV-Vis spectroscopy use Beer's Law (Beer-Lambert Law) to determine the relationship between absorbance and concentration of a substance in a solution. Beer's Law states that absorbance is directly proportional to the path length, b, and the concentration, c, of the absorbing species.

$$A = \varepsilon bc \qquad \ldots\ldots\ldots\ldots\ldots\ldots \quad (2.6)$$

Where ε is a constant of proportionality called the absorptivity. In general there is a linear relationship between the increasing amount of substance and a decreasing percentage or light transmitted through the target sample. If there is more of a substance to absorb the UV light less light will pass through the detector. Correspondingly, less absorption by the target sample allows increased transmission light through the sample.

In this project UV-Vis spectroscopy studies have been carried out by PerkinElmer, Lamda 950 UV/VIS/NIR spectrometer at DTU, New Delhi.

Figure: 2.15. Perkin Elmer, Lambda 950 UV-Vis Spectrophotometer at DTU, Delhi

2.4.1.4. Scanning Electron Microscopy (SEM)

The scanning electron microscope (SEM) is a type of electron microscope that images the sample surface by scanning it with a high-energy beam of electrons in a raster scan pattern wherein, electrons interact with the atoms that make up the sample producing signals that contain information about the sample's surface topography, composition and other properties such as electrical conductivity. This is an extremely useful tool for the study of the surface morphology because it offers a better resolution than the optical microscope. It uses electron emitted from tungsten or lanthanum hexaborate thermionic emitters for the visualization of surface of the sample. The filament is heated resistively by a current to achieve a temperature between 2000-2700 K. This results in an emission of thermionic electrons and accelerates them to energy in the range 0.1 - 30 keV towards the sample. A series of lenses focus the electron beam on the sample where it interacts with the sample to a depth of approximately 1 mA [43].

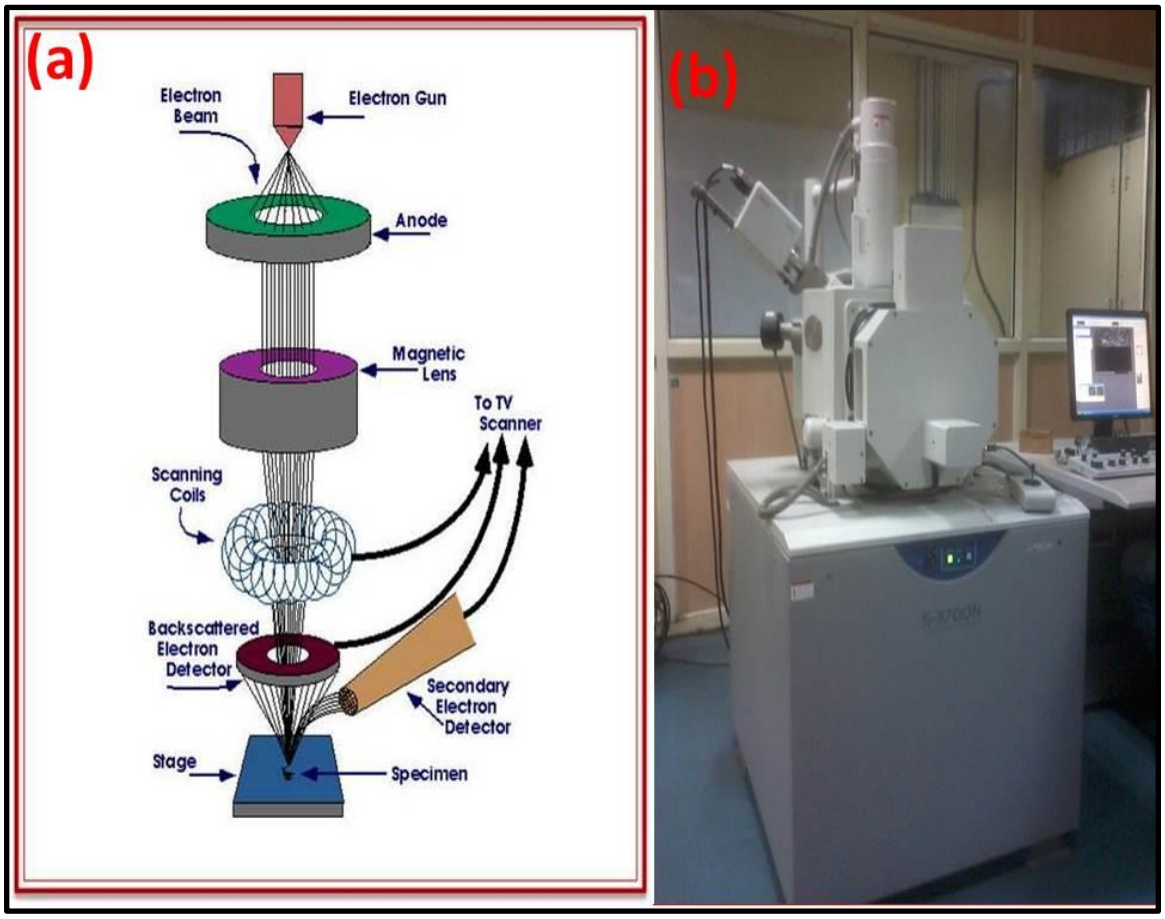

Figure: 2.16: Shows the (a) component of a scanning electron microscope and (b) SEM HITACHI, Model No.S-3700N at DTU, Delhi

When electron beam impinges on the specimen, many type of signals are generated and any of these can be displayed as an image. The two signals most often used to generate SEM image are secondary electron (SE) and backscattered electron (BSE). Most of the electrons are scattered at large angle ($0\text{-}180^0$) when they interact with positively charged nucleus. These scattered electrons usually called BSE are used for SEM imaging. Some electron are scattered in-elastically due to the loss in kinetic energy upon their interaction with orbital shell electron. Incident electron may knock off loosely bound conduction electron out of the sample. These SE and along with BSE are widely used for SEM topographical imaging. Both SE and BSE signal are collected when a positive voltage is applied to the collector screen in front of the detector. When a negative signal is capture and the low energy SE gets repelled. Electrons captured by the scintillator/photomultiplier are then amplified and used to form an image in the SEM. The limitations of SEM are that the sample must be solid and stable in vacuum on the order of 10^{-5} to 10^{-6} torr. However the SEM image relies on surface processes

rather than transmission it is able to image bulk samples up to several centimeters in size (depending on instrument design) and has a much greater depth of view, and so can produce images that are a good representation of the 3D structure of the sample.

In this project SEM studies have been carried out by using HITACHI, Model No.S-3700N Scanning electron microscope, at DTU, New Delhi.

2.4.1.5. Energy-dispersive X-ray microanalysis (EDX)

Energy-dispersive X-ray microanalysis (EDX) is complementary to SEM. It is also used in SEM for the elemental analysis of the specimen. Here, X-ray spectrometer converts X-ray photon into an electrical pulse, which is measured by a multi-channel analyser. The analyser records increments in corresponding "energy slot" and shows on a monitor display. The location of the slot is proportional to energy of the X-ray photon entering the detector. The display is a histogram of the X-ray energy received by the detector, with individual peaks, the heights of which are proportional to the amount of a particular element in the specimen being analyzed. The basic steps involved in SEM sample preparation include surface cleaning, stabilizing the sample with a fixative, rinsing, dehydrating, drying, mounting the specimen on a metal holder, and coating the sample with a layer of a material that is electrically conductive.

2.4.1.6. Atomic Force Microscopy (AFM)

Atomic force microscopy (AFM) is a very high-resolution type of scanning probe microscopy, with demonstrated resolution on the order of fractions of a nanometre, more than 1000 times better than the optical diffraction limit. AFM provides a 3D profile of the surface on a nanoscale, by measuring forces between a sharp probe (<10nm) and surface at very short distance (0.2-10 nm probe-sample separation). The AFM consists of a flexible cantilever with a sharp tip (probe) at its end as shown in Figure 2.17 that is used to scan the specimen surface. The AFM tip gently touches the surface and records the small force between the probe and the surface. The cantilever is typically silicon or silicon nitride with a tip radius of curvature on the order of nanometers. When the tip is brought into proximity of a sample surface, forces between the tip and the sample lead to a deflection of the cantilever according to Hooke's law. Depending on the situation, forces that are measured in AFM include mechanical contact force, van-der-Waal forces, capillary forces, chemical bonding,

electrostatic forces, magnetic forces etc. Typically, the deflection is measured using a laser spot reflected from the top surface of the cantilever into an array of photodiodes. Other methods that are used include optical interferometry, capacitive sensing or piezo-resistive AFM cantilevers. These cantilevers are fabricated with piezo-resistive elements that act as a strain gauge. Using a Wheatstone bridge, strain in the AFM cantilever due to deflection can be measured, but this method is not as sensitive as laser deflection or interferometry.

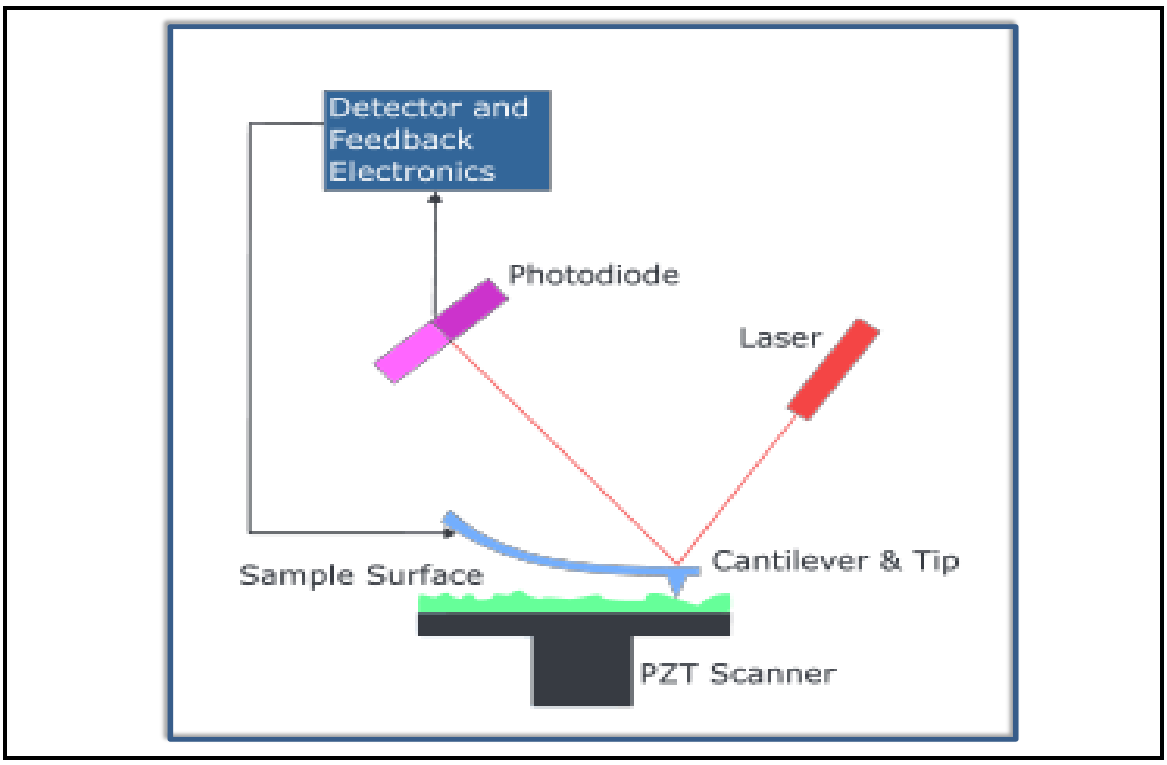

Figure: 2.17: Block diagram of atomic force microscope

If the tip was scanned at a constant height, a risk would exist that the tip collides with the surface, causing damage. Hence, in most cases a feedback mechanism is employed to adjust the tip-to-sample distance to maintain a constant force between the tip and the sample. Traditionally, the sample is mounted on a piezoelectric tube that can move the sample in the *z* direction for maintaining a constant force, and the *x* and *y* directions for scanning the sample. Alternatively a 'tripod' configuration of three piezo crystals may be employed, with each responsible for scanning in the x, y and z directions. This eliminates some of the distortion effects seen with a tube scanner. In newer designs, the tip is mounted on a vertical

piezo-scanner while the sample is being scanned in x and y using another piezo block. The resulting map of the area $z = f(x,y)$ represents the topography of the sample.

The AFM can be operated in a number of modes, depending on the application. In general, possible imaging modes are divided into static (also called contact) modes and a variety of dynamic (non-contact or "tapping") modes where the cantilever is vibrated.

In this project AFM studies have been carried out by using Park Systems, XE-100 Atomic force microscope, at DTU. New Delhi.

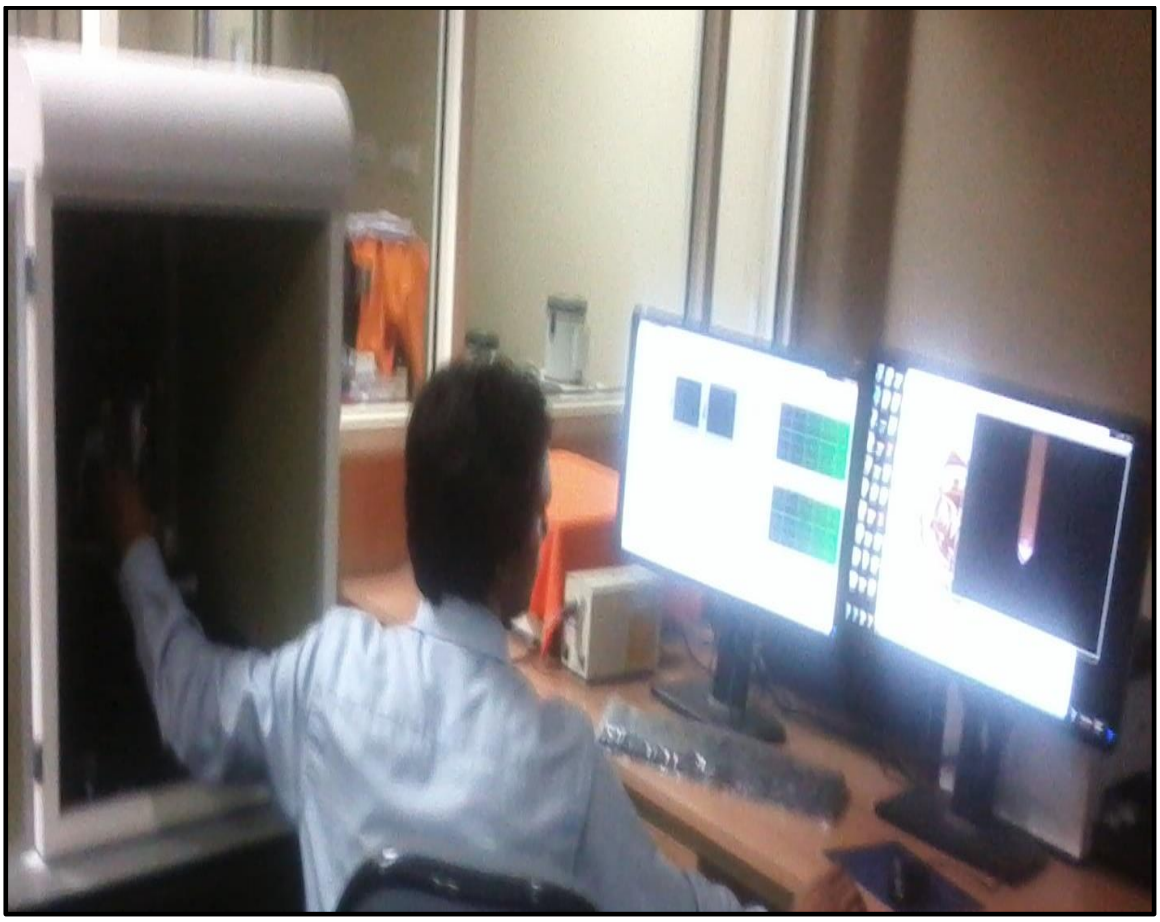

Figure: 2.18: Atomic force microscope Model No. XE-100, Park Systems, at DTU, Delhi

2.4.1.7. Photoluminescence spectroscopy

Photoluminescence study is a contactless, non-destructive method for probing the electronic structure materials. Light is directed onto a sample, where it is absorbed and imparts excess energy into the material in a process called photo-excitation. One way this excess energy can be dissipated by the sample is though the emission of light, or luminescence. In the case of photo-excitation, this luminescence is called photoluminescence. PL spectroscopy provides a good method for the study of luminescent properties of a fluorophore. There are many forms of PL, one is resonant radiation. In this method, a photon of a specific wavelength is absorbed and an equivalent photon is immediately emitted out, hence no significant energy transitions are involved between absorption and emission. The process is usually of the order of 10 nanoseconds. In case of fluorescence, the chemical substrate undergoes energy transitions before coming back to its ground state by emitting photons; some of the absorbed energy is dissipated out so that the emitting electrons are of lower energy than the absorbed ones. This phenomenon has a shorter lifetime (10^{-8} to 10^{-4} s). Phosphorescence is a radiational transition, in which the absorbed energy undergoes intersystem crossing into a state with a different spin multiplicity. The lifetime of phosphorescence is usually from 10^{-4} - 10^{-2} s, much longer than that of Fluorescence.

The basic elements of a PL spectroscopy set-up consist in an optical source, a spectrophotometer and a detector. A typical PL set-up is shown in Figure 2.19. The excitation laser beam is focused on the sample with a lens of typically f = 20-30 cm focal length. The emitted light can be collected by a single lens (2f/2f geometry) or by two lenses F_1 and F_2. The advantage of this latter geometry is to allow the use of a short focal length for F_1 in order to improve the collection efficiency of the emitted light. Moreover, F_2 can be chosen in order to match the optical aperture of the spectrometer, avoiding unnecessary supplementary losses.

PL emission studies in this project have been carried out by using Fluorolog 3, made by Horiba, at DTU, New Delhi.

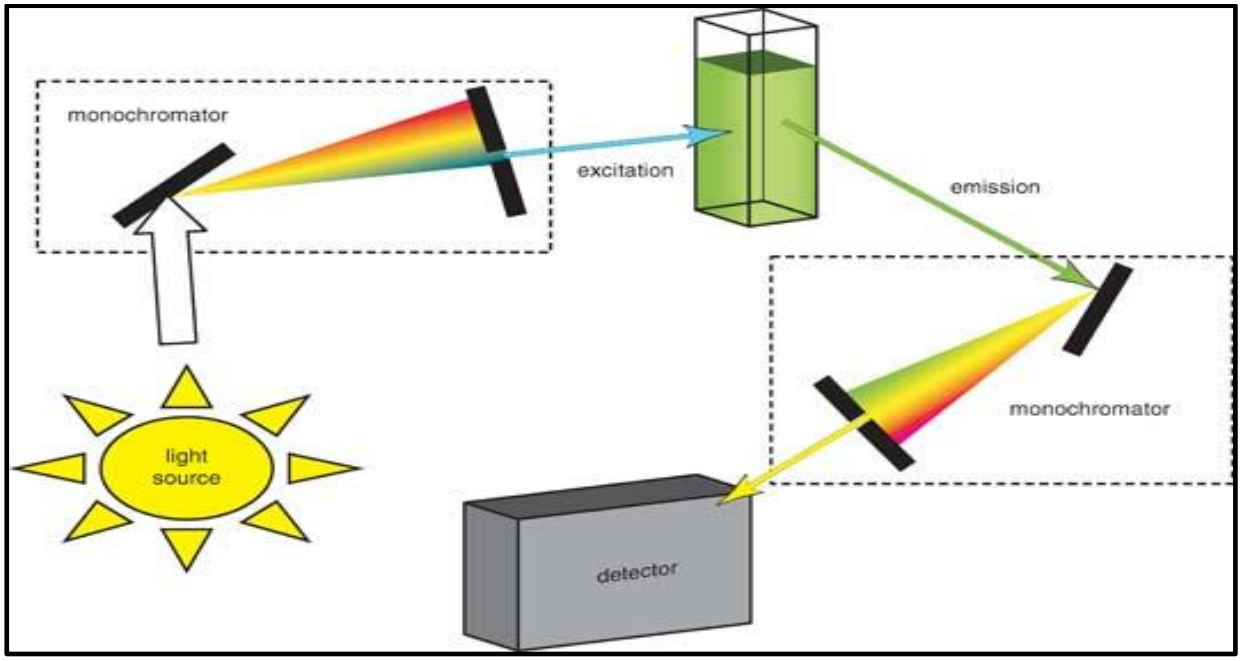

Figure: 2.19: Basic scheme of a photoluminescence experimental set up.

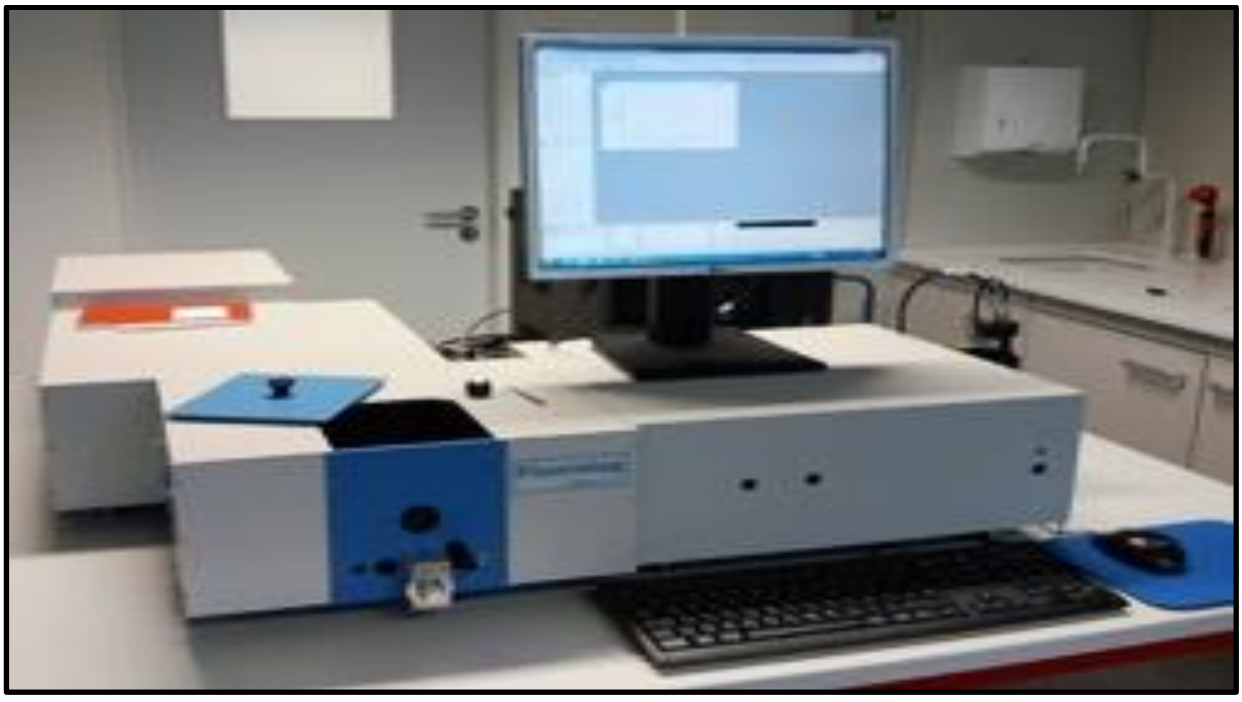

Figure 2.20: Photoluminescence Instrument, Fluorolog 3 made by Horiba.

2.4.1.8. Transmission Electron Microscopy (TEM)

Transmission Electron Microscopy (TEM) has the advantage over SEM that morphology, particle size and structure of the specimen can be viewed at very high magnifications at nanoscale level. In TEM, a thin solid specimen (< 200 nm) is bombarded in vacuum with a highly focused, mono-energetic beam of electrons. The high-resolution results from the smaller de Broglie wavelength associated with high-energy electron beam and its ability to focus the electron beam. For example, electrons having energy of 100 keV corresponds to a de Broglie wavelength of 3.7×10^{-3} nm. Generally, TEM operates with the electron beams having energy in the range of 20-200 keV. The spatial resolution is large for higher energy electron beam. The beam has sufficiently high energy to propagate through the specimen. The transmitted electron signals are magnified by a series of electromagnetic lenses. TEM offers two modes to study a desired specimen: image and diffraction. The image mode contrast must be induced in order to produce image for analysis. Many contrast-forming mechanisms exist and the interpretation of images is complicated due to the interplay of the different mechanisms. The most common imaging techniques in TEM are mass-thickness imaging, diffraction imaging, and phase contrast imaging. In the diffraction mode, the pattern of the diffracted electrons is obtained from the electron-illuminated sample. When the electron beam is incident on the sample, scattering events occur since all the illuminated parts of the sample act as scattering sources. Interference causes coherently scattered beams when Bragg's law is fulfilled. The coherently scattered beams are recorded as a "spot". This spot pattern of the diffracted electron beam from the selected sample area is called the selected area electron diffraction (SAED) pattern. It provides the information about the crystalline and crystal orientation. The diameter of the diffraction ring in SAED pattern is proportional to $(h^2 + k^2 + l^2)^2$ where (hkl) are the Miller indices of the planes corresponding to the ring, counting from the centre.

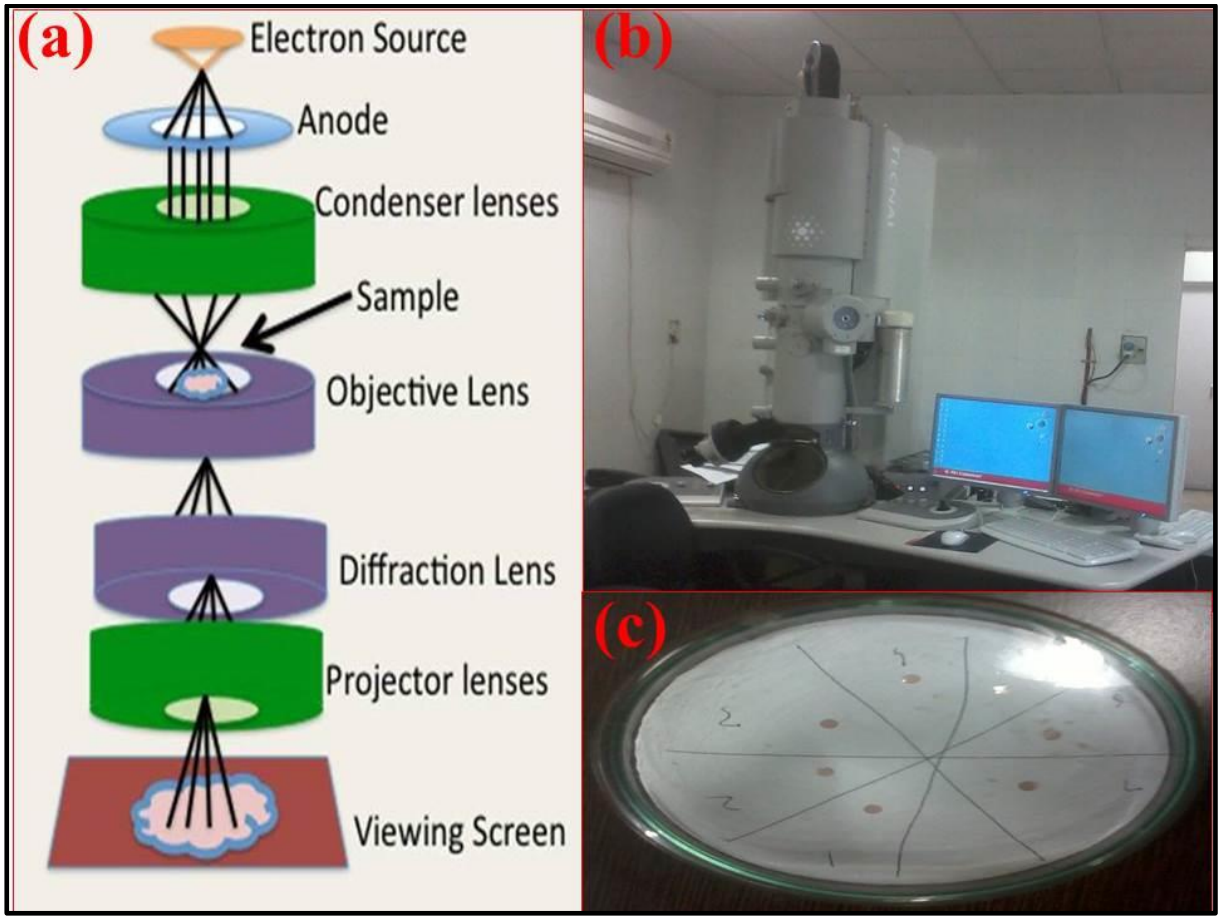

Figure: 2.21: Main components of (a) TEM (b) TEM machine at AIIMS, New Delhi (c) Copper grid dipped and dried with the naonoparticle sample.

A key requirement for TEM samples is the electron transparency, as a thick sample would cause too many interactions leaving no intensity in the transmitted beam. A thick sample also increases the risk that an electron is scattered on multiple occasions and the resulting image would be difficult to interpret. In the present work, TEM samples have been prepared by dispersing powder sample in acetonitrile and a small drop of that solution was casted onto the carbon coat copper grid.

In this project TEM studies have been carried out by using FEI Tecnai S Twin, at AIIMS, New Delhi.

2.4.1.9. Electrochemical Measurements

Electrochemistry is a branch of chemistry that studies chemical reactions which take place in a solution at the interface of an electron conductor (a metal or a semiconductor) and an ionic conductor (the electrolyte), and which involve electron transfer between the electrode and the electrolyte or species in solution. The electrochemical method is the most popular useful relation between biochemistry and electronics. The electrochemical method is used to determine the electroactive species present in the sample solution under test. It works on the principle of measurement of current or voltage in an electrochemical cell under the application of voltage or current in pre-defined manner respectively. If a chemical reaction is driven by an external applied voltage, as in electrolysis, or if a voltage is created by a chemical reaction as in a battery, it is an electrochemical reaction. Chemical reactions where electrons are transferred between molecules are called oxidation/reduction (redox) reactions. In general, electrochemistry deals with situations where oxidation and reduction reactions are separated in space or time, connected by an external electric circuit to understand each process. Electrochemical methods of measurements exploit the basic principles of electrochemistry to figure out the physical change in the system and hence the change occurred due to any specific constituent indicating its role and characteristics in the system.

In a solution, the equilibrium concentrations of the reduced and oxidized forms of a redox couple are linked to the potential (E) via the Nernst's Equation.

$$E = E_0 + \frac{RT}{nF} \ln \frac{C_{oxi}}{C_{red}} \qquad \text{..... (2.7)}$$

where, E_0 is equilibrium potential, F is Faraday's constant, T is absolute temperature, C_{oxi} and C_{red} are concentrations of oxidation and reduction centers. For each redox couple, there exists a potential, known as the standard potential E_0 at which the reduced and oxidized forms are present at equal concentrations. If the potential E with respect to the reference electrode is applied to the working electrode, e.g. by the use of a potentiostat, the redox couples present at the electrode respond to this change and adjust their concentration ratios according to Eq. (2.7). The analysis of the measured parameters namely current or voltage helps in identification and quantification of the species under studies.

The measurement set-up for a typical electrochemical 3-electrode measurement is shown below.

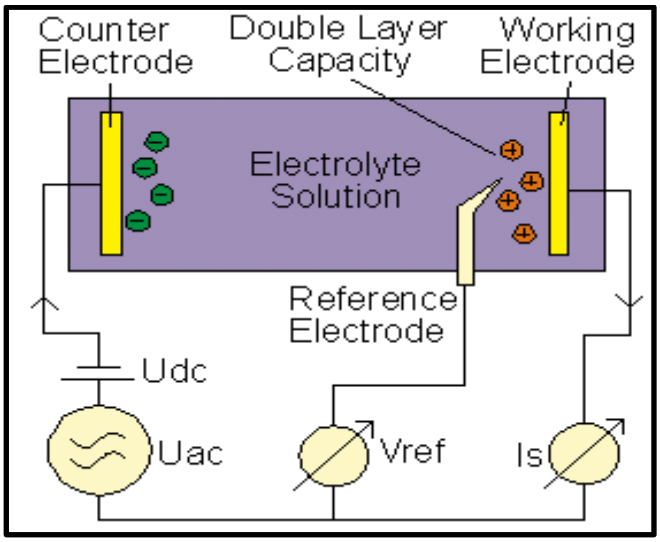

Figure: 2.22: Principle set-up of a three electrode electrochemical cell for cyclic voltammetric and differential pulse voltammetric measurement.

In addition to the two parallel plate electrodes (denoted as Counter and Working electrode), a third voltage reference electrode is placed close to the polarization layer and measures the voltage difference of the polarization double layer capacity to the working electrode. In contrast to dielectric, conductivity and impedance material spectroscopy where all electrodes are made of inert metal as e.g. gold, stainless steel or platinum, this applies for the electrochemical cell only for the counter electrode feeding current into the electrolyte.

The working electrode consists of the metal to be characterized in combination with the electrolyte. The reference electrode is usually an open tipped glass capillary filled with a standard electrolyte coupled to a standard metal in order to create a defined electrochemical potential to the electrolyte.

The total potential drop across the cell is summed up by all contributions of the chemical process like mass transport, chemical and adsorption steps, electron transfer, etc. By measuring the impedance spectrum $V_{Ref}^{*}(\omega)/I_S^{*}(\omega)$ and fitting it with an equivalent circuit model, the several process contributions can be separated from each other. The typical evaluation includes determination of Warburg impedance related to mass transport, electron transfer resistance, electrolyte resistance and double layer capacity.

As on the working electrodes an electrochemical reaction takes place, it is necessary to keep the DC potential V_{Ref} at a defined value or alternatively apply a constant DC current to the cell. This can be done by a Potentiostat / Galvanostat DC circuit as shown below.

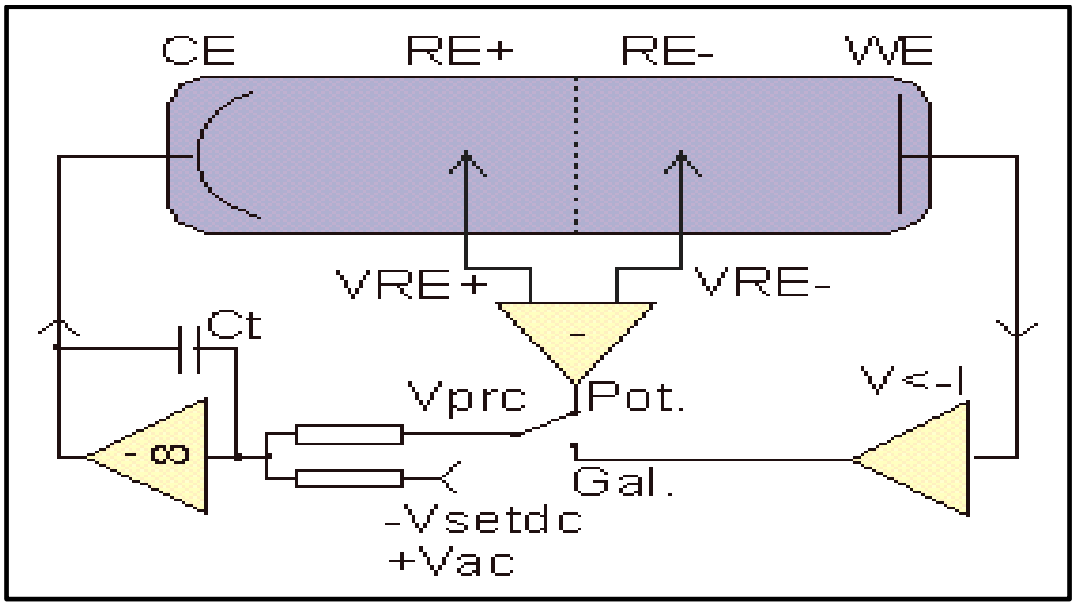

Figure: 2.23: Principle of Potentiostat / Galvanostat circuit with differential reference voltage inputs.

The voltage amplifier connected to CE electrode compares in potentiostat mode the differential voltage $V_{Prc} = V_{RE+} - V_{RE--}$ of both reference electrodes with the intended voltage V_{setdc}. The amplifier adjusts its output voltage until V_{Prc} and V_{setdc} match resulting in a constant and sample impedance independent reference voltage differential which can be adjusted by V_{setdc}. In galvanostat mode V_{Prc} is created proportional to the measured cell current by a current to voltage converter (V<-I), resulting in constant sample cell current. In both modes, the variable capacitor C_t adjusts the control loop time constant in order to avoid free high frequency oscillations caused by too high open loop gain.

In this project electrochemical studies have been carried out by using Metrohm Autolab Potentiostat/Galvanostat at DTU, Delhi.

Figure: 2.24: Metrohm Autolab Potentiostat/Galvanostat at DTU, Delhi.

The electrochemical method facilitates performing various electrochemical experiments in a single unit. Some of the electrochemical techniques are elucidated below:

2.4.1.9.1. Cyclic Voltammetry (CV) Measurement:

Cyclic voltammetry (CV) is widely used for the study of redox processes, for understanding reaction intermediates, and for obtaining stability of reaction products [44]. This technique is based on varying the applied potential at a working electrode in both forward and reverse directions (at some scan rate) while monitoring the current. For example, the initial scan could be in the negative direction to the switching potential. At that point the scan would be reversed and run in the positive direction. Depending on the analysis, one full cycle, a partial cycle, or a series of cycles can be performed. The important parameters in a cyclic voltammogram are the peak potentials (E_{pc}, E_{pa}) and peak currents (i_{pc}, i_{pa}) of the cathodic and anodic peaks, respectively. If the electron transfer process is fast compared with other processes (such as diffusion), the reaction is said to be electrochemically reversible, and the peak separation is

$$D_{Ep} = E_{pa} - E_{pc} = 2.303\ RT \log n \quad \text{.....(2.8)}$$

Irreversibility due to a slow electron transfer rate results in $D_{Ep} > 0.0592/n$ V.

The formal reduction potential (E_o) for a reversible couple is given by

$$E_0 = (E_{pc}+E_{pa})/2 \qquad \text{.....(2.9)}$$

For a reversible reaction, the concentration is related to peak current by the Randles–Sevcik expression (at 25 °C):

$$i_p = 2.686x10^5 n^{3/2} A c^0 D^{1/2} \boldsymbol{\nu}^{1/2} \qquad \text{..... . (2.10)}$$

where i_p is the peak current in amps, A is the electrode area (cm^2), D is the diffusion coefficient ($cm^2\ s^{-1}$), C^0 is the concentration in mol cm^{-3}, and n is the scan rate in V s^{-1}. Cyclic voltammetry is carried out in quiescent solution to ensure diffusion control. A three-electrode arrangement is used. Working electrodes include glassy carbon, platinum, gold, graphite, and carbon paste.

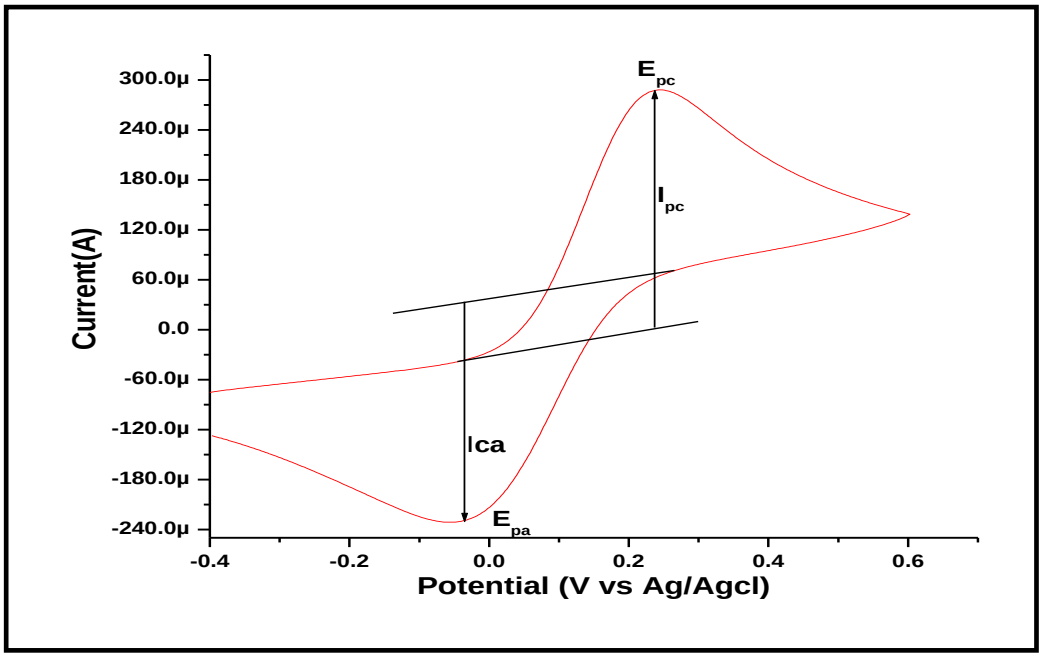

Figure: 2.25: Typical cyclic voltammogram

2.4.1.9.2. Differential Pulse Volta metric (DPV) measurement

Differential Pulse Voltammetry (DPV) is another kind of electrochemical measurement. In this series of regular voltage, pulses superimposed on a linearly changing voltage are applied and the resulting current is measured between the ramped baseline voltage and the pulse

voltage. A digital staircase voltage is commonly used as the ramped baseline. The system of this measurement is usually the same as that of CV. The potential between the working electrode and a reference electrode is changed as a pulse from an initial potential to an inter-level potential and remains at the inter level potential for about 5 to 100 milliseconds, then it changes to the final potential which is different from the initial potential. The pulse is repeated, changing the final potential and constant difference is kept between the initial and inter-level potential. The values of the current before and after the pulse are recorded and their differences are plotted versus potential [45].

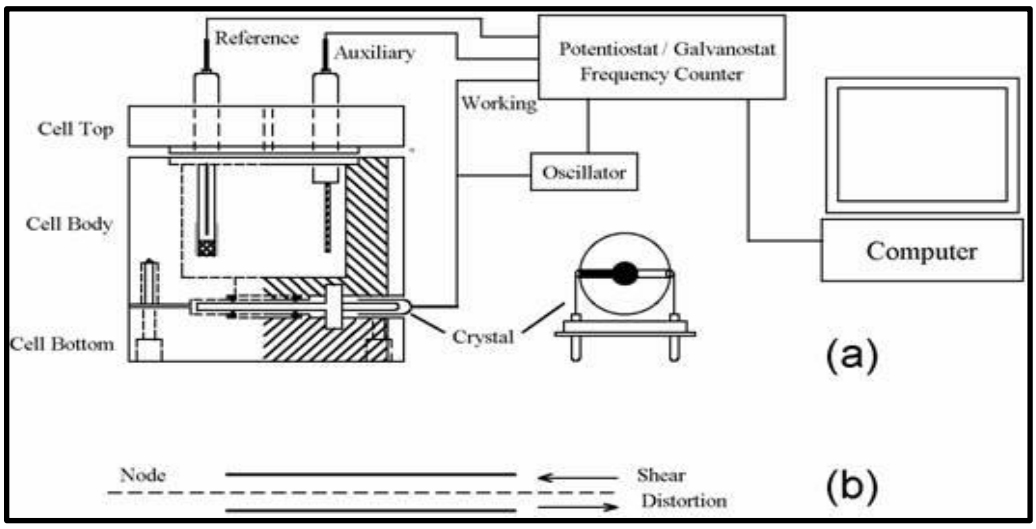

Figure: 2.26. Block diagram of DPV.

3.1 Structural and Optical Characterization

3.1.1. X-ray diffraction study

Figure 3.1 (curve a), shows the X-ray diffraction spectrum of CHIT. It shows broaden peak at 20.03° which indicates the existence of an amorphous structure. CHIT shows very broad lines especially for the smaller diffraction angle, thereby indicating that long range disorder is found in polymer samples. The broader small angle peaks in CHIT suggest that CHIT exhibits higher long range order.

The XRD spectrum of V_2O_5 nanoparticles, prepared by hydrothermal method is shown in Figure 3.1 **(**curve b) .The pattern shows the reflection planes from (2 0 0), (0 0 1), (1 0 1), (1 1 0), (4 0 0) ,(0 1 1), (1 1 1), (3 1 0) , (2 1 1), (4 0 1), (0 0 2), (1 0 2) (4 1 1) and (3 0 2) which indicates the presence of the orthogonal symmetry of V_2O_5. These diffraction lines provide a clear evidence of the formation of pure V_2O_5 nanoparticles with the reported values (JCPDS File No. 41-1426; a = 11.5160 Å, b = 3.5656 Å, and c = 4.3727 Å) [46, 47]. However, broadening of the reflection peak indicates formation of fine nanocrystalline particles. No foreign phases (diffraction peaks of any impurities) have been detected, proving the high purity of the synthesized V_2O_5 samples. The average crystallite diameter d, is calculated, using the Scherrer's equation, from the full width at half maximum (FWHM) of the most intense peak of the XRD for (1 1 0).

$$d = \frac{o.9\lambda}{\beta \cos\theta} \quad \text{.....} \quad (3.1)$$

where β is the broadening of diffraction line measured at half maximum intensity (radians) and λ = 1.5406 Å, the wave length of Cu Kα. The crystallite size estimated from the Scherrer's equation, is found to be (~25) nm and (~21) nm of V_2O_5 nanoparticle and V_2O_5-CHIT nanocomposite respectively.

Figure 3.1 (curve c), shows the XRD pattern of V_2O_5-CHIT nanocomposite in which a broader peak with increased intensity is obtained at the reflection plane (0 0 1), confirming the formation of V_2O_5-CHIT nanocomposite.

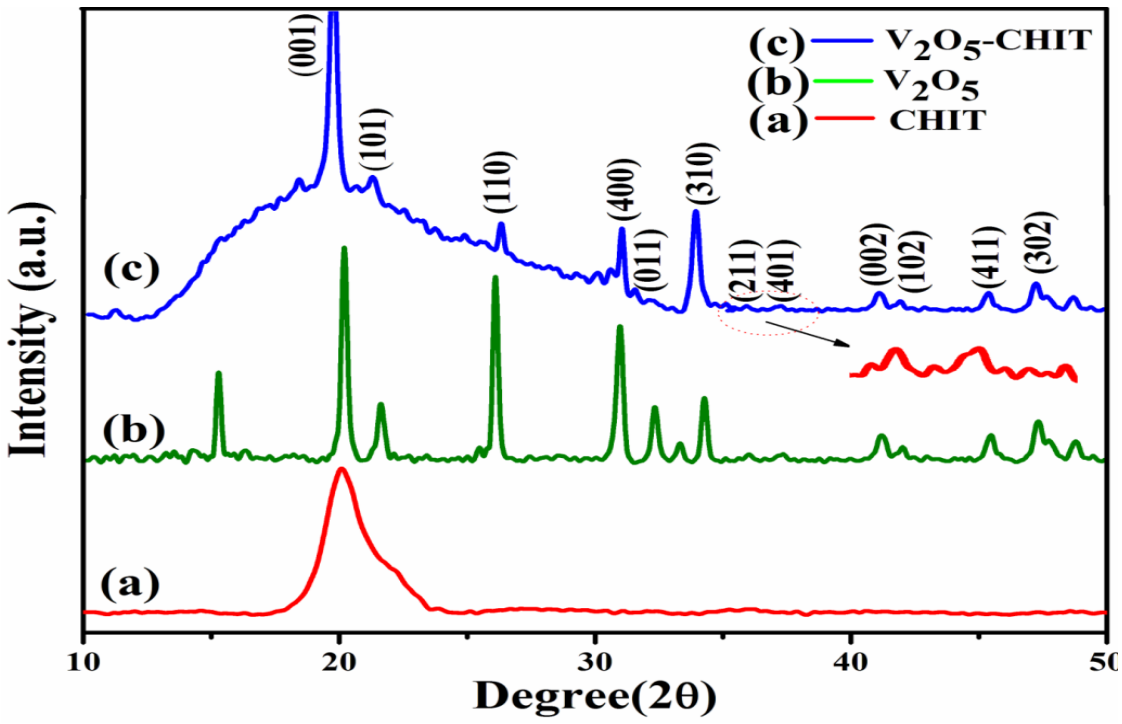

Figure 3.1: X-ray Diffraction pattern of (a) CHIT, (b) V_2O_5 nanoparticles and (c) V_2O_5-CHIT nanocomposite

3.1.2. FT-IR Spectroscopy study

The FT-IR spectra of nanostructured CHIT film (curve a), V_2O_5 (curve b), and V_2O_5-CHIT composite film (curve c) are shown in Figure 3.2 in the range of 400–4000 cm^{-1}. The CHIT/ITO film (Figure 3.2, curve a,) exhibits characteristic absorption bands of amino saccharide at 3430 cm^{-1} is due to overlapping of –OH and $–NH_2$ stretching, 2920 cm^{-1} are due to CH_2 stretching and 1650 cm^{-1} for carbonyl stretching (C=O) band of amide I and amide II, peak at 1380 cm^{-1} assigned to –C–O stretching mode of $–CH_2–OH$ groups and 1070 cm^{-1} stretching vibration of C–O–C in glucose circle of CHIT [48,49].

The FTIR spectrum of V_2O_5 (Figure 3.2, curve b) exhibits weak bands at 3440 cm^{-1} corresponding to different vibration modes of O–H stretching due to physically adsorbed water. Curve (b) reveals three obvious bands centred at 573, 812 and 1030 cm^{-1}, which are assigned to the V–O stretching vibration, V–O–V bending vibration and the stretching vibration of the shortest bond between vanadium and oxygen, respectively [50,51].

The FTIR spectrum of the V_2O_5-CHIT nanocomposite film (Figure 3.2, curve c) exhibits characteristic IR bands of the functional group corresponding to pure CHIT (Figure 3.2, curve b) and additional band at 571 and 813 cm^{-1} revealing to the V-O starching and V-O-V

bending vibration. This reveal the formation of complex between surface charged V_2O_5 nanoparticles and cationic CHIT matrix, indicating the formation of V_2O_5-CHIT nanocomposite. This indicates that the V-O-V network is bonded with CHIT macromolecules and indicates the formation of V_2O_5-CHIT nanocomposite.

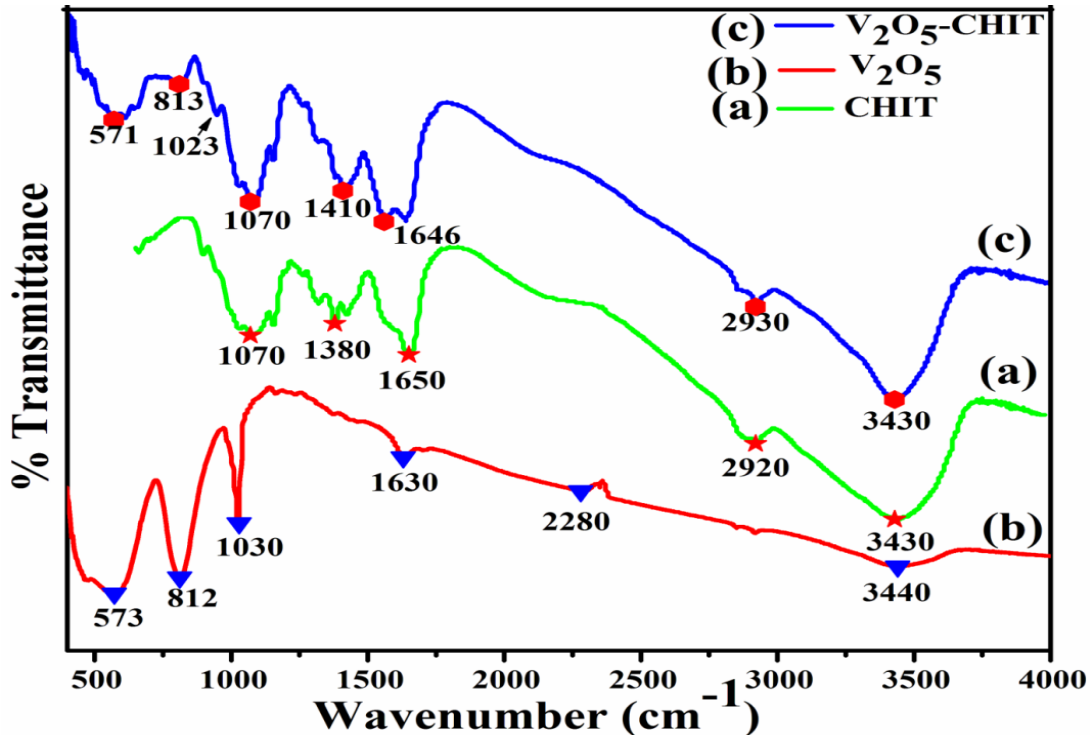

Figure 3.2: FT-IR transmission spectra of (a) CHIT (b) V_2O_5 nanoparticles and (c) V_2O_5-CHIT nanocomposite.

3.1.3. UV-Vis Spectroscopy study

The UV−visible spectroscopic studies were conducted by using Perkin Elmer, Lamda 950 to characterize the CHIT, V_2O_5 nanoparticles and V_2O_5-CHIT nanocomposite. Figure 3.3 (curve a) shows spectrum of CHIT. CHIT itself is transparent in the UV and visible region, so its optical properties are hard to characterize by spectroscopy methods.

Figure 3.3 (curve b) shows spectrum of V_2O_5 nanoparticles which gives absorption peak at 247.89 nm and 208.26 nm while the broad band arises at 244 nm is due to the combination of π-π* transition and n-π* transition in V_2O_5-CHIT nanocomposite (Figure 3.3, curve c).

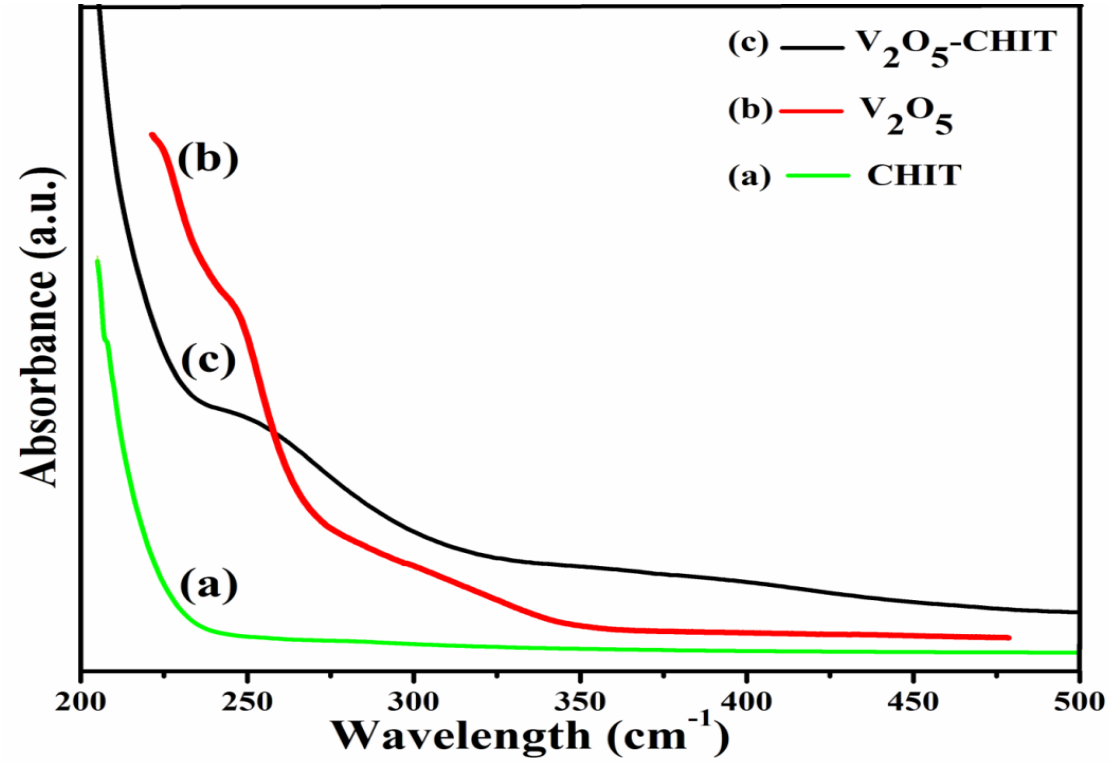

Figure 3.3: UV absorbance spectra of (a) CHIT, (b) V_2O_5 nanoparticles and (c) V_2O_5-CHIT nanocomposite.

3.1.4. PL Spectroscopy study

PL spectrum of chitosan was performed at 280 nm excitation wavelength and the emission spectrum shows a peak at 417 nm (Figure 3.4, curve a). PL spectrum of V_2O_5 nanoparticles was performed at 420 nm excitation wavelength and its gives peak at 359 nm (Figure 3.4, curve b). PL spectrum of V_2O_5 nanocomposite was performed at 420 nm excitation wavelength which gives a peak at 487 nm (Figure 3.4, curve c). A red shifted emission is observed in the V_2O_5-CHIT nanocomposite due to the electron rich polymer main chain. The result indicates the formation of nanocomposite [52].

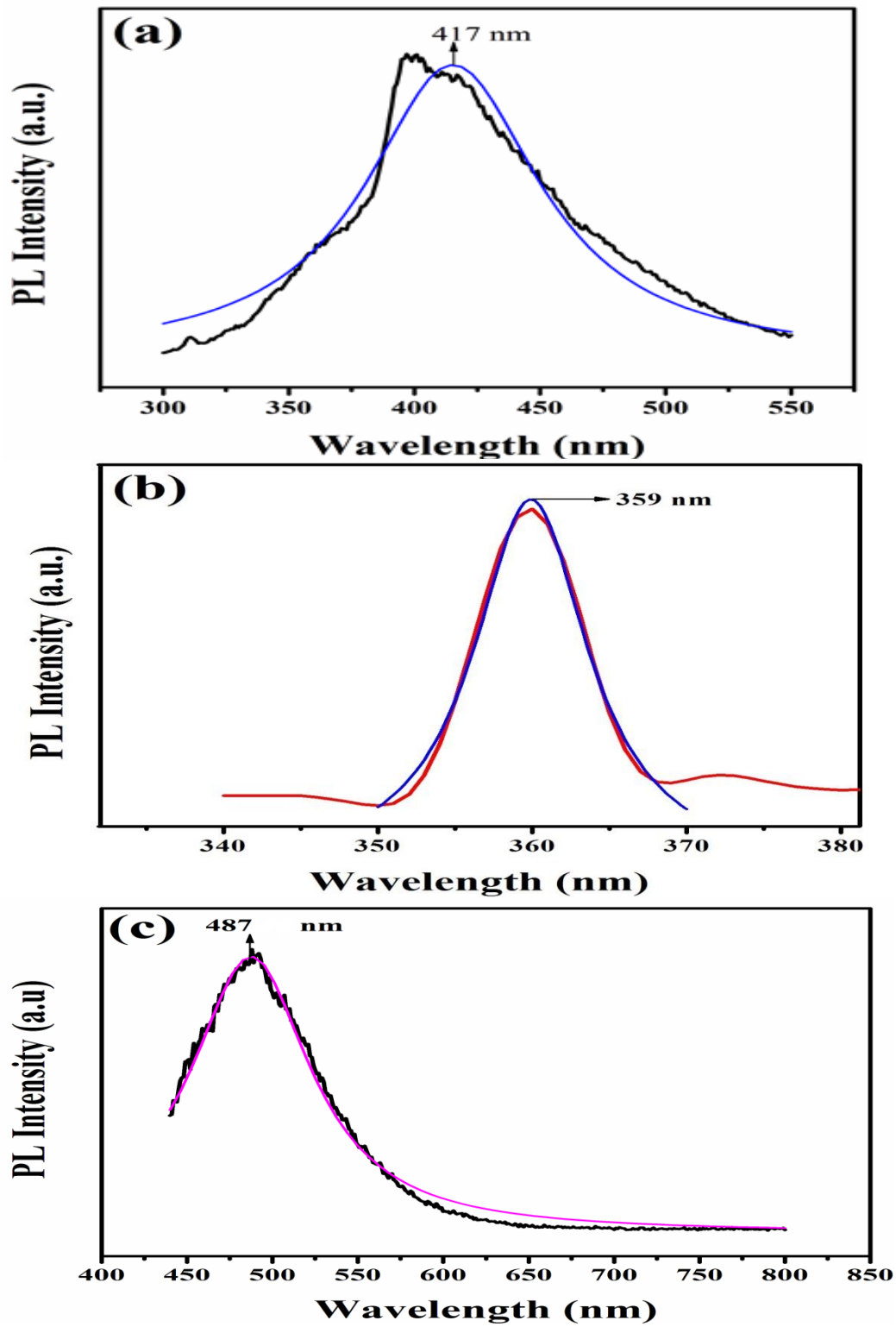

Figure 3.4: Photoluminescence emission spectra of (a) CHIT, (b) V_2O_5 nanoparticles and (c) V_2O_5-CHIT nanocomposite.

3.2 Morphological study

3.2.1. Atomic force microscopy (AFM) study

AFM evaluation was performed by using XE-100, Park System digital instrument by non-contact mode; AFM studies were carried out to investigate the surface properties for CHIT/ITO film, V_2O_5/ITO film and V_2O_5-CHIT/ITO nanocomposite film electrode in air environment. Figure 3.5 depicts 2D and 3D atomic force microscopy images of for CHIT/ITO film, V_2O_5/ITO film and V_2O_5-CHIT/ITO nanocomposite film electrode where from 3D view, the uniform height distribution throughout the surface is seen.

Figure 3.5 (a) Demonstrate the 3D surface morphology of CHIT/ITO film showed smooth, homogeneous and bulbous structural elements. The morphology of Figure 3.5 (b) exhibit uniformly distributed V_2O_5 nanoparticles on the surface of ITO; with root mean square roughness (R_q) = 6.087 nm, average roughness (R_a) = 5.193 nm, maximum profile peak height = 11.376 nm. It can be seen that all nanoparticles on ITO surface are uniformly distributed.

Figure 3.5 (c) demonstrate the 2D and 3D morphology of V_2O_5-CHIT/ITO nanocomposite film which shows that nanoparticles get incorporated in chitosan layer with root mean square roughness (R_q) = 3.280 nm, average roughness (R_a) = 2.575 nm, maximum profile peak height = 9.359 nm. It can be seen that roughness is decreased as compared to the V_2O_5/ITO nanoparticle surface because of chitosan. We obtained a smoothed nanocomposite film with very well incorporated V_2O_5 nanoparticles due to biopolymer.

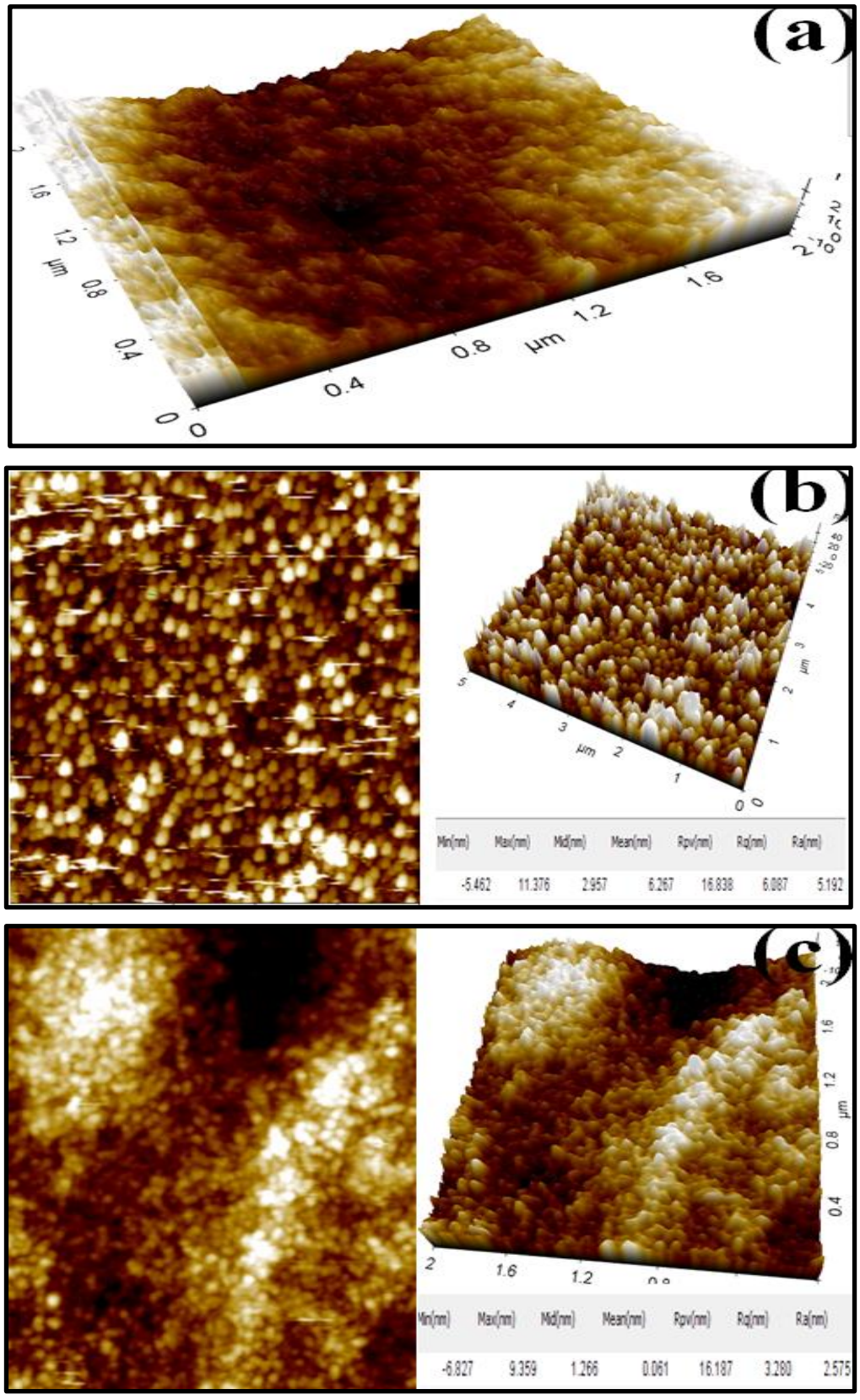

Figure 3.5: AFM result obtained for (a) CHIT/ITO film, (b) V_2O_5/ITO film and (c) V_2O_5-CHIT/ITO nanocomposite film.

3.2.2. Scanning electron microscopy (SEM) study

CHIT film, V_2O_5 nanomaterial and V_2O_5-CHIT nanocomposite film were investigated using Hitachi S-3700N, scanning electron microscope for studying its surface morphologies shown in Figure.3.6 (a, b, c). The CHIT film (micrograph a) shows homogenous with relatively smooth and crack-free surface. The SEM image of nanocrystalline V_2O_5 nanoparticles (micrograph b) exhibits rough nanostructured sheets and rod like morphology. However, some nanostructured sheets were stacked together due to high surface charge of vanadium. The SEM images of V_2O_5-CHIT nanocomposite film (micrograph c) show granular and fibre nanoporous morphology embedded uniformly in the porous CHIT matrix. Nanostructured V_2O_5 particles are uniformly incorporated in the porous chitosan and some also forms agglomerates, containing several particles. This indicates formation of the V_2O_5-CHIT nanocomposite.

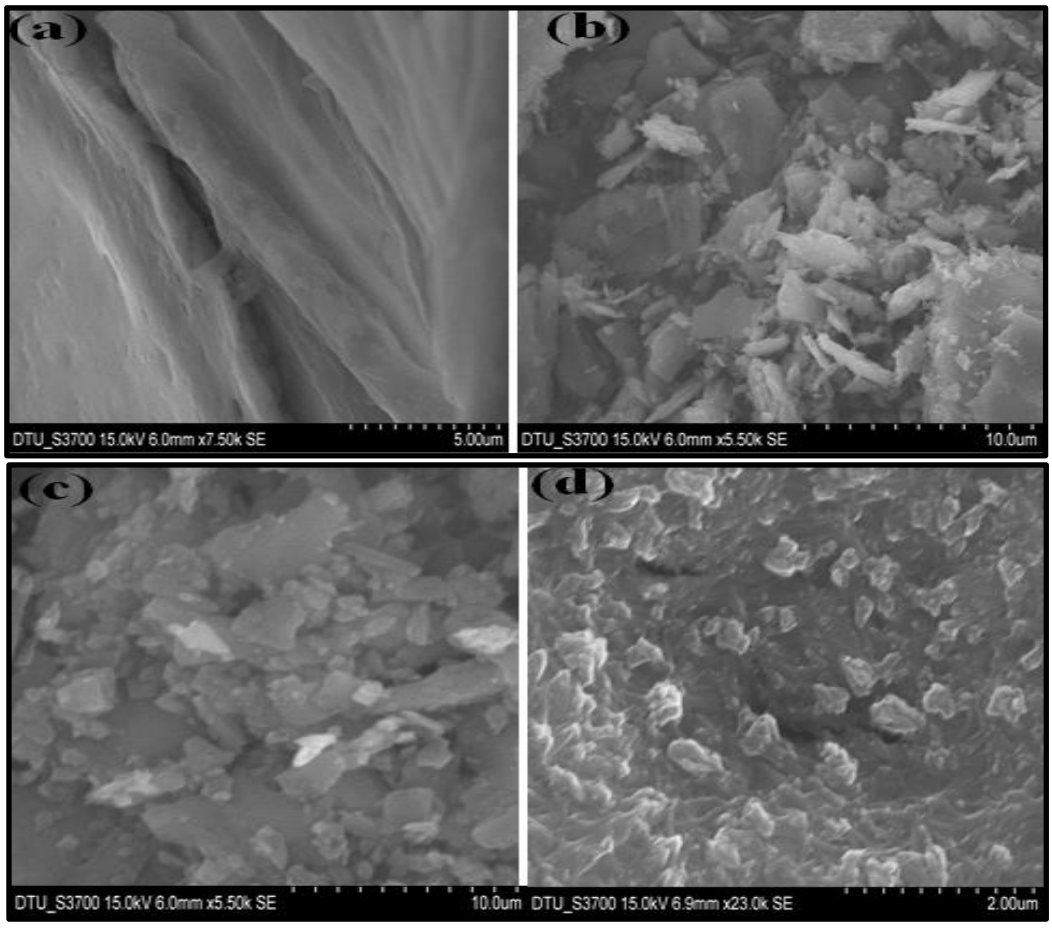

Figure 3.6: SEM micrograph of (a) CHIT film, (b, c) V_2O_5 nanomaterial and (d) V_2O_5-CHIT nanocomposite film.

3.2.3. EDX Analysis

The chemical composition of V_2O_5 nanoparticles prepared hydrothermally at the optimized conditions was extracted from the energy dispersive X-ray spectrum (EDX) which is shown in Figure 3.8. The EDS analysis exhibited clear peaks of only V and O elements, whereas no additional peaks were detected, which means that the as-prepared powder is exempted from impurities that arise from the starting precursors like silicon and carbon. The atomic percentages of V and O elements present in the as-prepared nanoparticles are 31.54 and 68.46 atom %, respectively.

The EDAX analysis of CHIT clearly indicates C, O and N peaks with atom% -46.28 %, 37.15 % and 16.57 % respectively at different keV (Figure 3.7). On preparation of the V_2O_5-CHIT nanocomposite, the EDAX analysis Figure 3.9 confirms the presence of only V, O, C and N elements with atom % composition of 8.31, 76.03, 2.94 and 12.72 % respectively. It confirms the nanocomposite formation and indicates that thus formed V_2O_5-CHIT nanocomposite is free from any form of impurity.

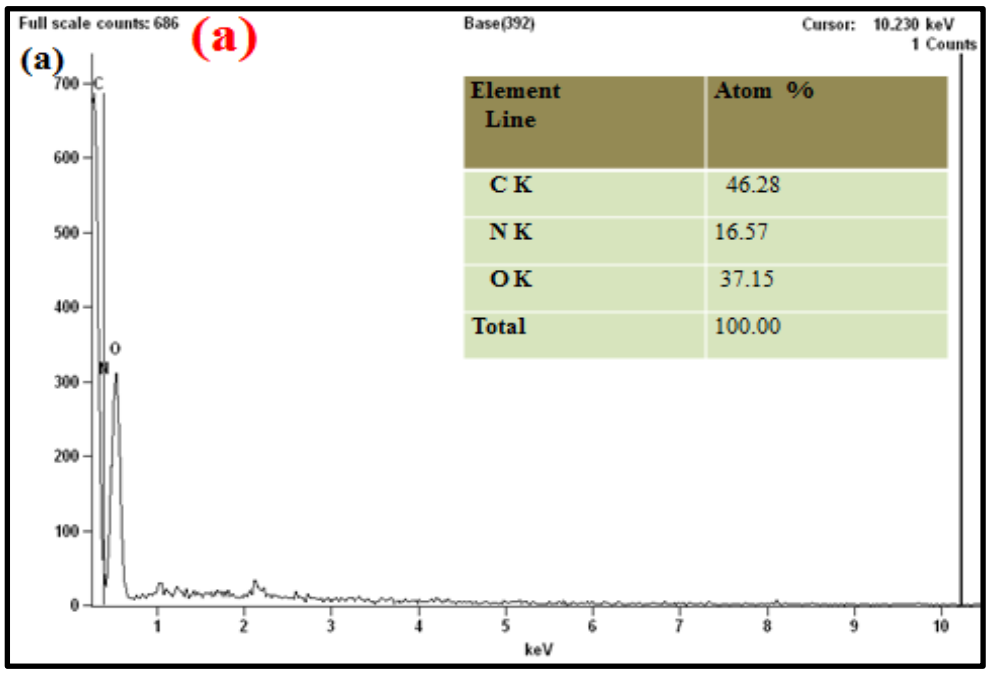

Figure 3.7: EDX analysis of CHIT showing atom % composition of C, N and O at different keV.

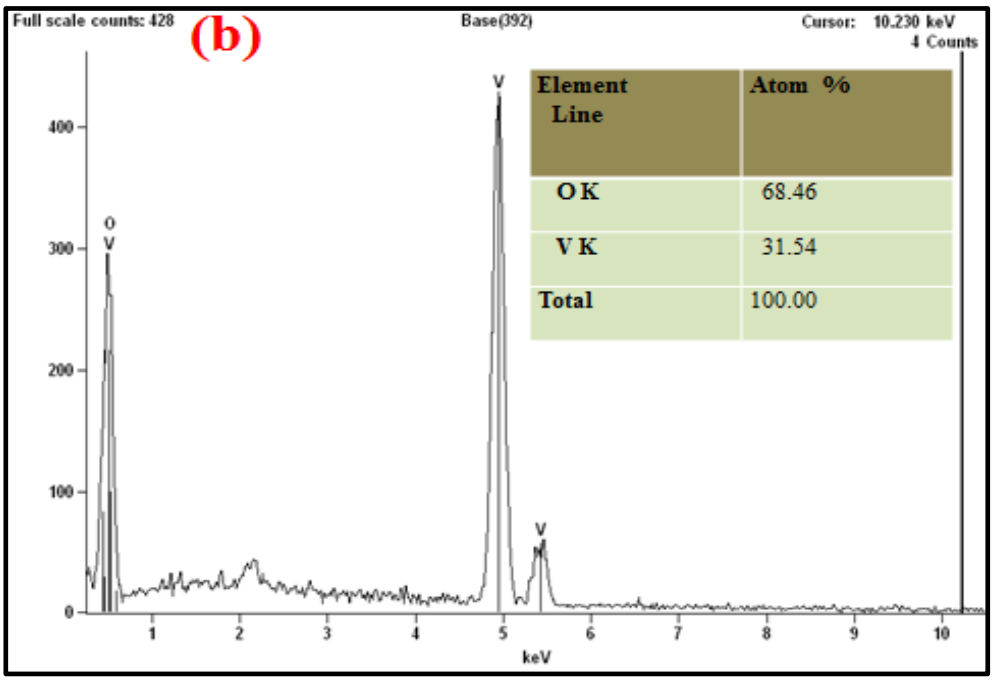

Figure 3.8: EDX analysis of V_2O_5 nanoparticles showing atom % composition of V and O at different keV.

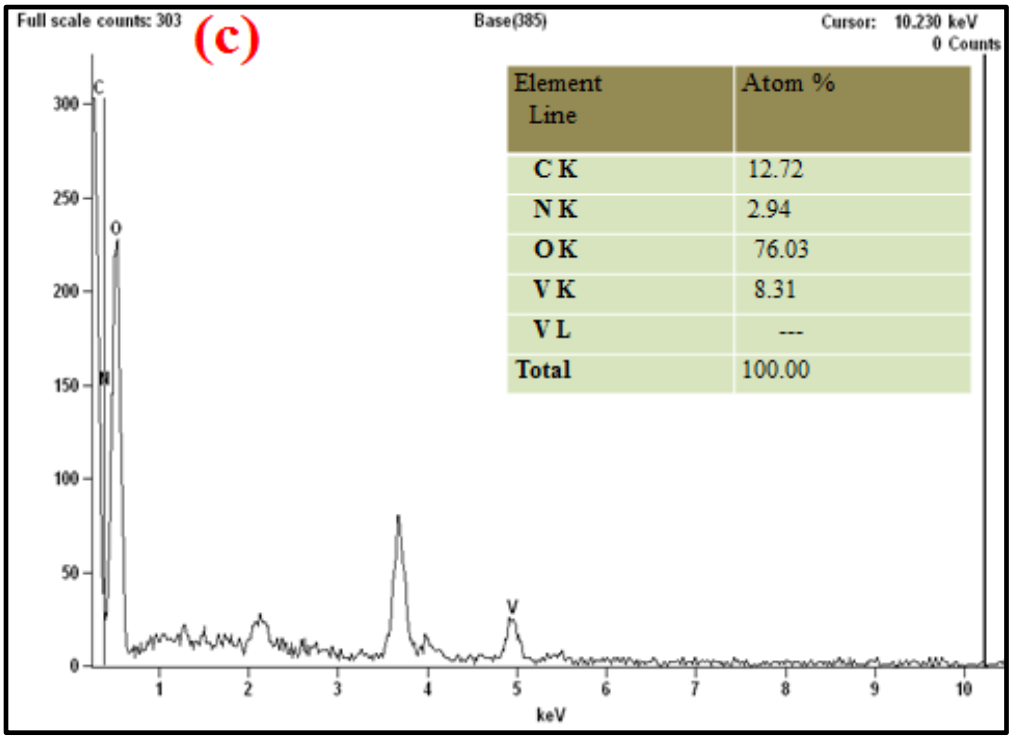

Figure 3.9: EDX analysis of V_2O_5-CHIT showing atom % composition of C, N, O and V at different keV and confirming nanocomposite formation.

3.2.4. Transmission electron microscopy (TEM) study

Transmission electron microscope (TEM) FEI Tecnai S Twin was used for Particle size and shape investigation of V_2O_5 nanoparticles. TEM analysis reveals formation of rectangular nano sheets with length 45-70 nm and diameter 40-45 nm in agreement with SEM observation. Some of these sheets are also stacked together in some areas and their individual thickness is 0.04 to 0.06 µ. Nano rods were also observed which are of dimension 0.07 × 0.40 µ. TEM analysis confirms the formation of nanostructured sheets and rods.

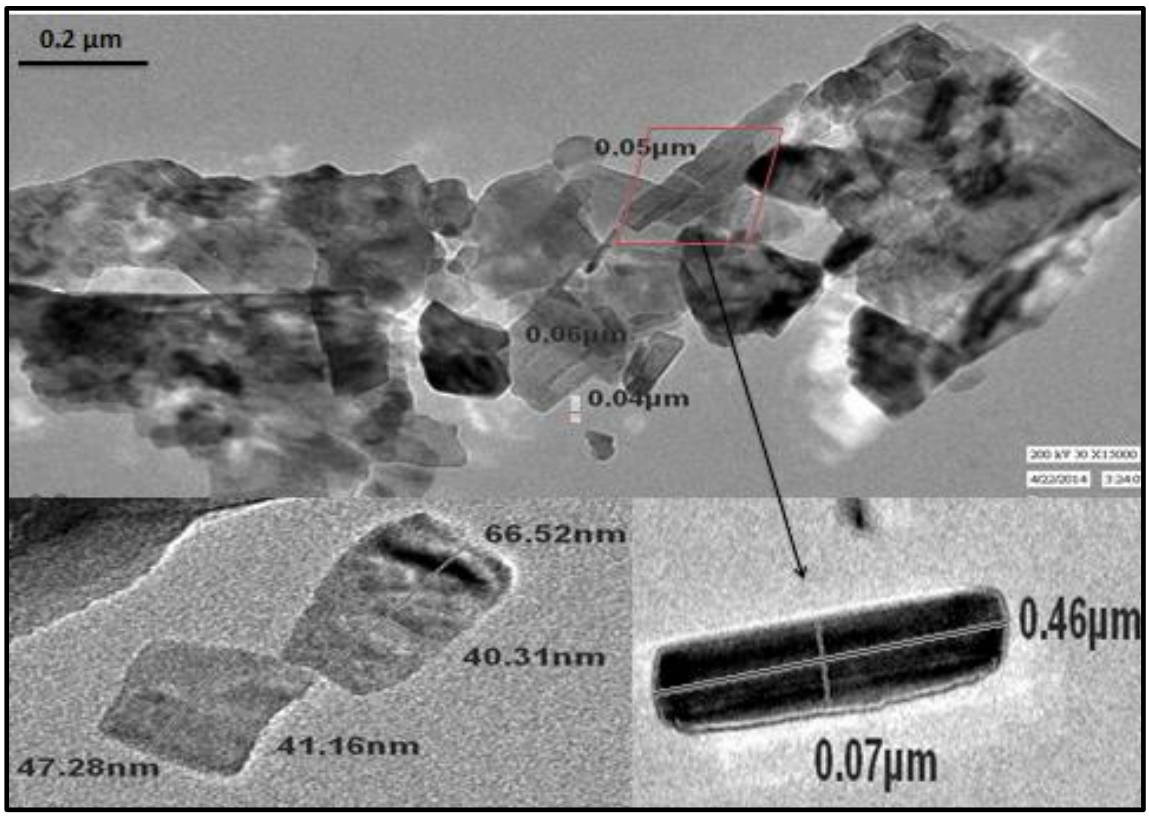

Figure 3.10: TEM micrograph of V_2O_5 nanoparticles which confirm the formation of nanostructured V_2O_5

3.3 Electrochemical study

3.3.1. Cyclic voltammetry and Differential pulse voltammetry studies

Figure 3.11 shows cyclic voltammograms (CV) obtained for bare ITO electrode (a), CHIT/ITO electrode (b), V_2O_5-CHIT/ITO electrode (c) and V_2O_5-CHIT/ITO electrode (d) in phosphate buffer (5 mM [pH 6.4] and 0.9% NaCl) containing $[Fe(CN)_6]^{3-/4-}$ at a scan rate of 50 mV/s. The CV of bare ITO (curve a) exhibits a well-defined electrochemical characteristics with a couple of redox peaks for $[Fe(CN)_6]^{3-/4-}$ mediator and shows oxidation peak current (I_{pa}) at 0.303 mA. In CHIT/ITO (curve b) electrode, the oxidation peak current (I_{pa}) increases to 0.477 mA (curve b) due to the cationic nature of CHIT which accepts electrons from the medium and transfers them to the electrode [53]. CV of V_2O_5/ITO nanoparticles electrode (curve c) shows oxidation and reduction peaks at 0.43V and -0.03 V respectively and the magnitude of peak current (0.631 mA) that is more than that of bare ITO (curve a) and CHIT/ITO (curve b), which can be ascribed to the excellent conductivity and large surface area of the V_2O_5 nanoparticles. On incorporation of V_2O_5 nanoparticles into the CHIT matrix, the I_{pa} (0.709 mA) is found to increased further for V_2O_5-CHIT/ITO electrode (curve d) due to high electro catalytic mobility, increased electro-active surface area resulting an improvement in electron transfer.

Differential pulse voltammetry (DPV) studies (Figure 3.12) have been carried out for (a) bare ITO, (b) CHIT/ITO, (c) V_2O_5/ITO and (d) V_2O_5-CHIT/ITO electrode, in PBS (5 mM, pH 6.4, 0.9% NaCl) containing $[Fe(CN)_6]^{3-/4-}$ in the potential range of 0 to 1.2 V. The results of DPV studies indicate that magnitude of peak current (0.145 mA) of CHIT/ITO (curve b) is enhanced as compared to that of bare ITO (curve a) (0.139 mA) due to diffusion of electrons onto cationic CHIT matrix and transfer to electrode. In DPV V_2O_5/ITO (curve c) electrode peak current is found 0.174 mA which is higher than that of bare ITO (curve a) and CHIT/ITO (curve b). After incorporation of V_2O_5 nanoparticles into CHIT matrix, the magnitude of peak current response further increases to 0.183 mA (curve d) for V_2O_5-CHIT/ITO electrode. This suggests that V_2O_5 nanoparticles provide improved electrocatalytic behaviour and enhanced electron transport between the medium and electrode.

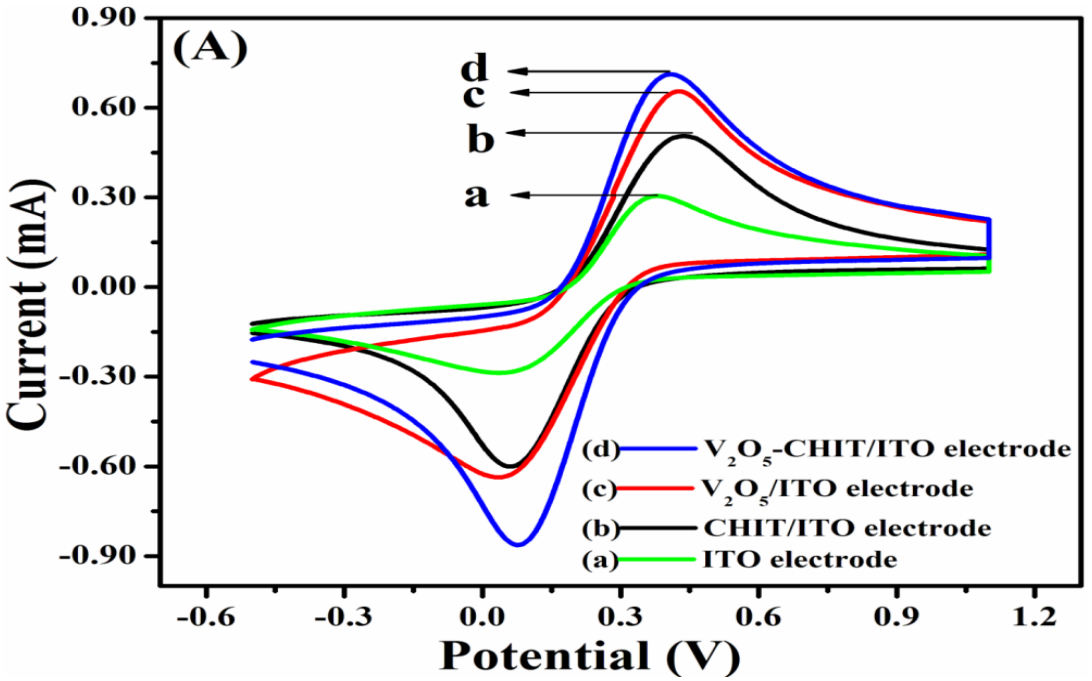

Figure 3.11: Cyclic voltammograms of (a) bare ITO electrode, (b) CHIT/ITO electrode, (c) V_2O_5-CHIT/ITO electrode and (d) V_2O_5-CHIT/ITO electrode

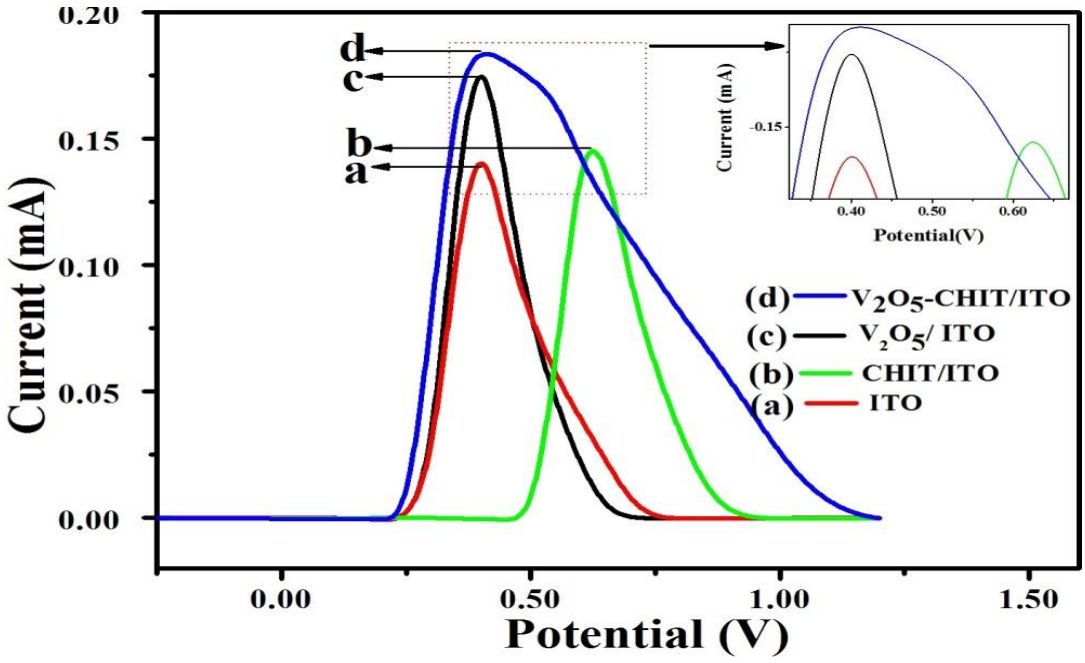

Figure 3.12: Differential pulse voltammograms of (a) bare ITO, (b) CHIT/ITO, (c) V_2O_5-CHIT/ITO and (d) V_2O_5-CHIT/ITO electrode

3.3.2. Effect of scan rate

To investigate the interfacial kinetics of the V_2O_5-CHIT/ITO electrode surface, CV studies in PBS (pH 6.4) have been conducted as a function of scan rate varying from 10 to 100 mV/s (Figure 3.13). It can be seen that magnitudes of both anodic (I_{pa}) and cathodic (I_{pc}) peak currents increase linearly with square root of scan rate ($v^{1/2}$) (Figure 3.13). With increasing scan rate the oxidation peak shifts towards more positive potential and similarly reduction peak shifts towards more negative potential, indicating that the redox process is quasi-reversible and potential peak shift ($\Delta E_p = E_{pa} - E_{pc}$) exhibit a linear relationship (inset(1), Figure 3.14) with scan rate suggesting that the electrochemical reaction at electrode is a diffusion controlled process. The observed linear dependence of peak height with sweep rate (with a linear regression co-efficient of 0.9993) indicating improved electrocatalytic behaviour.

The value of electron transfer co-efficient (α), for n number of electrons, has been calculated from two straight lines with a slope equal to $2.3RT/(1 - \alpha)nF$ for the anodic peak and $-2.3RT/\alpha nF$ for the cathodic peak, using Laviron's equations. The electron transfer co-efficient (α) for the V_2O_5-GG/ITO electrode has been found to be 0.965524 V for anodic peak and 0.0255 V for cathodic peak.

The change in value of the charge transfer rate constant (K_s) of the electrode due to surface modification has been calculated by following equation

$$K_s = mnF\, v/RT \quad \ldots\ldots\ldots\ldots\ldots\ldots\ldots\ldots \quad (3.2)$$

where m is the peak-to-peak separation (V), F is the Faraday constant (96 485 C mol^{-1}), v is the scan rate (30 mV/s), n is the number of transferred electrons (1), R is the gas constant (8.314 J mol^{-1} K^{-1}) and T is the room temperature (25 °C).

The K_s value of the V_2O_5/ITO electrode and the V_2O_5-CHIT/ITO electrode has been found to be 1.495 and 1.284 s^{-1} respectively. The increased K_s value at the surface of the V_2O_5/ITO electrode clearly indicates that both the electronic structure and surface physicochemistry of the V_2O_5 nanoparticles contribute to increased electron transfer arising from high catalytic behaviour of V_2O_5 nanoparticles.

The surface concentration of the electrodes can be calculated from the following relation of Brown-Anson model [54].

$$Ip = \frac{n^2F^2\ I^*\ AV}{4RT} \quad \ldots\ldots\ldots\ldots\ldots\ldots \text{(3.3)}$$

where *n* is the number of electrons transferred (2), *F* is the Faraday constant (96,485 C/mol), I* is the surface concentration of the corresponding electrode (molcm^{-2}), *A* is the surface area of the electrode (0.25 cm^2), *V* is the scan rate (20 mV/s), R is the gas constant (8.314 Jmol^{-1}K^{-1}) and *T* is the room temperature (25 °C). The surface concentration of V_2O_5-CHIT/ITO (1.5173 × 10^{-8} molcm^{-2}) is higher than that of V_2O_5/ITO (1.395 × 10^{-8} molcm^{-2}). The higher surface concentration of V_2O_5-CHIT/ITO electrode suggests that deposition of V_2O_5 nanoparticles increase the electroactive surface area.

The diffusion co-efficient value (D) for free diffusion of $[Fe(CN)_6]^{3-/4-}$ from electrolyte solution to the corresponding electrode surface has been calculated using the Randles–Sevcik equation.

$$I_p = (2.69 \times 10^5) n^{3/2} A D^{1/2} C\, v^{1/2} \ldots\ldots\ldots\ldots\ldots\ldots \text{(3.4)}$$

where I_p is the peak current of the corresponding electrode (I_{pa} anodic and I_{pc} cathodic), *n* is the number of electrons involved or electron stoichiometry (1), *A* is the surface area of the electrode (0.25 cm^2), *D* is the diffusion co-efficient, *C* is the surface concentration in mol (5 mM) and ν is the scan rate (50 mV s^{-1}). D value is obtained for V_2O_5-CHIT/ITO electrode is 1.2198 x 10^3 cm^{2}s^{-1}.

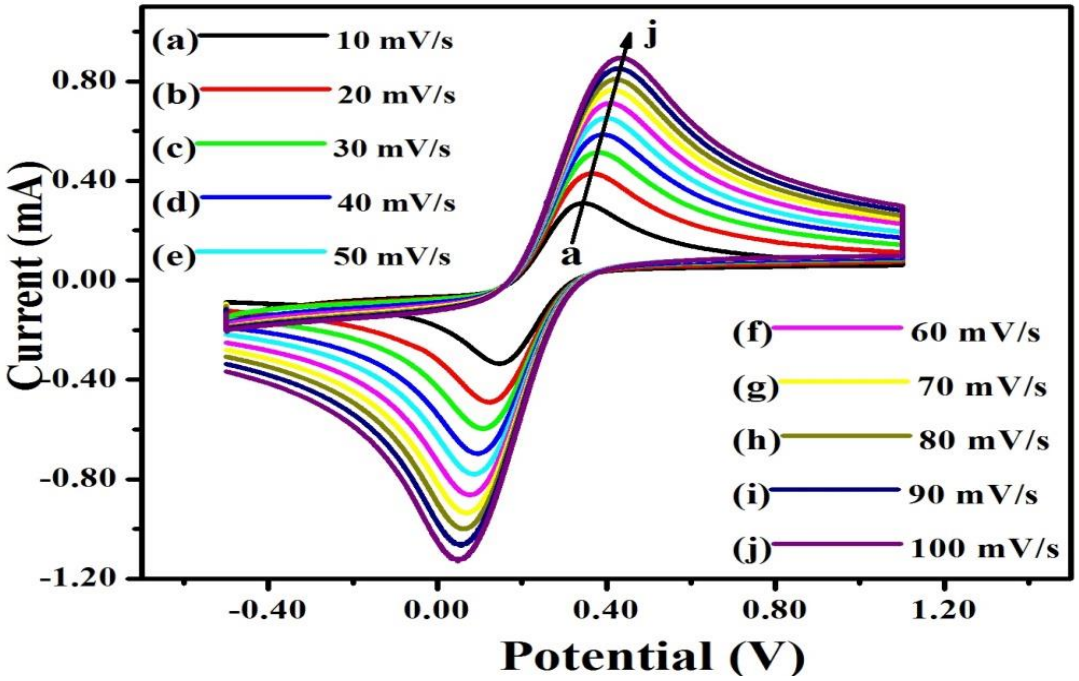

Figure 3.13: CV curve of the V_2O_5-CHIT/ITO using an increasing scan rate of 10 to100 mV/s

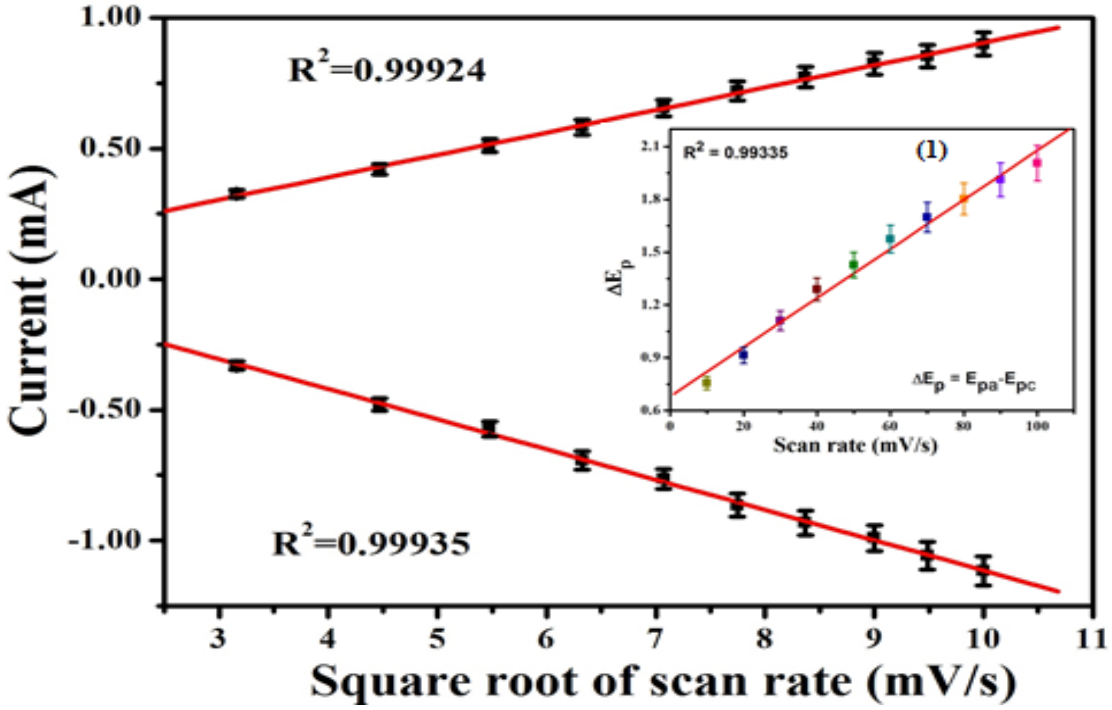

Figure 3.14: Magnitude of current and of potential difference v/s function of square root of scan rate (10–100 mV/s), in inset: (1) potential peak shift v/s scan rate

3.3.3. Optimisation of pH

Investigation of the effect of pH value on the performance of the V_2O_5-CHIT/ITO nanocomposite electrode is of great importance. The effect of solution pH (5.7 to 8) studies (Figure 3.15) have been carried out on V_2O_5-CHIT/ITO nanocomposite electrode at different pH (5.7-8) using CV techniques in PBS (5 mM, 0.9% NaCl) containing $[Fe(CN)_6]^{3-/4-}$ (5 mM) at scan rate of 50 mV/s. It can be seen that the oxidation peak current increases from pH 5.7 to 6.4 and the peak potential shifts towards lower potential and the highest magnitude of current is obtained at pH 6.4 (Fig 3.16). When pH further increases from 6.4 to 8, the oxidation peak current decreases gradually and the potential peak shifts to the higher value. The limited electron transport between the medium and the electrode may lead to a decrease in the electrochemical signal at higher pH. These changes in the peak current may arise due to a decrease in concentration of the positively charged moieties present at the matrix as the pH of PBS approaches its isoelectric point (IEP); this could result in decreased interaction between redox ions $[Fe(CN)_6]^{3-/4-}$ and the n-V_2O_5/ITO surface. The highest magnitude of current is obtained at pH 6.4 indicates that the V_2O_5-CHIT/ITO nanocomposite electrode is most active at pH 6.4. Thus all the experiments in this study have been conducted at pH **6.4.**

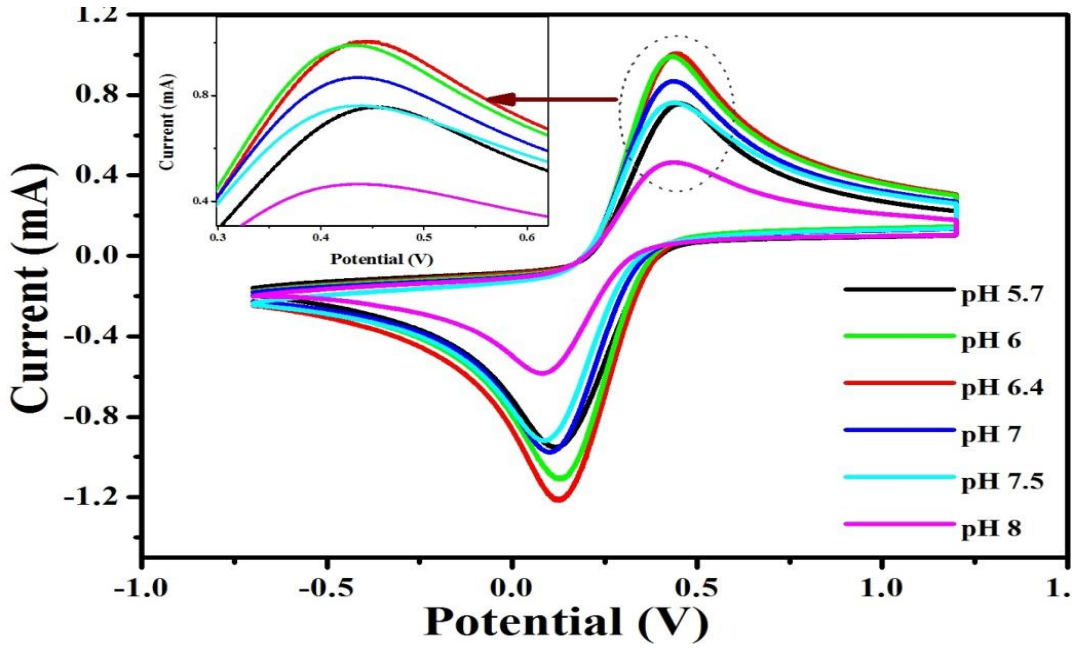

Figure 3.15: Cyclic voltammetric studies of V_2O_5-CHIT/ITO electrode as a function of pH ranging from 5.7 to 8.

`

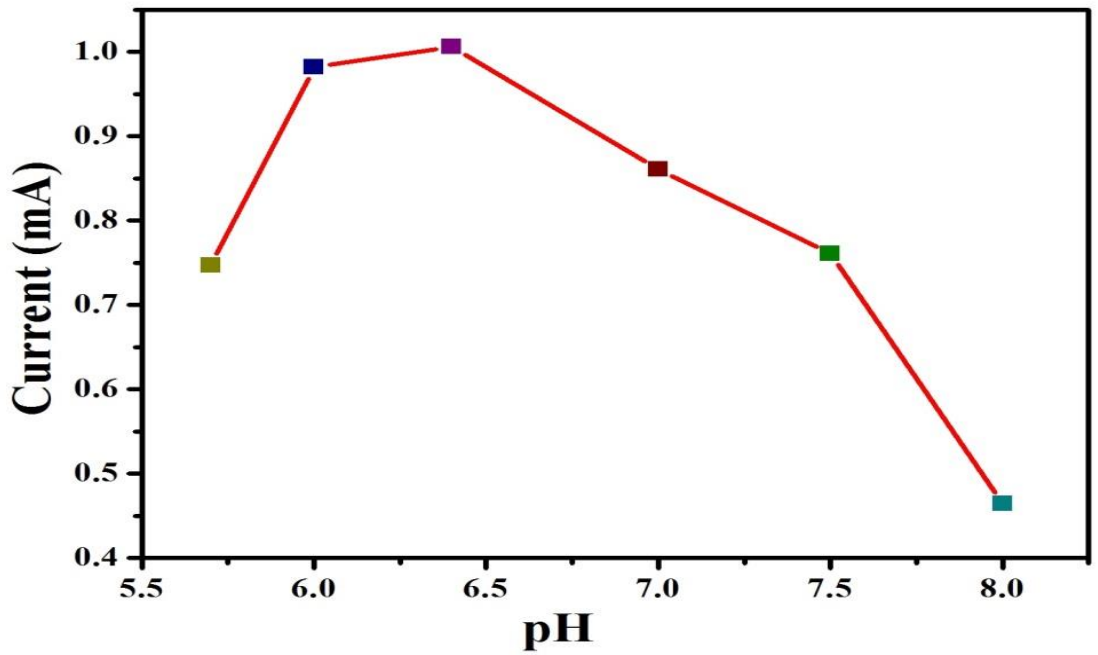

Figure 3.16: Conjugative change in current as a function of pH (from 5.7 to 8) on V_2O_5-CHIT/ITO electrode

3.3.4. Electro-oxidation study of hydrazine

The overall reaction for the oxidation of hydrazine can be written as follows:

$$N_2H_4 + 4OH^- \rightarrow N_2 + 4H_2O + 4e^- \quad \ldots\ldots\ldots\ldots\ldots\ldots\ldots\ldots\ldots\ldots \quad (3.5)$$

The effect of Hydrazine concentration on the CV response of V_2O_5-CHIT/ITO nanocomposite electrode has been investigated in 5 mM phosphate buffer (PBS, pH = 6.4, 0.9% NaCl) containing $[Fe(CN)_6]^{3-/4-}$ at a scan rate of 50 mV/s. Figure 3.17 shows CV of the V_2O_5-CHIT/ITO nanocomposite electrode as a function of N_2H_4 concentration varying from 2-22 mM. With increasing hydrazine concentration in the solution, the anodic and cathodic peak current increases. It is observed that the oxidation current of hydrazine first rises and then reaches a maximum value at ~ 0.5163 V. This catalytic peak current has a linear relationship with the concentration of hydrazine in the range of 2-22 mM. The linearity of V_2O_5-CHIT/ITO electrode is found from 2 to 22mM with linear regression co-efficient of 0.9712. The sensitivity of the V_2O_5-CHIT/ITO nanocomposite electrode obtained from the slope of the curve is found to be 0.00460 µA/(mM cm^2). The standard deviation and low

detection limit for the nanocomposite electrode have been found as 0.00249µA and 1.6239 mM respectively. From these results, it can be concluded that electro-oxidation of N_2H_4 at this electrode can be used for quantitative determination of hydrazine in given samples and it thus has a potential application as electro-oxidation device.

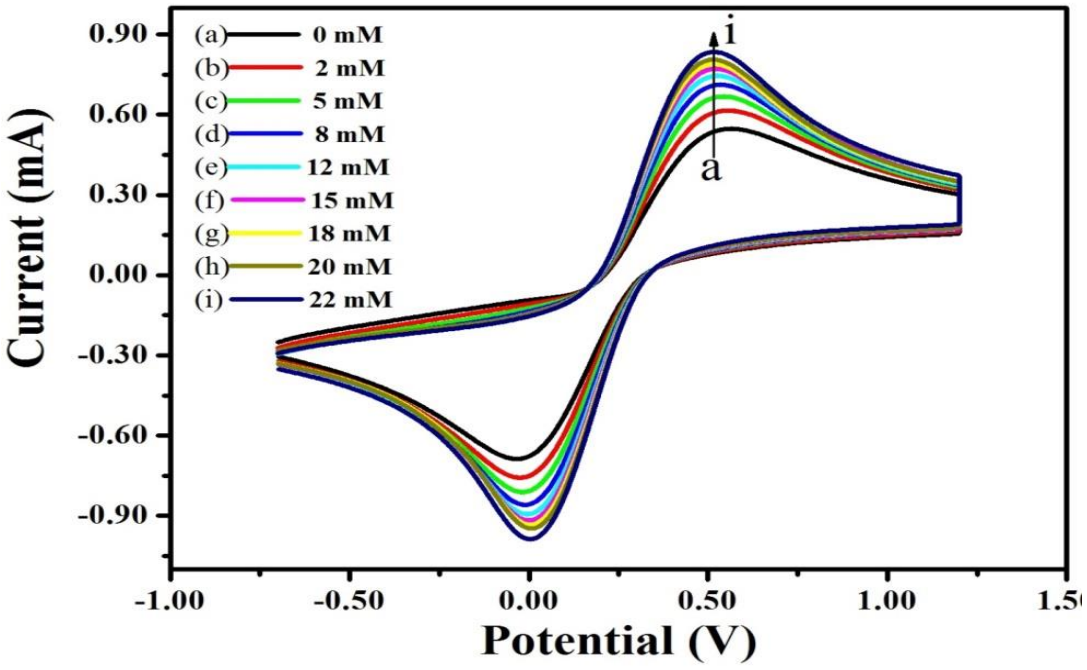

Figure 3.17: Electrochemical response of the V_2O_5-CHIT/ITO electrode with respect to hydrazine concentration (2-22 mM) in PBS (5 mM, pH 6.4, 0.9% NaCl) containing $[Fe(CN)_6]^{3-/4-}$ at a scan rate of 50 mV/s

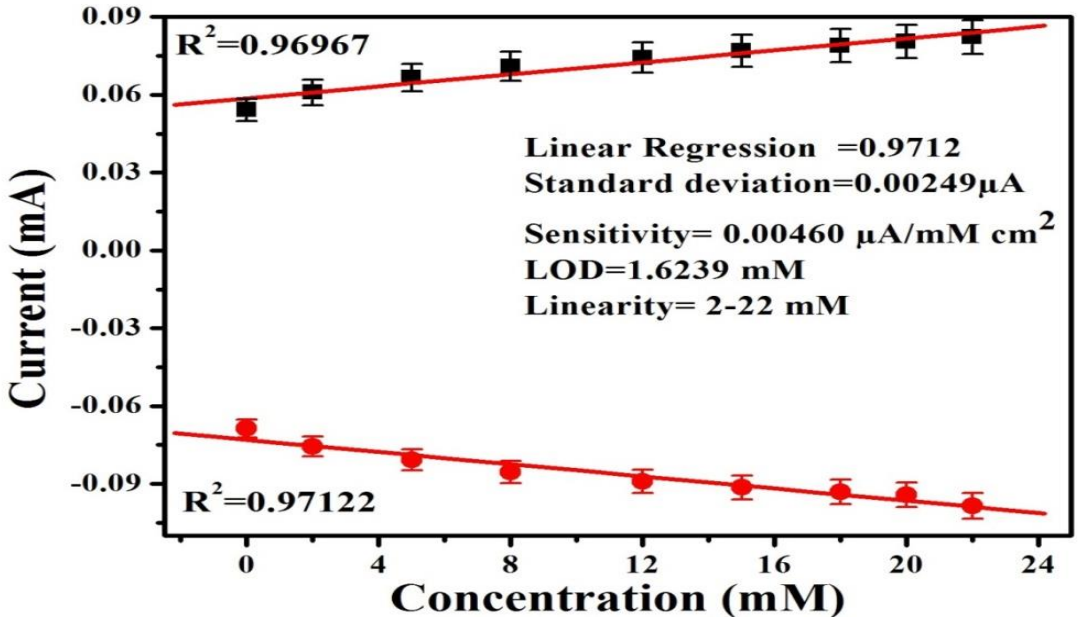

Figure 3.18: Calibration curve of the V_2O_5-CHIT/ITO electrode and the variation in current as a function of Hydrazine concentration (2-22 mM) in PBS (5 mM, 6.4 pH, 0.9% NaCl) containing $[Fe(CN)_6]^{3-/4-}$ at a scan rate of 50 mV/s.

3.3.5. Response time study of V_2O_5-CHIT/ITO electrode

For the determination of response time (Figure 3.19) of V_2O_5-CHIT/ITO nanocomposite electrode, we have measured electrochemical current response from 2 to 30 s. The magnitude of current increases initially (2 to 20 s) and after 20 s current started decreasing indicating that 20 s is the response time of V_2O_5-CHIT/ITO nanocomposite electrode.

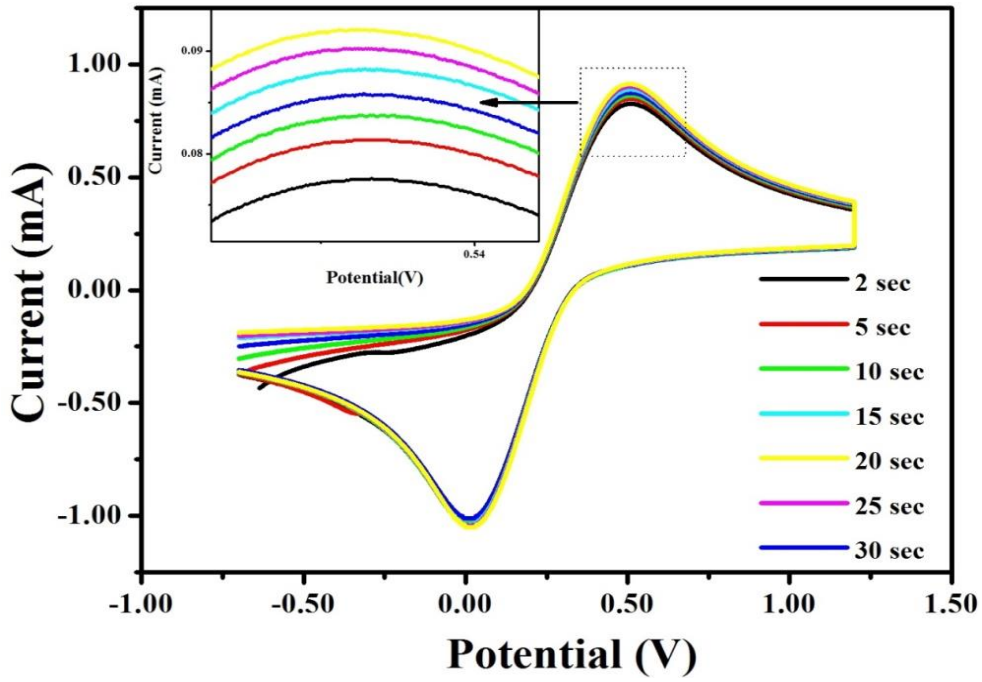

Figure 3.19: CV study of electrochemical response time of V_2O_5-CHIT/ITO nanocomposite electrode as a function of time during the incubation period from 2 to 30 s

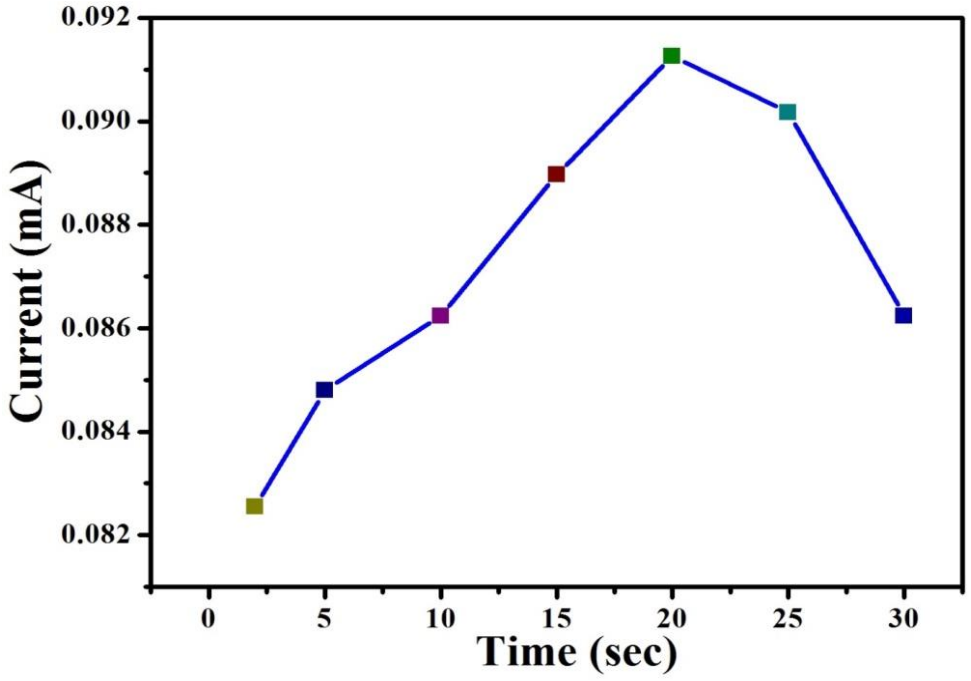

Figure 3.20: Electrochemical response time V_2O_5-CHIT/ITO nanocomposite electrode of during the incubation period from 2 to 30 s.

3.4 Antimicrobial activity assay

The antibacterial activity of the V_2O_5 nanoparticles, CHIT and V_2O_5-CHIT nanocomposite was tested against both gram positive and gram negative bacteria i.e. *Bacillus cereus* and *Pseudomonas aeruginosa* respectively. **Figure 3.21 (A)** shows the result after 24 h incubation of the *B. cereus* agar plate loaded with (a) V_2O_5 nanoparticles, (b) CHIT, (c) V_2O_5-CHIT nanocomposite (d) water as control. In Figure 3.21 (A) the uniform bacterial growth was observed, indicating no bacterial retardation activity by V_2O_5 nanoparticles (a), CHIT has given a zone of inhibition of 2 mm against Gram positive bacteria (b). This is attributed to the interaction between positively charged chitosan and negatively charged microbial cell wall, leading to the leakage of intracellular constituents. The binding of chitosan with DNA and inhibition of mRNA synthesis occur via the penetration of chitosan into the nuclei of the microorganisms and interfering with the synthesis of mRNA and protein s [55]. However, V_2O_5-CHIT nanocomposite gives a zone of inhibition of 3 mm because of CHIT but, the diameter is increased in nanocomposite as compared to that of CHIT due to change in the surface properties of CHIT, which was due to loading of V_2O_5 nanoparticles on the CHIT surface. Simultaneously control does not show any bacterial retardation (d).

Bacterial Strain	Bacterial Strain Name	Inhibition zone of various samples against bacterial Species (mm)			
		(a) V_2O_5	(b) CHIT	(c) V_2O_5-CHIT	(d) H_2O (control)
Gram +ve	*Bacillus cereus*	-	2	3	-
Gram -ve	*Pseudomonas aeruginosa*	-	5	6	-

Table 3.1: Zone of inhibition (mm) given by antibacterial activity of (a) V_2O_5 nanoparticles,(b) CHIT,(c) V_2O_5-CHIT nanocomposite (d) Water as control.

Figure 3.21 (B) shows the result after 24 h incubation of the *Pseudomonas aeruginosa* (Gram negative) agar plate loaded with (a) V_2O_5 nanoparticles, (b) CHIT, (c) V_2O_5-CHIT nanocomposite (d) H_2O. Similarly no zone of inhibition was observed in V_2O_5 nanoparticles (a) and control (d). While an increased zone of inhibition of diameter 5 mm and 6 mm were observed for CHIT (b) and V_2O_5-CHIT nanocomposite (c) respectively.

Increased zone of inhibition (diameter) by CHIT and V_2O_5-CHIT nanocomposite is observed in case of Gram negative bacteria as compared to gram positive bacteria. This is due to difference in cell wall structure of the Gram positive and Gram negative bacteria. Hydrophilicity in Gram-negative bacteria is significantly higher than in Gram-positive bacteria, making them more sensitive to chitosan.

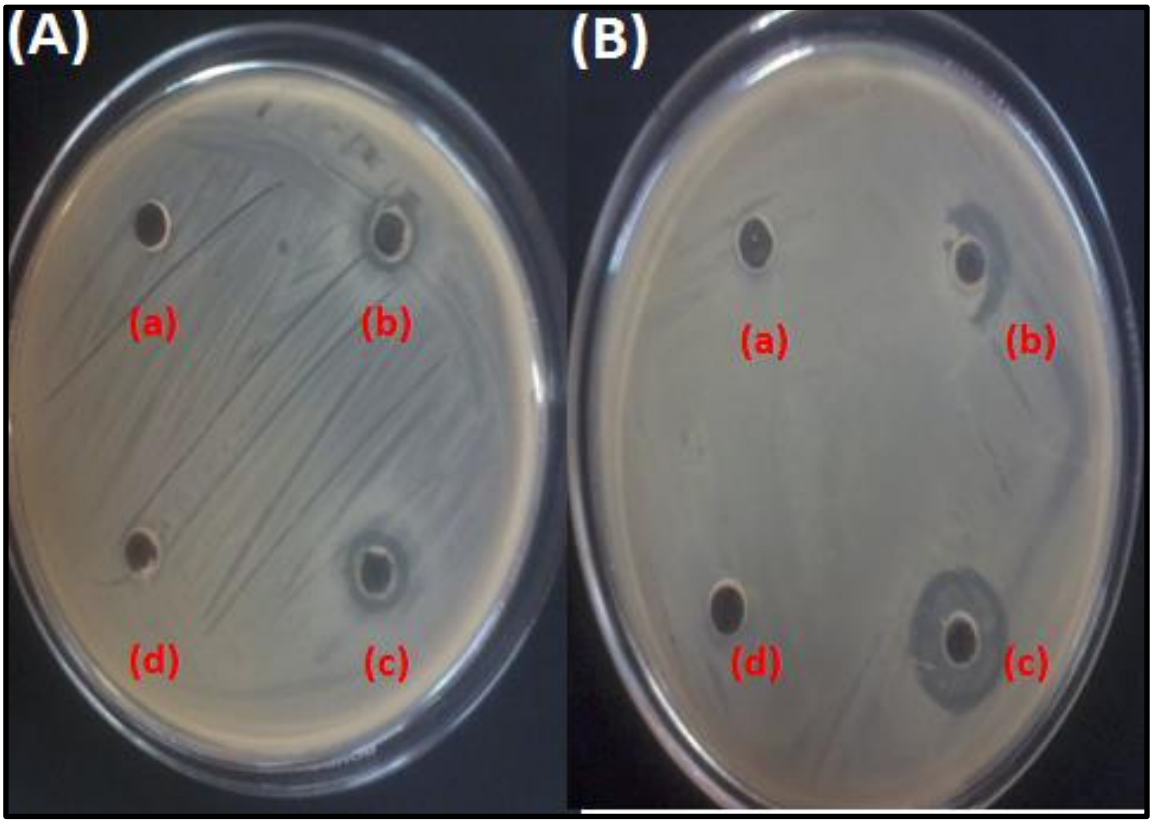

Figure 3.21: Snap shot of Agar plate after 24 h of incubation (A) Antibacterial activity against Bacillus cereus (Gram positive) bacteria (B) Antibacterial activity against *Pseudomonas aeruginosa* (Gram negative) bacteria where (a) V_2O_5 ,(b) CHIT (c) V_2O_5-CHIT nanocomposite and (d) Water.

4. Conclusion and future prospects

4.1. Conclusion

The main aim of this project work was the synthesis of vanadium penta oxide nanostructures, their characterization and fabricating V_2O_5/CHIT nanocomposite electrode for electro-oxidation of hydrazine. The V_2O_5 nanoparticles were synthesized by hydrothermal method. We have fabricated an amperometric non enzymatic sensor by binding the V_2O_5 nanoparticles (~25 nm) with the CHIT matrix. The prepared electrode has been characterized by XRD, SEM, FTIR, UV-Vis, PL and electrochemical techniques for enhancing the electrocatalytic properties of hydrazine. V_2O_5 nanoparticles were dispersed in CHIT solution ultrasonically and were casted onto ITO surface by drop casting method. The V_2O_5-CHIT/ITO electrode showed rapid response (20 s), high sensitivity 0.00460 μA/(mM cm^2), linearity (2-22 mM), standard deviation (0.00249 μA), lower detection limit (1.6239 mM). The wide detection range and high sensitivity may be assigned to the amplification of the magnitude of current response since the presence of V_2O_5 nanoparticles in CHIT matrix and its good biocompatibility improves the electron transfer between analyte (hydrazine) and V_2O_5-CHIT/ITO electrode surface. The results clearly suggest that V_2O_5-CHIT nanocomposite electrode provides an attractive matrix for impregnation of metal-oxide nanoparticles and an improved non-enzymatic sensor for the electrochemical studies.

4.2 Future prospects

Hydrazine and its derivatives have found a wide range of applications, including as antioxidants, pharmaceutical intermediates, pesticides, plant-growth regulators, blowing agents, corrosion inhibitors, dyes and in photography. Furthermore, hydrazine is a high energy fuel molecule and reducing agent as well and can be used as the fuel in explosives and rocket propulsion systems.

Nevertheless, hydrazine is toxic and probably even potentially carcinogenic. In order to better utilize hydrazine as a fuel and resolve these environmental issues, the development of a

catalyst that can oxidize at a high rate is required. However, a major barrier to the wide application of direct hydrazine (N_2H_4)-air fuel cells is the expensiveness of the noble metal catalysts that are generally required. To overcome this problem, research has been focused on developing various types of catalysts for the electro-oxidation of hydrazine.

However, very limited research has been done towards the sensing and electro-oxidation of hydrazine. This project work has tried to work towards this field using metal oxide-biopolymer nanocomposite. Nanoparticles have suitable physical and chemical properties for the development of electrochemical sensors and sensor with improved sensitivity and selectivity can be developed making use of the catalytic properties of nanoparticles.

The emergence of nanotechnology is opening new horizons for electrochemical sensors. Recent years have witnessed the development of a variety of nanomaterials based devices exhibiting novel functions. The use of nanomaterials in such sensing devices has taken off rapidly and will surely continue to expand. Nanoparticles, nanowires and nanotubes have already made a major impact on the field of electrochemical sensors and the unique properties of nanomaterials suggest that future interdisciplinary research could lead to a new generation of electrochemical biosensors.

Due to carcinogenic nature of hydrazine, to better utilize hydrazine as a fuel and resolve environmental issues there is an ever increasing demand for the fabrication of cheap, simple devices for electro-oxidation of hydrazine by exploiting the bottom up approach of nanotechnology, for the design of new improved electrochemical nanosensors. Still there is plenty of room for fabricating different nanomaterial based sensors for the electro-oxidation of hydrazine, which may become facilitated in the near future due to the revolutionary advancements in the field of nanotechnology. The metal oxide nanostructures might be suitable for these applications.

References

(1) P. Ball, "Made To Measure: New Materials for the 21st Century" Princeton, NJ: Princeton University Press, (1997).

(2) C. N. Rao, J. Mat. Chem 14, E4 (2004). DOI: 10.1039/b400318.

(3) J. M. Thomas, Pure Appl. Chem. 60, 1517 (1988). 28 A. P. Alivisatos, Science 271,933 (1996).

(4) S.G. Penn, L. He, M. J. natan, curr. Opin. Chem. Biol. 2003, 7, 609.- J.Lui, Y. Li, X. Huang, Z. Zhu, Nanoscale Res. Lett. 5,1177 (2010).

(5) S. Mickevicius, V. Bondarenka, S. Grebinskij, H. Tvardauskas, M. Andriulevicius, S. Tamulevicius , S. Kaciulis, The metals chemical states in hydrated vanadium oxides. 40 (2009) 126–129.

(6) J. Swiatowska-Mrowiecka , F. Martin , V. Maurice , S. Zanna, Klein, J. Castle, P. Marcus, The distribution of lithium intercalated in V_2O_5 thin films studied by XPS and ToF-SIMS.53 (2008).

(7) S. Mickevicius, V. Bondarenka, S. Grebinskij, H. Tvardauskas, M. Andriulevicius, S. Tamulevicius , S. Kaciulis, The metals chemical states in hydrated vanadium oxides. 40 (2009) 126–129.

(8) H. Cui, V. Teixeira, L. Meng , R. Wang , J. Gao , E. Fortunato.Thermochromic properties of vanadium oxide films prepared by dc reactive magnetron sputtering.Thin Solid Films 516 (2008).

(9) C.Q. Feng, S.Y.Wang, R. Zeng, Z.P. Guo, K. Konstantinov, H.K. Liu, Synthesis of spherical porous vanadium pentoxide and its electrochemical properties.184 (2008).

(10) Y. Kim, S. Gopukumar, K. Kim, B. Cho, Performance of electrostatic spray- deposited vanadium pentoxide in lithium secondary cells. 117 (2003) 110–117].

(11) Anqiang Pan,ab Ji-Guang Zhang, Facile synthesized nanorod structured vanadium pentoxide for high-rate lithium batteries.

(12) Waldir Avansi Jr., Caue Ribeiro, Edson R. Leite, and Valmor R. Mastelaro, Vanadium Pentoxide Nanostructures: An Effective Control of Morphology and Crystal Structure in Hydrothermal Conditions.

(13) Li Li, Zifeng Yan, Synthesis and Characterization of Self-Assembled V2O5 Mesostructures Intercalated by Polyaniline.

(14) Miao andTan, 2000; Xu et al., Amperometric phenol biosensor based on laponite clay-chitosan nanocomposite matrix 22 (2007) 816-821.

(15) R. Khan, A. Kaushik, P.R. Solanki, A.A. Ansari, M.K. Pandey, B.D. Malhotra, Zinc oxide nanoparticles-chitosan composite film for cholesterol biosensor, Analytica Chimica acta 616, (2008), 207–213.

(16) H. Huang, X. Yang, Chitosan mediated assembly of gold nanoparticles multilayer, Colloids and Surfaces A: Physicochem. Eng. Aspects 226, (2003), 77–86.

(17) X.L. Luo, J.J. Xu, Q. Zhang, G.J. Yang, H.Y. Chen, Electrochemically deposited chitosan hydrogel for horseradish peroxidase immobilization through gold nanoparticles self-assembly, Biosensors and Bioelectronics 21, (2005), 190–196.

(18) H.L. Zhang, X.Z. Zou, G.S. Lai, D.Y. Han, F. Wang, Direct electrochemistry of horseradish peroxidase based on biocompatible carboxymethyl chitosan–gold nanoparticle nanocomposite, Biosensors and Bioelectronics 22, (2006), 768–773.

(19) H.L. Zhang, X.Z. Zou, G.S. Lai, D.Y. Han, F. Wang, Direct Electrochemistry of Hemoglobin Immobilized on Carbon-Coated Iron Nanoparticles for Amperometric Detection of Hydrogen Peroxide, Electroanalysis 19, (2007), 1869 – 1874.

(20) A. Kaushik, P.R. Solanki, A.A. Ansari, S. Ahmad, B.D. Malhotra, Chitosan-Iron Oxide Nanobiocomposite Based Immunosensor for Ochratoxin-A, Electrochemistry Communications, 2008 (In press).

(21) J. Qiu, H. Peng, R. Liang, Ferrocene-modified Fe_3O_4-SiO_2 magnetic nanoparticles as building blocks for construction of reagentless enzyme-based biosensors, Electrochemistry Communications 9, (2007), 2734–2738.

(22) Y.L. Liu, Y.H. Yang, H.F. Yang, Z.M. Liu, G.L. Shen, R.Q. Yu, Nanosized flower-like ZnO synthesized by a simple hydrothermal method and applied as matrix for Horseradish Peroxidase immobilization for electro-biosensing, Journal of Inorganic Biochemistry 99, (2005), 2046–2053.

(23) J.T. Yeh, C.L. Chen, K.S. Huang, Synthesis and properties of chitosan/SiO_2 hybrid materials, Materials Letters 61, (2007), 1292–1295.

(24) R. Khan, M. Dhayal, Nanocrystalline bioactive TiO_2–chitosan impedimetric immunosensor for ochratoxin-A, Electrochemistry Communications, 10, (2008), 492–495.

(25) K.J. Feng, Y.H. Yang, Z.J. Wang, J.H. Jiang, G.L. Shen, R.Q. Yu, A nano-porous CeO_2/Chitosan composite film as the immobilization matrix for colorectal cancer DNA sequence-selective electrochemical biosensor, Talanta 70, (2006), 561–565.

(26) L. Aldous, R. G. Compton, The mechanism of hydrazine electrooxidation revealed by platinum microelectrodes: role of residual oxides, 2011,13, 5279-5287.

(27) B. Sheng, L. Hu, T. Yu, X. Cao, H. Gu, Selective hydrogenation of cinnamaldehyde over Pt nanoparticles deposited on grapheme oxide, 2012, 2,5520-5523.

(29) M. Hosseini, M. M. Momeni, M. Faraji, Characterization of in situ grown ceria nanoparticles on reduces grapheme oxide as catalyst for electrooxidation of hydrazine, 2011, 335, 199–204.

(30) Q. Yi, L. Li, W. Yu, Z. Zhou, G. Xu,, 2008, 295, 34-38.

(31) K. Asazawa, K. Yamada, H. Tanaka, M. Taniguchi, K. Oguro, Aerosol derived Ni, Zn electrocatalyst for direct hydrazine fuel cell, 2009, 191, 362-365.

(32) J. Wang, Z. Dong, J. Huang, J. Li, X. Jin, J. Niu, J. Sun, J. Jin, J. Ma, Appl. Surf. Sci., http://dx.doi.org/10.1016/j.bbr.2011.03.031.

(33) S. I. Yamazaki, T. Ioroi, K. Tanimoto, K. Yasuda, K. 45 Asazawa, S. Yamaguchi, H. Tanaka, J. Power Sources, 2012, 204, 79-84.

(34) Y. B. Jang, T. H. Kim, M. H. Sun, J. Lee, S. J. Cho, Catal. Today, 2009, 146, 196–201.

(35) S. Ivanov, U. Lange, V. Tsakova, V. M. Mirsky, Sensor Actuat 50 B-Chem, 2010, 150, 271-278.

(36) S. K. Singh, Y. Iizuka, Q. Xu, Int. J. Hydrogen Energ., 2011, 36, 11794-11801.

(37) J. S. Chinchilla, K. Asazawa, T. Sakamoto, K. Yamada, H.Tanaka, P. Strasser, J. Am. Chem. Soc., 2011, 133, 5425–5431 55.

(38) X. Zhong, H. Yang, S. Guo, S. Li, G. Gou, Z. Niu, Z. Dong, Y. Lei, J. Jin, R. Li, J. Ma, J. Mater.Chem., 2012, 22, 13925- 13927.

(39) Ming Li. Fengyu kong, Guanghi Li, Honggiang Wanq, Synthesis of vanadium pentoxide (V_2O_5) ultralong nanobelts via an oriented attachment growth mechanism, 5317-5320

(40) K.Nishimaki, S.Ohmae, T.A.Yamamoto, M.Katsura; Nanostruct.Mater. Vol-12, 1999, 527-530.

(41) A. Cuesta, P. Dhamelincourt, J. Laureyns, A. Martínez-Alonsoand J. M. D. Tascón, Comparative performance of X-ray diffraction and Raman microprobe techniques for the study of carbon materials, J.mat. Chem., 1998, 8, 2875-2879.

(42) Griffiths, P.; de Hasseth, J.A. (18 May 2007). Fourier Transform Infrared Spectrometry (2nd ed.).Wiley-Blackwell. ISBN 0471194042.

(43) J. J. Storf, A. D. Lucas, V. Garmella, Y. P. Bao, U. R. Muller, W. Kemp, Organic Spectroscopy, The Macmillan Press Ltd, 1991, Houndmills, Basingstoke, Hampshire, , Nat. Biotechol, 22, 2004, 283.

(44) J. M. Chalmer and P. R. Griffith, H. F. Shurvell, in Handbook of Vibrational Spectroscopy, Edited, John Willey and Sons, Ltd. Vol 3, 2002, 1783.

(45) G. Lia, J. M. Liao, G. Q. Hu, N. Z. Ma and P. J. Wu, Biosens. Bioelectron.20, 2140 (2005).

(46) J. Wang, Analytical electrochemistry, 3 Ed., Analytical electrochemistry, Wiley-VCH 2006.

(47) Anqiang Pan,ab Ji-Guang Zhang, Zimin Nie,b Guozhong Cao,c Bruce W. Arey,b Guosheng Li,b Shu-quan Liang and Jun Liu, Facile synthesized nanorod structured vanadium pentoxide for high-rate lithium batteries.

(48) Woi pei meng and Irmawati ramli, Optimization of the surface area of V_2O_5 nanocrystals through number of washing.

(49) A. Kaushik, R. Khan, P.R. Solanki, P. Pandey, J. Alam, S. Ahmad, B.D. Malhotra, Iron oxide nanoparticles–chitosan composite based glucose biosensor, Biosens. Bioelectron. 24 (2008) 676–683.

(50) F. Tian, Y. Liu, K. Hu, B. Zhao, The depolymerization mechanism of chitosan byhydrogen peroxide, J. Mater. Sci. 38 (2003) 4709–4712.

(51) C. Xiong, A. E. Aliev, B. Gnade and K. J. Balkus, ACS Nano, 2008, 2, 293–301.

(52) Ming Li, Fengyu Kong, Hongqiang Wang and Guanghai Li, Synthesis of vanadium pentoxide (V_2O_5) ultralong nanobelts via an oriented attachment growth mechanism.

(53) Santosh Kumara, Nidhi Nigama, T. Ghosha, Pradip K. Duttaa, S.P. Singhb,Prashant K. Dattab, Lijia Anc, Tong Fei Shic, Preparation, characterization and optical properties of a novel azo-based chitosan biopolymer.

(54) A. Caski, G. Maubach, D. Born, J. Reichert and W. Fritzsche, Single Mol.,275 (2002).

(55) Steven J. Setford and Jeffrey D. Newman,Enzyme Biosensor, Methods in Biotechnology, 2005, Volume 17, 29-60, DOI: 10.1385/1-59259-846-3:029.

(56) Jay Singh & P. K. Dutta , Preparation, Antibacterial and Physicochemical Behavior of Chitosan/ Ofloxacin Complexes.(International Journal of Polymeric Materials and Polymeric Biomaterials.